UNIVERSITY OF COPENHAGEN
FACULTY OF SCIENCE

**Master's Thesis**

Søren Borg Nielsen

# On The Arctic Temperature Bias in a Climate Model and its Cause

Academic Supervisor: Prof. Markus Jochum

Submitted: 4/11 2016

# Abstract

A temperature bias in the Arctic Ocean in the coarse resolution Community Climate System Model version 4 (CCSM4) is documented and the cause is analyzed. The bias is attributed to a too warm ocean inflow from the Nordic Seas and it is shown that the inflow temperature bias is connected to the parameterized mesoscale eddy mixing of temperature in the Norwegian Current. A series of model setups are created with different parameterization settings, forcings and resolution and run for 300 years. It is shown that by reducing either horizontal or thickness diffusivities, or both, the Arctic temperature bias is reduced. Side effects of reduced diffusivities include deepening of the upper Atlantic water, improving the depth in the Canadian basin but not in the Eurasian basin, as well as an improved circulation around the Canadian basin slope when reducing thickness diffusivity.

It is further shown that the cause of the temperature bias in the Nordic Seas is a spurious, vertical 2-core structure of the Norwegian Current, shielding the lower branch from the atmosphere and the associated heat loss related to poleward advection. Reducing the diffusivities causes the separation of the Norwegian Current to be weaker, and ultimately it loses more heat to the atmosphere and reduces the temperature bias of the inflowing water to the Arctic. One caveat is that it cannot be determined if the cause of the 2-core structure is excessive eddy diffusion, or if the eddy diffusion in the Nordic Seas is caused by the formation of the 2-core Norwegian Current, but the results clearly call for more sophisticated eddy tracer mixing parameterizations.

# Resumé

En temperaturanomali i det Arktiske Ocean er dokumenteret i klimamodellen Community Climate System Model version 4 (CCSM4), og årsagen analyseres. Fejlen tilskrives en alt for varm havtilstrømning fra Norskehavet og det påvises at den for varme tilstrømning er forbundet med parameteriseret mesoskala eddy diffusion af temperatur i den Norske Havstrøm. En række numeriske forsøg sættes op med forskellige ændringer i parametriseringer af sub-grid processer, modelforcering og -opløsning, og integreres i 300 år. Det er vist, at ved en reduktion af enten horisontal eller isopyknal diffusivitet reduceres den arktiske temperaturanomali. Bivirkninger af reducerede diffusiviteter omfatter sænkning af den den øverste 0°C-isoterm, hvilket forbedrer dybden i det canadiske bassin, men ikke i det eurasiske bassin, samt en forbedret cirkulation omkring det canadiske bassin, når den isopyknale diffusivitet sænkes.

Det er endvidere vist, at årsagen til temperaturanomalien i Norskehavet er en dobbeltkernestruktur af den norske havstrøm, som afskærmer en del af havstrømmen fra atmosfæren og det tilhørende varmetab relateret til den polgående advektion. Reduceret diffusivitet bevirker at adskillelsen af den norske strøm, der bliver svagere, hvilket er forbundet med et øget varmetab til atmosfæren. Et forbehold er, at det ikke kan afgøres, om årsagen til dobbeltkernestrukturen er urealistisk høj eddy diffusion, eller om den simulerede eddy diffusion er forårsaget af dannelsen af den dobbeltkernede norske havstrøm, men resultaterne kalder på mere sofistikerede eddy-parameteriseringer.

# Preface

The present work is supposed to be the conclusion of several years of studies, but it feels only as the beginning. During the past few years I have learned a lot regarding climate physics, yet I feel as though I am only getting to the point where I start to think the right things and ask the right questions. To think back I realize how little I knew two years ago, and I wonder if in two years I will think the same about today.

Learning is seldom an individual achievement, and this feels like the perfect occasion to thank all that helped me get this far. One thing I have learned is that the world is chaotic, and every person I ever met might have played an important role in getting me to this point, and you therefore all have my thanks. Some people, however, deserve special attention.

First, I would like to thank my supervisor, Prof. Markus Jochum, who in his own way has kept the grand overview when I was caught in the details, and Jonas for his indispensable help in setting me up with CCSM, Python and Linux, as well as Helen and Roman and the rest of Team Ocean for insightful comments and help when it was needed, and to my collegues at CIC and ClimGeo for the pleasant work environment and important coffee breaks.

I would also like to direct a very special thanks to Mads, Kasper and Christian for the help with my academic work and with some proof-reading when it was needed the most. It has been a pleasure to journey through geophysics with you, and your support has been essential in the darkest hours.

But thanks should also be sent to those outside of work. I would therefore like to thank Kristian for the most philosophical workout sessions, David for being my everlasting link to my childhood, Peter and Freja for always opening their door to me, Martin for the laughs, the quotes and always letting me win best out of three, Simon and Morten for the funniest three course dinner nights, Silke for the adventures, Anders, Anders, Anders and Lasse for the music, Mikkel for helping me through first year, everyone at Hørhus Kollegiet's second floor and finally Peder for teaching me that solving a problem starts by understanding it. I bet I have forgotten some, I hope you all bear with me.

Finally, I would like to thank my family, my parents for raising me the way they did, and especially my brother, Flemming, for teaching me to read and write.

Without you all, where would I be?

Søren Borg Nielsen
November, 2016

# Contents

# 1 Introduction

Numerical models play a crucial role in our understanding of the climate system. Without models it is impossible to test hypotheses on how the climate react to different changes, locally or globally. As such, models need to be continuously evaluated and improved, and it is desired that all model errors be analyzed and corrected. One particular region that has proved very difficult to simulate in climate models is the Arctic Ocean.

The polar regions are extremely interesting as the ocean here is not only in touch with the atmosphere, but sea ice and ice sheets as well, bringing together all components of the climate system in one relatively small region. One particular feature that is unique to the North Pole is the warm, salty subsurface Atlantic Water, which causes stratification in the Arctic to be fairly weak and contains a huge amount of heat that, should it be brought to the surface through some process, has the potential to release this heat to the atmosphere and possibly melt sea ice.

The present study follows a simple approach in the hope of increasing understanding of the processes that cause a temperature bias to occur in the Arctic. The train of thought is rather simple: a warm temperature bias is observed in the Atlantic layer in the ocean component of the Community Climate System Model version 4, CCSM4, the Parallel Ocean Program, POP2, and a hypothesis for the cause of this bias is developed and tested. The hypothesis is that too strong eddy diffusion of tracers in the northern high latitudes changes the structure of the Norwegian Current and thus the entire structure of the Nordic Seas and Arctic Ocean temperature fields. In order to test the hypothesis the same model is modified in different respects in an attempt to minimize the hypothezised eddy-induced temperature bias. In the course of the project different observations of model performance have been made, making way for other aspects that need to be illuminated. This includes the role of ocean viscosity as well as the role of the surface forcing, as both seem to have an effect in the development of the bias. The focus, however, remains on eddy mixing parameterizations and their implications in the northern high latitudes.

In section 2 a description of the Arctic Ocean and Nordic Seas is given, focused primarily on the observed temperature and flow characteristics as well as basin bathymetries. In section 3 a description of the theory of tracer mixing parameterizations is presented as well as mixing of momentum. In section 4 the CCSM4 Arctic temperature bias is documented. In section 5 the model used throughout this study, POP2, is described along with the different model runs, leading to a presentation of the results in section 6. Section 7 discusses the observations and tries to tie together all loose ends as well as to discuss whether or not the hypothesis holds and section 8 concludes the project.

# 2 The Northern High Latitude Oceans

The starting point of this thesis is to describe the observed characteristics of the Northern high latitude oceans, which here refer to the Nordic Seas and the Arctic Ocean. The focus is observed bathymetry and circulation. Focus in the litterature has been on the Arctic Ocean, but as discussed later, the Nordic Seas are very important for the present study, and therefore a short description of this small basin is also presented.

## 2.1 The Arctic Ocean

Global warming and the observed reduction in sea ice in the Arctic Ocean has increased the public and political interest in the Arctic. Especially the reduced sea ice cover has increased the possibility of the Arctic as a more accessible region for shipping lanes and extraction of resources. Scientific interest has also increased; not only does the Arctic play a vital role in the climate system, it appears to be a region very sensitive towards climate change as well, making it crucial to understand feedback mechanisms associated with the current change within the regional and global climate. The scientific community also benefits from the current sea ice trends in the respect that more observations are now possible in what used to be a region of extremely limited access. Thus, the amount data in and knowledge of the Arctic Ocean, in particular below the sea ice, is increasing.

The ocean bathymetry of the Arctic Ocean and Nordic Seas is plotted in figure 1 (based on the Jakobsson et al., 2012, dataset). The plot is overlaid with acronyms of the different basins, shelves and ridges. The explanation for all acronyms is given in table 1 and will be used throughout this section for reference. The Arctic Ocean is connected to the Atlantic through three channels: The Canadian Archipelago (CA) connects the Arctic to the Baffin Bay (BB) and through the Labrador Sea to the North Atlantic. The Barents Sea (BAS) and Fram Strait (FS) connect the basin to the Nordic Seas (NS) and over the Greenland-Scotland Ridge and the Denmark Strait to the rest of the North Atlantic. The Bering Strait (BES), a shallow and narrow pathway providing the Arctic with a modest net transport of 0.8 Sv (1 Sv

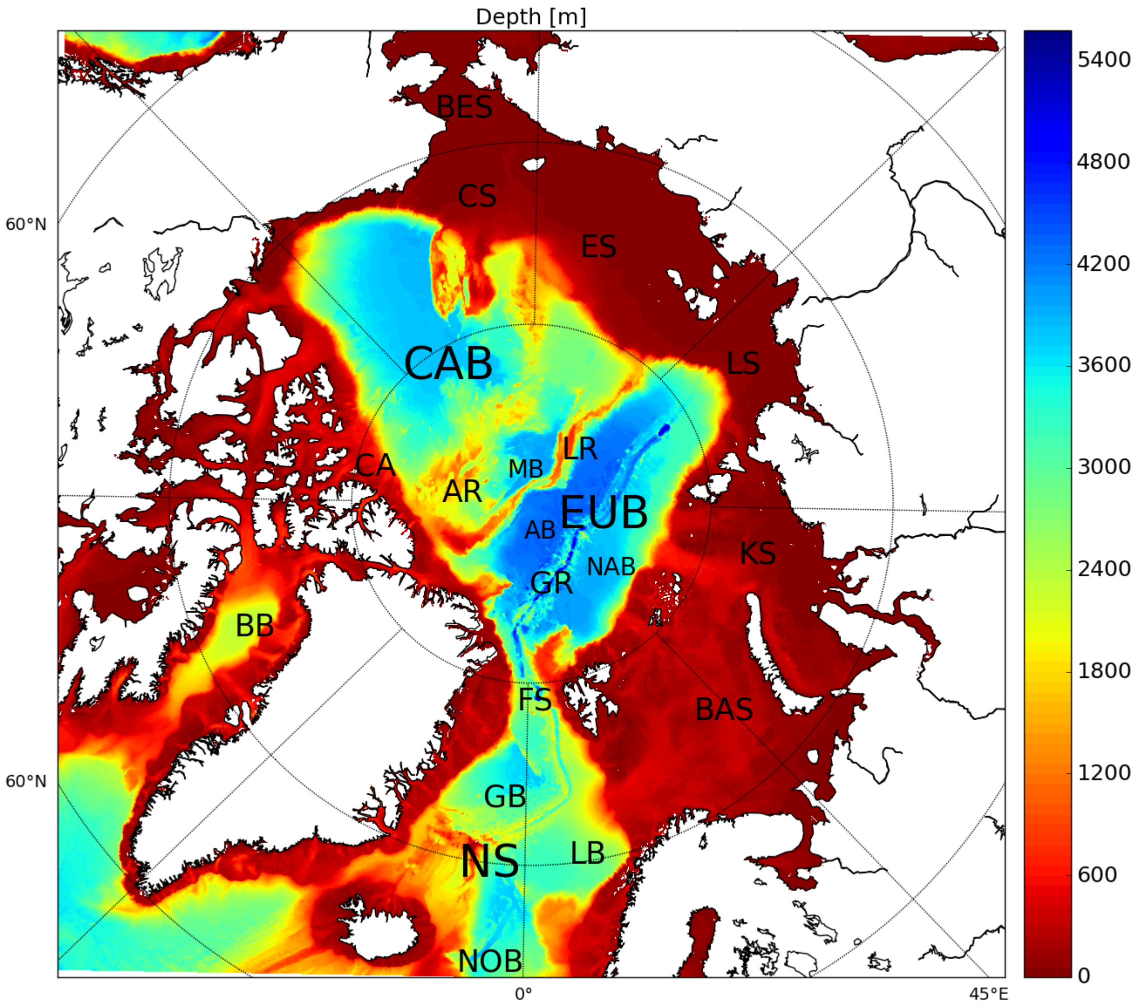


**Figure 1:** Bathymetry of the Arctic Ocean in metres (from the Jakobsson et al., 2012, dataset). For explanation of basin acronyms see table 1.

$= 10^6$ m$^3$s$^{-1}$) (Woodgate and Aagaard, 2005), is the only connection to the Pacific Ocean. The salinity of the ocean is largely determined by the series of river outflows that surround the Arctic providing the biggest fresh water source in the region (as estimated by Aagaard and Carmack, 1989). Besides the FS, all passages to the Arctic are shallow as seen in figure 1. Thus, the FS is the only channel through which the Arctic exchanges deep waters with the Atlantic. For simplicity, and because the largest volume transports are observed to occur through the FS, the Arctic is often described in the literature and simulated as a semi-enclosed basin. Such studies, despite their crude assumptions, have shown in large to capture most of the dynamic and important features of the region (see for instance Spall, 2013). However, despite the success of these models, the shallow channels are suggested to play important roles in setting the watermass properties of the Arctic. As an example the BAS has been suggested to be a source of cold, halocline water overlying the Atlantic layer, separating the sea ice from the underlying warm waters that would otherwise melt the sea ice (Steele et al., 1995).

The circulation in the Arctic is determined by the local bathymetry, especially the ridges that lie across the interior basin. The bathymetry of the Arctic and Nordic Seas is plotted in figure 1. The Lomonosov Ridge (LR, the ridge connecting the northern edges of Greenland and Siberia) separates the Arctic in two basins, the Eurasian basin (EUB), surrounded by the FS, the BAS and the LR, and the Canadian basin (CAB), surrounded by the CA, the BES, the Chuchki Shelf (CS) and East Siberian Shelf (ES) and the LR. The EUB is warmer and saltier than the CAB, as it is dominated by the inflow of Atlantic water.

When looking at figure 1, one thing that captures the eye is that a large part of

**Table 1:** Legend explanation for figure 1.

| | | | |
|---|---|---|---|
| AB | Amundsen Basin | GB | Greenland Basin |
| AR | Alpha Ridge | GR | Gakkel Ridge |
| BAS | Barents Sea | KS | Kara Shelf |
| BB | Baffin Bay | LB | Lofoten Basin |
| BES | Bering Strait | LR | Lomonosov Ridge |
| CA | Canadian Archipelago | LS | Laptev Shelf |
| CAB | Canadian Basin | MB | Makaraov Basin |
| CS | Chuchki Shelf | NAB | Nansen Basin |
| EUB | Eurasian Basin | NOB | Norwegian Basin |
| ES | East Siberian Shelf | NS | Nordic Seas |
| FS | Fram Strait | | |

the area of the ocean is in fact coastal shelves with depths of only a few hundreds of metres. The basin is connected to the global oceans through beforementioned straits and openings, and is otherwise confined by the Siberian and Canadian shelves. The Arctic interior can be split into several sub-basins on through the different ridges. As mentioned, the major basins, the Eurasian and Canadian basins, are separated by the LR, stretching from Greenland to Russia close to the North Pole. The EUB is further separated by the Gakkel Ridge (GR) into the Nansen (NAB) and Amundsen basins (AB). The former is surrounded by the BAS, the Kara Sea (KS) and the GR, and the latter is located between the two ridges. The CAB is separated in two basins by the Alpha Ridge (AR), gives rise to a small basin, the Makarov basin (MB), surrounded by the AR and LR. The litterature sometimes refer to the CAB and MB as the Amerasian basin, and sometimes to both as the Canadian basin. As the MB is largely unimportant for the present study, the term Canadian basin shall be used to cover also the MB.

Rudels et al. (1994) studied the watermass properties of the intermediate waters in primarily the EUB, obtained from Conductivity-Temperature-Depth (CTD) measurements covering the NAB and AB (and a few excursions to the MB, for a full description of observations, see Anderson et al., 1994). The spatial structure of the observed temperature-salinity (TS) fields led to the current theory of the Arctic intermediate circulation: The FS and BAS branch of Atlantic water merge North of BAS and KS and form a boundary current along Siberian shelf. When meeting the GR and LR, the water current splits into branches that either continue along the shelf or flow along the ridges. When the currents flowing along the ridges reach the Greenland shelf they merge again with the boundary current and flow along the shelf and out the western part of the FS, except for a small recirculating branch that forms a closed circulation between the LR and GR. Eddies transfer heat and salt from the boundary current into the interior, and as the boundary current travels along the perimeter of the Arctic, it loses heat and salt. As a result, the CAB is cold and fresh compared to the warmer and saltier EUB.

The intermediate waters in two basin interiors are composed of cyclonic circulations, the Beaufort Gyre in the CAB being the strongest of the two. What drives the Beaufort Gyre, an important feature in the Arctic which stores vast amounts of freshwater, has been suggested to be the local wind stress curl, but som recent numerical studies (Spall, 2013) with uniform wind stress suggest that the ice stress curl on the ocean surface is in fact an even more important mechanism. As such, the important mechanisms in setting the circulation of the Arctic are still debated.

The interiors are strongly stratified by the large freshwater fluxes from rivers and melting sea ice. The deep waters are, however, rather complicated in their watermass properties, as some deep waters are formed in the Nordic Seas and some on the Arctic shelves, but it is worth mentioning that they follow an cyclonic flow like the intermediate waters but unlike the surface waters (Aagaard, 1981).

## 2.2 The Nordic Seas

The Nordic Seas is a common term covering the basins that separate Norway and Greenland. The bathymetry is also plotted in figure 1 with legend description in table 1. The Nordic Seas (NS) can generally be decomposed into three sub-basins, the Norwegian basin (NOB), the Lofoten basin (LB) and the Greenland basin (GB). The watermass properties of the basins are dominated by the currents transporting waters between the North Atlantic and the Arctic Ocean. The inflow of Atlantic Waters is split in several branches in the NOB, primarily a branch flowing in between Iceland and the Faroe Islands, the other between the latter and Scotland. The entire section, including the Denmark Strait between Greenland and Iceland is generally referred to as the Greenland-Scotland Ridge. The current structure gets fairly complicated. Here we shall follow the terminology of Raj et al. (2015). The inflow branch between the Faroe Islands and Iceland, the Norwegian Atlantic Front Current, flows along the slope of the Norwegian shelf, rounding the western side of the Vøring Plateau (the plateau between NOB and LB) and the LB, where as the Norwegian Atlantic Slope Current flows on the eastern side along the Norwegian coast, before splitting in the BAS current and a branch joining the front current to flow through the FS. The western part of the basin is dominated by the waters flowing from the Arctic Ocean to the Atlantic, forming the East Greenland Current (EGC). Between all these currents, a lot of recirculation takes place. Upon reaching the FS, some waters return to join the EGC, and upon reacing the Denmark Strait, waters of the EGC recirculates to join with the front current. The LB is also dominated by standing eddy activity, creating a form of vortex where waters reside in long recirculation before ending up in either the front or slope current. This basin is important in the overall proces of heatloss from the Atlantic Water to the atmosphere and deep water formation (Raj et al., 2015).

An important concept regarding the Atlantic Water and the circulation in the Nordic Seas and the Arctic is the subduction of the waters under cold, fresh waters formed at the surface especially in the Arctic from sea ice and river outflows. The current generally subducts close to the FS (e.g. Beszczynska-Möller et al., 2012) and after this loses contact with the atmosphere.

# 3 Mixing parameterizations

The following chapter deals with the idea of representing mixing in global ocean and atmospheric models, which requires several approximations in the step of going from continuous fluids to discrete ones.

Since the 70's computer models have been increasingly used in the study of the climate system. This is partly because of the huge leaps technological advances have allowed in the past half century, but also because climate science, unlike most other physical sciences, is not tested through thorough experiments on the entire climate system, as this is impossible (or at least raises serious ethical questions). In order to learn something about the climate system we therefore must turn to climate models, and the need to continuously improve these is obvious. Recent advances in numerical modelling has increased model performances, and these are getting better every year. This is manifested in some great results obtained using global, coupled general circulation models (GCM's) in the recent decade. Several important climatic features are now captured in the socalled "state of the art" climate models such as CCSM, MPI-ESM, NorESM and others. Despite the advances within modelling it is important to stress that no model is perfect, and each has its own biases (see e.g. Ilicak et al., 2016). This is a logical consequence of modelling as one has to make certain compromises when going from a continuous real world to a discrete model world.

The primary focus is eddy mixing parameterizations and their ability to mix tracers. Mixing of momentum is also an important feature and will be discussed briefly in the end of the chapter.

In general, primitive equation models attempt to solve the momentum equation

$$\frac{D\mathbf{V}}{Dt} = -2\mathbf{\Omega} \times \mathbf{V} - \frac{1}{\rho}\nabla\rho + \mathbf{g} + \mathbf{F} \tag{1}$$

and the tracer equation,

$$\frac{\partial}{\partial t}\varphi + \mathbf{V} \cdot \nabla\varphi = \mathcal{D}\left(\varphi\right). \tag{2}$$

Here $\mathbf{V}$ is the 3-dimensional velocity vector, $t$ is time, $\mathbf{\Omega}$ is the rotation vector of the Earth, $\rho$ is density, $\mathbf{g}$ is the gravitational accelaration vector and $\mathbf{F}$ represents friction. $\varphi$ is a tracer (e.g. temperature or salt), and $\mathcal{D}$ represents diffusion. $\nabla$ denotes the three-dimensional gradient operator. The total derivative is defined as the sum of the local rate of change and the advective term,

$$\frac{D}{Dt} = \frac{\partial}{\partial t} + \mathbf{U} \cdot \nabla. \tag{3}$$

Solving these equations in a model requires discretization, and at any level one has to choose a cut-off length scale, under which all processes happen on a sub-grid level. Sub-grid processes then constitute the frictional and diffusive terms in the two equations, and determining these is the subject of this chapter, starting with the tracer diffusion.

## 3.1 Mixing of tracers

The ideal ocean model has a high spatial resolution horizontally and vertically. In the uppermost extreme scenario one would be able to track each individual water parcel throughout the ocean. This is the far future of models, if it is even realistic to ever obtain, thus, for now we have to settle with ocean general circulation models (OGCM's) of poorer resolution. So far the highest resolution global ocean models are at the level where they are eddy-resolving or eddy-permitting. This means that baroclinic instabilities evolve naturally within the model, causing eddies to be formed at a rate comparable to that observed in the ocean. However, as a result of limited computational power, climate models must often include ocean components of coarser, non-eddy-resolving, resolution. This follows as the integration time of centuries to millenia which is required for climate simulation purposes increases exponentially as the spatial resolution is increased. Thus, working with climate modelling means that processes below a certian spatial resolution are simply left unresolved in the model. However, if coarse resolution models are to be of any use they should preferably yield the same results as high resolution, eddy resolving models, or at least be of great similarity. Otherwise any use of coarse resolution climate models is extremely hard to justify. The challenge then arises in how to make the coarse resolution model mimic the high resolution model when the latter includes processes on the unresolved scale of the coarse resolution mode.

In order to accomplish this difficult task it is important to assess how sub-grid mixing processes interact with the resolved mean flow as the impact of small-scale processes on the large scale circulation might be crucial, and from this knowledge the relevant processes need to be parameterized. The continued development of global ocean and climate models is especially targeted at deriving new parameterizations for physics that may not be included in the model yet, either because the subject has not been investigated enough to develop a parameterization that can be justified, because the existing parameterizations are too numerically inefficient to be realistically implemented in the model or because the existing parametrizations are simply not good enough. One point that is currently particularly in focus in model development is to implement physical processes that are not yet included in the models in order to remove any artificial energy sources and sinks, and thus make them more energetically consistent. Recent research involves parameterizing e.g. the effect of near-inertial waves (Jochum et al., 2013) on vertical mixing as well as creating energy consistent models for the mixing proces of breaking of internal waves (e.g. Olbers and Eden, 2013).

For non-eddy-resolving ocean models, such as the nominal 1 and 3° resolution versions of POP2 discussed in this thesis, a longlasting challenge has been to parameterize the processes of eddy mixing. Eddies is a broad term which often refer to circular currents that break off the major currents, but in models often refer to any flow that is not captured by the mean flow. The effect of eddies is not straightforward to implement in sub-grid parameterizations, as turbulent mixing has different signatures depending on the local dynamics, and because the mixing happens on different length and time scales.

Essentially, eddy mixing has two different components, one along isopycnals, i.e. surfaces of constant density, and one across isopycnals. The former is referred to as isopycnal mixing, the latter as diapycnal mixing. Isopycnal mixing in ocean models happens in two ways, by simply diffusing higher tracer moments on isopcynal surfaces and through eddy advection of tracers. The latter proces is parameterized as thickness diffusion, as will be described below. Within the interior of the ocean diapycnal mixing is primarily tied to the vertical diffusion which is generally much weaker than isopycnal mixing as it requires more energy. However, in the proximity of (vertical) boundaries an eddy contribution to the diapycnal mixing occurs, referred to as horizontal mixing, which happens along the boundary rather than along isopycnals (see further below). The term diffusion will be used frequently in the rest of this study and will, unless otherwise specified, refer to the diffusive effects of eddies, as eddy mixing of tracers is often parameterized as a diffusive proces.

In the following, both forms of eddy mixing will be described, starting with the isopycnal, interior mixing. As each type of diffusion has its own diffusivity coefficient (although these are often set to be identical), all coefficients will be characterized by a $\kappa$ followed by a subscript depending on the diffusivity in question. This choice has been made to ensure consistency throughout the report.

### 3.1.1 Isopycnal mixing, GM90

In their paper on isopycnal mixing, Gent and McWilliams (1990) proposed a new parameterization for mesoscale eddies in an adiabatic ocean model, here referred to as the GM90-parameterization. They proposed a framework for parameterizing mesoscale eddies, derived from inspecting steady state solutions to fine-resolution ocean models, where mesoscale eddies were included. If working in isopycnal coordinates, the equations of isopycnal layer thickness, $\partial h/\partial \rho$, (from here simply thickness), with $h$ being the physical height of the density surface, and tracer transports were used to derive the parameterization. The thickness equation is derived from mass conservation and incompressible flow, giving that change in thickness is balanced by the local divergence of thickness:

$$\frac{\partial^2 h}{\partial t \partial \rho} + \nabla_\rho \cdot \left( \frac{\partial h}{\partial \rho} \mathbf{u} \right) = 0, \tag{4}$$

with $\nabla_\rho$ being the horizontal graident operator at constant density, $\rho$, and $\mathbf{u}$ being the horizontal velocity vector. The tracer equation states that the local tracer concentration is balanced by advection and diffusion:

$$\frac{D\varphi}{Dt} = \nabla_\rho \cdot \left( \kappa_I \frac{\partial h}{\partial \rho} \mathbf{J} \cdot \nabla_\rho \varphi \right) / \frac{\partial h}{\partial \rho}, \tag{5}$$

with $\kappa_I$ being tracer diffusivity and $\varphi$[1] being the tracer. Here, $D/Dt$ is the total derivative in isopycnal coordinates

$$\frac{D}{Dt} = \frac{\partial}{\partial t} + \mathbf{u} \cdot \nabla_\rho. \tag{6}$$

$\mathbf{J}$ is a non-diagonal matrix, and the elements of it are a function of the isopycnal slopes:

$$\mathbf{J} = \frac{1}{1 + h_x^2 + h_y^2} \begin{bmatrix} 1 + h_y^2 & -h_x h_y \\ -h_x h_y & 1 + h_x^2 \end{bmatrix}, \tag{7}$$

with

$$h_x \equiv \frac{\partial h}{\partial x}, h_y \equiv \frac{\partial h}{\partial y}. \tag{8}$$

When analyzing the steady state of eddy-resolving models Gent and McWilliams (1990) observed that the divergence of the mean flow is balanced by the mean divergence of eddy flow. In order to include this in a non-eddy resolving model, a non-conservative term, $\mathbf{F}$, is included in equation 4:

$$\frac{\partial^2 h}{\partial t \partial \rho} + \nabla_\rho \cdot \left( \frac{\partial h}{\partial \rho} \mathbf{u} \right) + \nabla \cdot \mathbf{F} = 0 \tag{9}$$

Incorporating this term in the thickness equation, however, requires that the coarse resolution model has to be locally diabatic (the alternative would require a compress-

[1] Note that Gent et al. (1995) and several other studies use $\tau$ to denote tracers. As the litterature offers several different choices for symbols for tracers, I have decided upon $\varphi$ in order to avoid any confusion with characteristic time scales.

ible flow and possibly lead to unphysical mass sources or sinks). As the parameterization is intended to represent adiabatic flow, the choice was made that, although diabatic effects were allowed locally, the global domain had to preserve the important adiabatic propoerties that a fine-resolution model produced (from equations 4 and 5). These are (Gent and McWilliams, 1990)

1. The domain averaged density should be constant, and likewise the volume of any specific density.

2. Without sinks or sources at the boundaries, the average tracer value between any two isopycnals should be conserved, and local gradients of any tracer on an isopycnal surface should decrease.

3. The tracer equation should be satisfied by the density as well.

The first property comes from the simple fact that in an adiabatic, eddy-resolving model, the change in local isopycnal thickness must be balanced by the convergence of thickness. The second property comes from a combination of simple conservation of tracers, whereas the local gradients decrease as tracers are diffused within a layer (Fickian diffusion, Redi, 1982). The final property was derived for the adiabatic as the total derivative of the local density must be zero. Gent and McWilliams (1990) referred to the model as quasi-adiabatic, given that it fulfilled the above listed global, adiabatic properties, despite the allowance for locally diabatic behaviour.

The non-conservative term, $\mathbf{F}$, in equation 9 now has to be chosen in order to satisfy the global adiabatic properties. The choice was to represent it as a diffusion of thickness, given in isopycnal coordinates as

$$\mathbf{F} = -\frac{\partial}{\partial \rho} \left( \kappa_{GM} \nabla_\rho h \right), \tag{10}$$

with $\kappa_{GM}$ being the thickness diffusivity. In their paper, Gent and McWilliams (1990) did not define if the thickness diffusivity had to be a constant or a function of space and time, but suggested that the latter might be the case.

Later, Gent et al. (1995) elaborated on the interpretation of the GM90 parameteriation. While it is tempting to interpret the physics of the parameterization as diffusion, the intended interpretation is meant to be as advection, as the large scale advection of tracers is not determined solely by the mean flow, but additionally by the mesoscale eddy flow. This can be illustrated by re-writing the tracer equation in terms of an effective transport velocity, $(\mathbf{U}, W)$ defined as the sum of the large-scale velocity and an included eddy-induced transport velocity:

$$\mathbf{U} = \mathbf{u} + \mathbf{u}^*, \qquad W = w + w^*, \tag{11}$$

where $\mathbf{u}$ and $\mathbf{u}^*$ denote the large-scale and eddy-induced transport velocities, respectively, and the same for the vertical components, $w$ and $w^*$ (Gent et al., 1995, split up the velocities in horizontal and vertical components as the form of these differ, to be seen shortly). The reason to include the eddy-induced transport is that the simple use of just the large-scale tracer transport is simply not physically justified, as eddies contribute significantly to the overall tracer transport observed. The covariance of velocity and tracer, i.e. the average of the product of velocity and tracer deviations, has a potentially non-zero value, and thus eddies can have have impact on the mean advective tracer transport, even though the average of velocity deviations are zero, e.g. (Holton, 2004):

$$\overline{u\varphi} = \overline{u}\,\overline{\varphi} + \overline{u^*\varphi^*}, \tag{12}$$

where overbars denote averages and stars denote deviations. When including the advection of tracers from eddies, the tracer equation for any tracer, $\varphi$, can be written as the sum of advection and isopycnal diffusion of tracers. By this re-interpretation, Gent et al. (1995) re-wrote the tracer transport equation in terms of the effective transport velocity, $\mathbf{U}$:

$$\frac{\partial}{\partial t}\varphi + \mathbf{U} \cdot \nabla_H \varphi + W \varphi_z = \nabla \cdot [\kappa_I \mathbf{K} \nabla \varphi], \tag{13}$$

where subscript $H$ denotes the two-dimensional, horizontal operator, $\kappa_I$ is the isopycnal diffusivity, and $\mathbf{K}$ is the three-dimensional small-slope approximation mixing tensor, which is an approximation of $\mathbf{J}$ in equation 5.

By using the parameterization proposed in equation 10, Gent et al. (1995) showed that the horizontal and vertical velocity components would take the form

$$\mathbf{u}^* = -\left(\kappa_{GM}\mathbf{L}\right)_z, \qquad w^* = \nabla \cdot \left(\kappa_{GM}\mathbf{L}\right), \tag{14}$$

with $\mathbf{L}$ being defined as the isopycnal slope vector

$$\mathbf{L} = \frac{\nabla \rho}{\rho_z}. \tag{15}$$

The implementation of the GM90 parameterization in OGCMs showed substantial improvements compared to the previous use of horizontal and vertical diffusivities only, as the implementation resulted in better global temperature distributions and thermoclines, meridional heat transports and areas of deep convection, to name the most notable (Danabasoglu et al., 1994). The original implemantations of GM90 used constant diffusivities, $\kappa_{GM}$, of order $10^3$ m$^2$ s$^{-1}$, but it is evident from equation 14 that there is a need to define whether the thickness diffusivity $\kappa_{GM}$ is constant in space and time or not and what physical implications this might have, as it will lead to substantially different results given that

$$\kappa_{GM} = \kappa_{GM}\left(\mathbf{x}, t\right). \tag{16}$$

with $\mathbf{x}$ being the position vector and $t$ the time.

### 3.1.2 Determining $\kappa_{GM}$

It is important to realize that the physical meaning of the diffusivity coefficient, $\kappa_{GM}$, has yet to be clarified. While using a constant value throughout the ocean might be the simplest choice, it requires some thoughts as to what physical properties determine this value, and if one value is representative for the entire ocean. Visbeck et al. (1997) used experience from atmospheric modelling and proposed a closure for $\kappa_{GM}$ that depended on the local Richardson number. This proposal was based on several numerical experiments of different ocean dynamics. Different setups included an implementation of the GM scheme with a constant diffusivity and a scheme including a parameterization based on baroclinic instability theory, setting

$$\kappa_{GM} = \alpha \frac{f}{\sqrt{\mathrm{Ri}}} l^2, \tag{17}$$

with $\alpha$ being a tuning parameter, Ri being the Richardson number, Ri$= N^2/(|\partial \mathbf{u}/\partial z|^2)$, with $N$ being the Brunt-Väisälä frequency, and $l$ being an eddy length scale. Visbeck et al. (1997) identified a physical interpretation of $\kappa_{GM}$ through mixing length theory in this parameterization as an eddy velocity, $\frac{f}{\sqrt{\mathrm{Ri}}} l$, times an eddy length scale, $l$. By comparing the performance of different numerical schemes they found that the performance of the GM scheme with both constant and variable diffusivity from equation 17 were good choices. However, the choice for a constant diffusivity depended very much on the dynamics of the experiment. The optimal choice for constant diffusivity ranged from 300 to 2000 $\mathrm{m^2 s^{-1}}$ depending on the characteristics of the problem that was being solved nummerically, whereas the tuning parameter in equation 17, $\alpha$, seemed to be confined within a more narrow parameter space in order to yield the best results, having a value of $0.015 \pm 0.005$. This parameterization choice for $\kappa_{GM}$, however, is constant through the entire water column, and thus does not include a vertical, but a horizontal dependency only. To have no vertical variations in the diffusivity coefficient seems about as physically justified as not having any horizontal variation, and naturally more recent efforts have focused on this topic.

Effects of a vertically varying thickness diffusivity were investigated by Danabasoglu and Marshall (2007). The reasoning behind a vertical dependency on $\kappa_{GM}$ comes from observations that eddy activity is more pronounced in the upper ocean, suggesting a surface enhanced mixing parameterization. Following Ferreira et al. (2005), the idea was to construct a diffusivity proportional to the square of the local buoyancy frequency in every grid point, i.e.

$$\kappa_{GM} = \frac{N^2}{N^2_{\mathrm{ref}}} [\kappa_{GM}]_{\mathrm{ref}}, \tag{18}$$

with $N_{\text{ref}}$ and $[\kappa_{GM}]_{\text{ref}}$ being reference values for the buoyancy frequency and thickness diffusivity, respectively. Ferreira et al. (2005) proposed this parameterization following analysis of a residual-mean circulation model. The implementation most notably showed improvements with respect to heat transport and zonal mean potential temperatures when compared to observations, as well as other modest improvements. The proposed parameterization, however, was based on the dynamic regions such as the ACC and the Gulf Stream, whereas regions such as the Tropics (where the diffusivities obtained from eddy stresses were negative) and the Northern high latitudes were not included, in particular, the model completely lacked the Arctic Ocean. The improvements following the $N^2$ parameterization were also found in the dynamic regions and the abyss, whereas little, if any, improvement was found in the upper ocean Tropics and in the Northern high latitudes (see figure 14 of Ferreira et al., 2005). The study of Danabasoglu and Marshall (2007) used a constant value for $[\kappa_{GM}]_{\text{ref}}$, but this could be spatially varying as well.

Other closures for $\kappa_{GM}$ have been proposed recently. Eden and Greatbatch (2008) developed a parameterization which is also based on the idea that the diffusivity can be viewed as a product of an eddy velocity and length scale. The particular idea in their parameterization is to construct an energetically consistent closure using the fact that the eddy velocity scales with the eddy kinetic energy (EKE). This choice of closure requires calculations of the EKE budget, which is found by considering all energy contributions (production, dissipation and radiation) seperately, adding their parameterizations and integrating to find a prognostic value for the EKE. The length scale is taken to be the minimum of the first baroclinic Rossby radius, $L_r = NH/(\pi f)$, and the Rhines scale, $L_{Rhi} = \sqrt{U/\beta}$, with $H$ being the water depth, $f$ the coriolis parameter and $\beta$ the meridional change in $f$. The scheme was evaluated by comparing results to high-resoution, eddy-resolving models, and was found to perform well. One problem occurs in the mixing length assumption, as results from eddy-resolving models suggest the existence of negative diffusivities (which was also found by Ferreira et al., 2005), which is dificult to obtain using mixing length theory, given velocity and length scales are defined as positive. The idea of a locally negative diffusivity was already suggested in the original paper by Gent and McWilliams (1990). The physical interpretation of negative diffusivities would require that eddy potential energy would be converted to mean potential energy instead of the other way around. The idea that eddies transfer energy from available potential energy (APE) of the mean flow to EKE reflects the proces of baroclinic instabilities. However, other eddy effects such as barotropic instabilities and backscattering would cause the opposite energy transfer, something that is not possible to obtain with positive diffusivities only. Allowing negative diffusion, however, is potentially very difficult numerically as diffusion also adds to dampen numerical waves.

Eden et al. (2009) provide a nice overview of the topic of diffusivity by comparing the four different closures for the choice of thickness diffusivity mentioned above in an OGCM (a constant choice, the Visbeck et al. (1997) parameterization, the Danabasoglu and Marshall (2007) diffusivity as well as the parameterization developed by Eden and Greatbatch (2008)). All simulations were shown to have biases, but changes within the thickness diffusivity showed systematic alterations in climatologic aspects such as increasing the surface diffusivity leads to decreased ACC transport. The study by Eden et al. (2009) shows that there is still a lot of improvements to be made on the question of thickness diffusivity (and maybe mesoscale eddy parameterizations in general, a discussion that will be picked up in section 7). While one choice of thickness diffusivity might result in better representation of the ocean in one aspect, it might show worse in others. Eden et al. (2009) suggest that the choice of diffusivity should be made on its resemblance to the a priori knowledge of the spatial variations found from observations. This suggestion is reasonable, as the optimal choice for diffusivity closure should not only result in climatological improvements, but also be based on physical principles. If observations or physical reasoning contrast a chosen parameterization it is difficult to justify this choice of closure, no matter how well it improves given biases in an ocean model.

In this respect, the idea of considering $\kappa_{GM}$ as a product of an eddy length scale times an eddy velocity scale seems appealing. The physics will never be perfect as parameterizations are, by definition, approximations, but scaling arguments provide a nice framework for determining the strength of eddies, defined by the parameter

$\kappa_{GM}$. The problem is then reduced to defining the right length and velocity scales. If one were to follow this mindset, the best choice of diffusivity parameterization would be that of Eden and Greatbatch (2008), as it is the most physically consistent and is one of the best performing schemes developed so far. At the same time, using energetically consistent schemes is a desired feature as it will eradicate existing problems with artificial energy sources and sinks within present climate model. However, problems with model set-up has made the use of the scheme in this work impossible. In section 5.3 I will return to the question of eddy length scales and velocity scales. In the following section, the eddy mixing properties are described for regions where the flow is not well-represented as adiabatic, which is primarily in the turbulent boundary layers. In the vicinity of boundaries the idea of isopycnal mixing is not complete, and an additional mixing must be introduced.

### 3.1.3 Horizontal mixing close to boundaries

The GM90 parameterization was developed for the interior, where adiabatic mixing is preferred, as mixing across isopycnals require much more energy than mixing along isopycnals. However, the concept of eddy mixing along isopycnals breaks down in the more turbulent boundary layers where eddy mixing should include a diabatic component. Accordingly, the normal component of eddy mixing at the boundary should be zero as a non-zero component would lead to unphysical mixing across the boundary. In order to accommodate the latter, tapering functions have often been implemented in OGCM's that reduce diffusivity coefficients when approaching boundaries. These tapering functions, however, often lead to unphysical eddy transports near the surface. Furthermore, lacking physical justification, one tapering scheme would lead to biased solutions that were difficult to prefer over other tapering schemes, and unlike observations, they would not necessarily include the diabatic component. Ferrari et al. (2008) addressed this problem and proposed a new tapering scheme, a Near-Surface Eddy Flux (NSEF) scheme that consisted of three distinct areas: (1) the interior, where the GM90 parameterization would control eddy mixing, (2) a boundary layer, where the normal component of the eddy flux goes to zero as the boundary is approached and mixing is along the boundary, and (3) a transition layer, representing the region where both types of mixing occur. This parameterization meant a new formulation of the eddy-induced velocities in eq. 11 where the velocities depended not only on the diffusivity constant and isopycnal slopes, but instead including spatial variations depending on which region the water parcel lies within. Danabasoglu et al. (2008) implemented a simplified version of the NSEF scheme in the CCSM3 and found that the implementation generated significant improvements, especially in regards to shallow eddy-induced circulations that were a result of the surface tapering functions and were undocumented in observations. Furthermore, the parameterization reduced a cold bias in the abyssal potential temperature.

The parameterization is developed through the consideration that mixing of tracers and buoyancy in the interior to a great extent is along isopycnals. The mixing is therefore split into two components, one along and one across isopycnals. In this framework, an along isopycnal component of the eddy mixing is described as the curl of a vector streamfunction. The job then is to define the proper streamfunction for the three regions of the ocean (interior, boundary layer and transition layer), as well as the residual diapycnal eddy-induced tracer flux. Ferrari et al. (2008) derives the formalism to define the streamfunction, $\mathbf{\Psi}$ and residual fluxes (for buoyancy), $\mathbf{F_e}\{b\}$ for horizontal boundaries as

$$\mathbf{\Psi} \equiv -\frac{\langle w_e b_e \rangle}{|\nabla_H b_m|^2}\mathbf{z} \times \nabla_H b_m - \frac{\langle \mathbf{u}_{he} b_e \times \nabla_H b_m \rangle}{|\nabla_H b_m|^2} \tag{19}$$

$$\mathbf{F}_e\{b\} \equiv \frac{\langle \mathbf{u}_e b_e \cdot \nabla b_m \rangle}{|\nabla_H b_m|^2}. \tag{20}$$

Here, subscripts $e$ and $m$ refer to eddy-induced and large-scale mean, respectively, brackets refer to mean fluxes and $b$ is the buoyancy. The first term in eq. 19 is in the horiontal direction, whereas the second term is in the vertical direction. The diapycnal flux, $\mathbf{F}_e\{b\}$ is in the horizontal gradient of the buoyancy and is therefore always in the horizontal, ensuring that no residual flux will happen across the horizontal boundary. The advective eddy transport, $\mathbf{u}_{me}$, of buoyancy is defined as the curl of the vector streamfunction:

$$\mathbf{u}_{me} = \nabla \times \mathbf{\Psi}. \tag{21}$$

When approaching the horizontal boundaries, the first term in eq. 19 goes to zero, setting the eddy induced transport to be along the boundary.

The NSEF parameterization incorporates the GM parameterization for the adiabatic interior, and then modifies the streamfunction and residual fluxes for the boundary layer and the transition layer. In order to make the vertical flux zero at boundaries, this flux is assumed to be linear in the boundary layer. This makes it easy to define the vertical flux in the boundary layer as a function of depth, which then puts a restriction on the value of the vertical flux in the top of the transition layer. The adiabatic interior determines the boundary condition at the bottom of the transition layer, and the formulation of the vertical flux puts the restriction on the streamfunction in the transition layer, as it must be continuous across the boundaries between the regions. The final streamfunction thus includes a function of depth, defining a function that changes shape in the different regions. The rest of the problem for the NSEF parameterization scheme is then to define at what depth the regions are defined. This procedure will be described in section 5.

Most earlier studies use the same values for the horizontal diffusivity, $\kappa_H$, the horizontal isopycnal diffusivity, $\kappa_I$, and the thickness diffusivity, $\kappa_{GM}$. The reason for this is the lack of physical reasoning as to why these values should differ, as well as in what range the magnitude of the differences should be. In the present study, the values will not necessarily be the same. This choice will not be based on a physical background, but will be used to identify the consequences of the different values of diffusivities. By altering just one parameter, it will be easier to identify what contribution the specific eddy mixing parameterization has on the climatology of the OGCM. The chosen values will be specified for different model runs in section 5.4.

## 3.2 Viscosity

Eddy mixing of tracers has been described in the previos section, but an important feature of eddies is that they also mix momentum. This momentum flux enters the momentum equation (equation 1) in the friction term. Momentum fluxes are often referred to as viscosity. Representation of viscosity is highly problematic as viscosity is limited not only by physics, but by numerical discretization as well. As such, too small values of viscosity will lead to increased grid-scale noise, whereas too high values cause numerical instability. Thus, modelling viscosity is a question of to what degree numerical noise is accepted in the solution compared to the loss of physics.

In POP2, the calculation of viscosity depends strongly on the regime of the flow. For instance, strong lateral viscosity is needed in the Munk layer to represent western boundary currents. The parameterization is anisotropic and involves two coefficients, one that acts in the direction of the flow, $A_{\text{visc}}$, and one that is perpendicular, $B_{\text{visc}}$. The way in which this complicated set of different constraints is orchestrated in POP2 will be described in the following (following Jochum et al., 2008; Smith et al., 2010).

Different viscosities are calculated depending on the physical or numerical requirements that gives rise for viscuous terms. These are eddies and effects from viscous western boundary layers. Lateral viscosity coefficients from eddy generation are based on observational estimates that suggest anisotropic coefficients around the equator. Thus, the parallel coefficient,$A_{SGS}$, is set to a constant value, $A_{eddy}$, whereas the perpendicular coefficient is designed to be equal to $A_{eddy}$ poleward of a certain latitude, $\phi_I$, through

$$B_{SGS} = B_{eddy}\left[1 + c_2\left(1 - \cos\left(2\phi'\right)\right)\right]. \tag{22}$$

Here $B_{eddy}$ and $c_2$ are constants and

$$\phi' = 90^\circ \min\left(|\phi|, \phi_I\right)/\phi_I,$$

ensuring that $A_{SGS} = B_{SGS}$ poleward of $\phi_I$, through the requirement that $A_{eddy} =$

$B_{eddy}\,(1+2c_2)$.
The viscous western boundary layer is designed to have a minimum width. This means that within $N$ grid points of the western boundary, a viscous coefficient is set to a specific value. More than three grid points from the western boundary, this coefficient decreases exponentially as

$$B_{Munk} = c_3 \beta dx^3 e^{-p(x)^2}, \tag{23}$$

where

$$p\,(x) = c_4 \max\,(0, x - x_N)$$

where $x_N$ is the zonal coordinate of the $N^{th}$ grid point east of the boundary, with $N$ as default being equal to 3. $c4$ is the inverse characteristic length scale of the boundary layer which by default is set to 1000 km, making $c4 = 10^{-6}\mathrm{m}^{-1}$.

Once the viscous terms have been calculated, the maximum of the two coefficients are taken, as it is the value required to include the necessary physics (or reduce noise satisfactorily). This gives a set of parameters, $A_1$,$B_1$, where

$$A_1 = \max\,(A_{SGS}, B_{Munk})\,, \tag{24}$$

$$B_1 = \max\,(B_{SGS}, B_{Munk})\,.$$

However, for numerical stability of the solution, the maximum of these coefficients is not allowed to be larger than a value required by the viscous CFL-criterion. This states that the value of any of the viscosity coefficients must not exceed a critical value, $\frac{1}{2}A_{\mathrm{CFL}}$, with $A_{\mathrm{CFL}}$ given by

$$A_{\mathrm{CFL}} = \frac{dx^2 + dy^2}{4dt}. \tag{25}$$

Thus, to secure numerical stability, too strong lateral viscosity is limited by setting

$$A_{\mathrm{visc}} = \min\left(A_1, \frac{1}{2}A_{\mathrm{CFL}}\right) \tag{26}$$

$$B_{\text{visc}} = \min\left(B_1, \frac{1}{2}A_{\text{CFL}}\right).$$

# 4 The Arctic temperature bias in CCSM4

Representing the observed watermass properties in the Arctic has proved to be problematic in most ocean models. Ilicak et al. (2016) compare the ability of 15 state-of-the-art climate models to simulate the Arctic Ocean watermass properties, and show that all models have issues in this particular basin, either the Atlantic water is too warm, cold, shallow, deep or somehow a combination of these. Both temperature and salinity fields are poorly simulated for most models, and this includes CCSM4, which appears to be much too warm in most parts of the water column. Jahn et al. (2012) assess the CCSM4 bias and speculate it to be caused by a tendency for too little cold water formation on the Arctic shelves. Ilicak et al. (2016) concludes the same, but also point towards a too warm Arctic intermediate water inflow through the Fram Strait.

Identifying the origin of a bias can be extremely tricky, as one might follow an infinite chain of precursors to the observed bias. Nevertheless, there is no obvious way to come around this issue, and as such the same procedure is followed here. The first logical step is to verify the existence of the bias. Jahn et al. (2012) analyze a coupled setup of the CCSM4 and Ilicak et al. (2016) use an ocean-ice sepup, both use the nominal 1° version. As running the 1° resolution model version is numerically expensive, we first wish to analyze if the bias occurs in the coarser, numerically cheaper setup of CCSM4. As with Ilicak et al. (2016) we use ocean-ice models with atmospheric forcing. When using ocean-ice setups without an active atmosphere, one must employ some sort of surface salinity restoring (e.g. Griffies et al., 2009). Using too strong surface salinity restoring caused the Atlantic layer to be too heavily mixed vertically before reaching the Arctic in the coarse resolution simulation, resulting in an extreme cold bias instead, and thus it was decided to use weak surface restoring. The Arctic was now analyzed over 300 years of a control simulation, to be referred to as DEFAULT. The potential temperature (hereafter also simply temperature) evolution averaged between 80 and 90°N is plotted in the left panel of figure 2, and the temperature anomaly, here defined as the potential temperature with the first year subtracted, is plotted in the right panel. One clearly sees a warm Atlantic layer

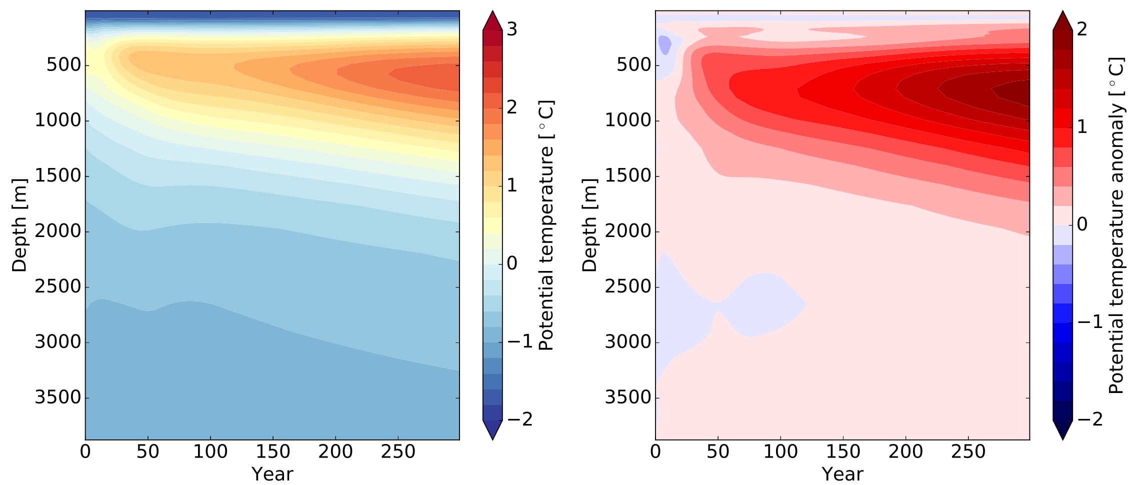


**Figure 2:** Left: Evolution of potential temperature (°C) in the Arctic Ocean, averaged between 80-90N. Right: Same as right, but with the the first model year subtracted.

building up early in the simulation. Not only is the temperature too warm in the core of the Atlantic layer, the temperature bias also propagates deep in the interior to about 2 km depth.

This verifies the existence of the temperature bias, but it does not illuminate the origin of it. To get a better understanding it is ideal to look at the spatial distribution of the anomaly. In figure 3 the Arctic Ocean potential temperature is plotted at a model depth of 580 m over the first 200 years to get an idea of how the evolution plays out. As can be seen, the temperature increases along the Kara Shelf and Laptev Shelf in Eurasian Basin and then propagates into the Canadian Basin. After 25 years the temperature is already warmer by a degree North of the island of the Kara Shelf. After a hundred years the temperature in the Canadian Basin has risen by more than a degree. The temperature increase appears to have an origin in the inflow from the Fram Strait, and possibly the Barents Sea. This is seen as the temperature just south of the Fram Strait is very warm after already 25 years.

This initial analysis point towards the fact that the bias builds up in the Nordic Seas rather than in the Arctic. The bias is simply advected or diffused into the

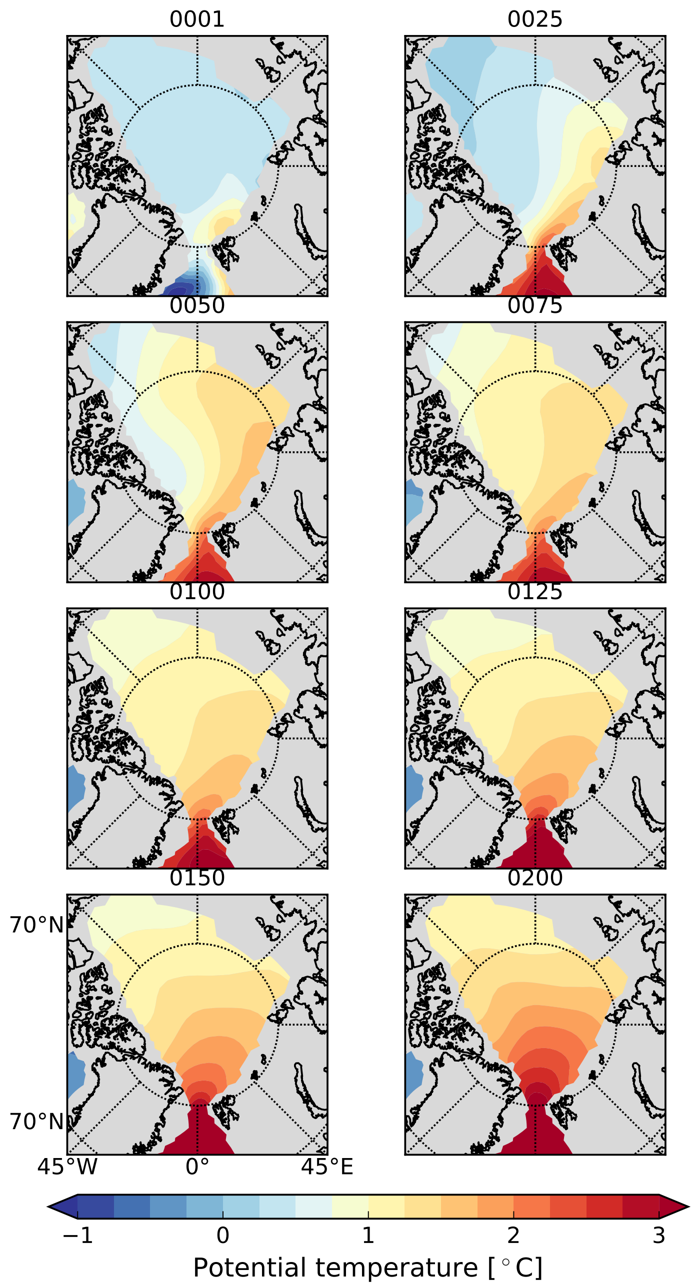


**Figure 3:** Evolution of Arctic potential temperature (°C) at a model depth of 580 m over the first 200 model years.

Arctic through the openings to the Atlantic. As such, the same analysis is made in the Nordic Seas, only at a shallower model depth, 197 m, as we expect the Atlantic layer to be much shallower in the Nordic Seas than the Arctic, as it is observed to be in contact with the surface until it reaches Spitzbergen. The situation is plotted in figure 4.

Within the first 75 years the model experiences a spin-up with a large temperature bias being generated during the first 20 years which then slowly decreases until model year 75 until it starts to increase again, an increase which appears to be growing at least for more than 100 years. The process has strong resemblence of too strong eddy diffusion. To confirm this, the horizontal diffusivity is plotted at the same model depth in figure 5. It is evident that there is a large region off the coast of Norway where diffusivities reach values of 1500 $m^2s^{-1}$. This supports the hypothesis that the temperature spreading in the Nordic Seas is possibly connected to too strong diffusion.

It is difficult to validate if this diffusivity is representative of the real ocean, as eddy diffusivity is not physically measurable. Koszalka et al. (2011) used drifters to estimate the eddy kinetic energy (EKE) in the Nordic Seas. Off the coast of Norway EKE is generally large, connected to the large eddy activity in e.g. the Lofoten Basin (Raj et al., 2015). As will be discussed below, EKE can be viewed as one of the key parameters to determine the eddy diffusivities, although, it is not directly comparable to eddy diffusivity, and although we might expect the diffusivity to be large off the coast of Norway, the model might still have too large diffusion. Andersson et al. (2011) estimated surface eddy diffusivity from surface drifters, with diffusivities ranging between 1000 and 5000 $m^2s{-}1$, with values around 2000 $m^2s{-}1$ along the Norwegian Current but larger near the Lofoten Basin. This does suggest that the POP2 surface diffusivity of 4000 $m^2s{-}1$ is indeed too large.

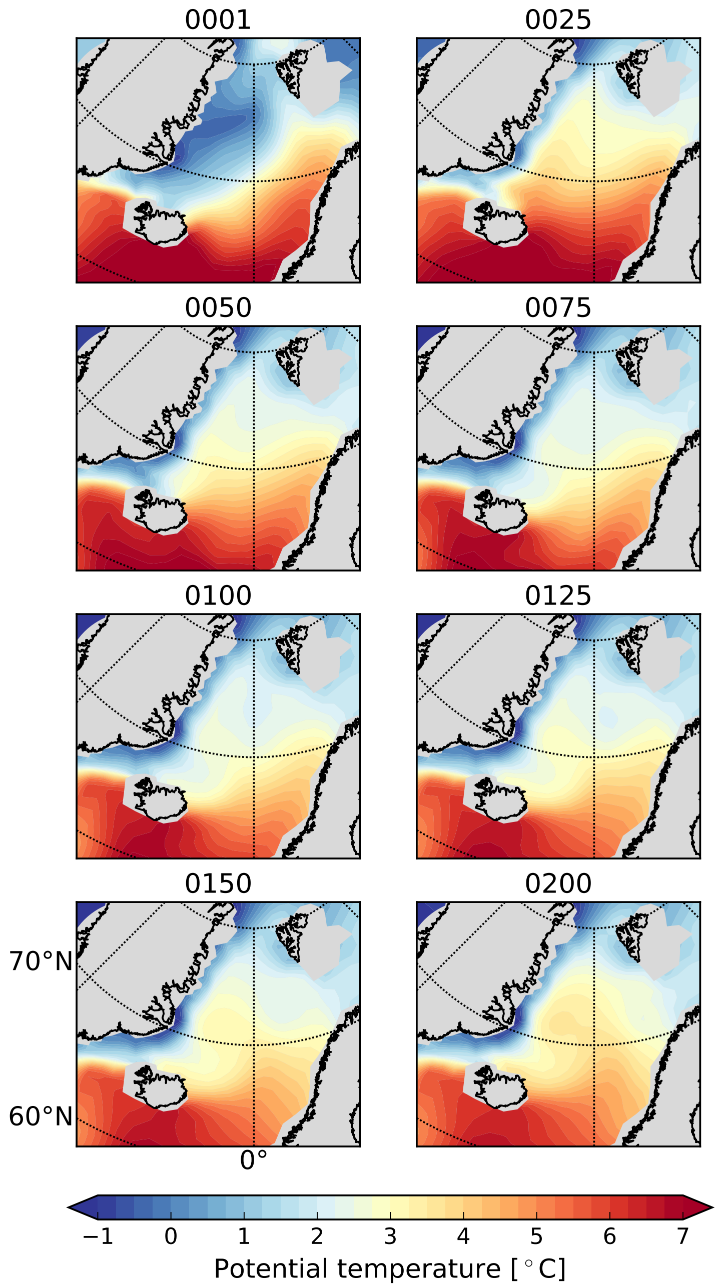


**Figure 4:** Evolution of potential temperature (°C) at a model depth of 197 m.

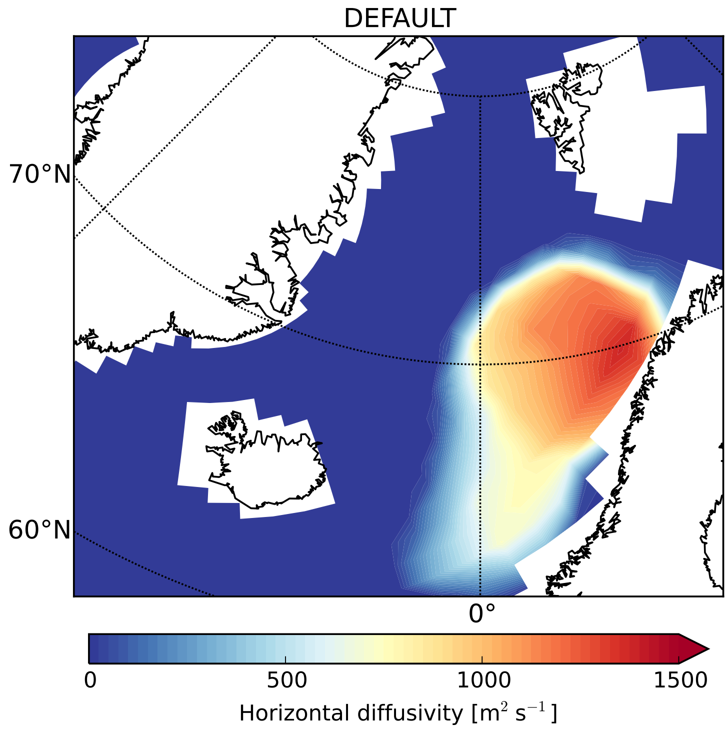


**Figure 5:** Horizontal diffusivity (m$^2$ s$^{-1}$) at a model depth of 197 m.

# 5 Model setup

The model used in the present study is the coarse resolution Parallel Ocean Program version 2 (POP2) which is the ocean component of the Community Climate System Model version 4 (CCSM4). A brief description with focus on the mixing parameterizations will be given here, but for a full in-depth description of the model, see Smith et al. (2010). For most experiments, the model is coupled to an active sea ice model, CICE. Despite apparent problems in the sea ice component of the simulations, it is out of the scope of this project to go into the details of the sea ice component. The same applies to the atmosphere component, CAM, also used in one coupled setup.

## 5.1 POP2

The CCSM4 use the POP2 which is an upgrade including several changes and improvements from POP, which was the older version used in e.g. CCSM3. The differences are all highlighted in Danabasoglu et al. (2012), but of important changes are reduced viscosities (following Jochum et al., 2008), an overflow parameterization for density driven flows in the Nordic Seas (Danabasoglu et al., 2010) and the increase in vertical levels from 40 to 60. The changes in the model for several cases are due to missing physics in the old version included through new parameterizations.

The results of the release of CCSM4 show improvements in both atmosphere (Gent et al., 2011) and ocean (Danabasoglu et al., 2012) components, but the model still have substantial biases and implications that call for further improvements. Some biases in the model have origin in the specific model physics, others from problems with unresolved physics in the coarse resolution model, to be described shortly. Thus, model biases will only be discussed when relevant to the results of this study.

POP2 is a so-called Bryan-Cox-Semtner class model, and is level-coordinate ocean model, using $z$ as vertical coordinate. It solves the primitive equations using hydrostatic and Boussinesq approximations. The former states that the vertical pressure gradient depends linearly on the density, that is $\partial p/\partial z = -\rho g$, and the latter states that density changes are small and therefore can be neglected, except in terms multiplied by $g$. Thus, the governing equations are conservation of momentum and conservation of mass, and the equation of state being a function of potential temperature, salinity and depth (instead of pressure). The equations are transformed from spherical coordinates to a general, orthorgonal coordinate system with dimensions $(q_x, q_y, z)$, which are two horizontal and a depth axis, respectively (see Smith et al., 2010).

The model uses a staggered Arakawa B-grid (Arakawa and Lamb, 1977) with all scalars (temperature, salt, pressure, ideal age) placed at the center of gridpoints and vectors (velocities) at the corners. The scalars are located in so-called T-cells, spanned by velocity points in each corner, with the variables defined in the center

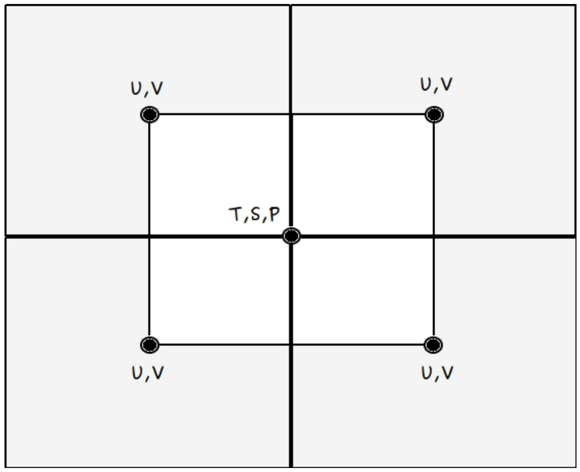


**Figure 6:** Illustration of the POP2 B-grid with T-cells containing scalars marked as white and U-cells containing vectors marked as grey.

of the cells (illustrated for simplicity in figure 6). The velocities are evaluated in the U-cells, but unlike for T-cells, values are not necessarily located in the center of the U-cells, as the grid spacings differ. The grid choice for global ocean models using the momentum equations as governing equations is often between B- and C-grids. C-grids have been shown to perform better with respect to dispersion of waves, however under the requirement that the grid spacings do not exceed that of the Rossby radius of deformation. The B-grid has moderate errors in the dispersion of all wave modes, whereas the C-grid has problems with high modes given too large grid spacings (Randall, 1994). As such, for coarse resolution a B-grid might be preferable to a C-grid. The first Bryan-Cox-Semtner model was the one by Bryan (1969) which for obvious numerical limitations at that time used a B-grid. Today, with the advance of high performance computing, increased horizontal resolution of ocean models typically make the C-grid preferable, but being based on an old model, POP2 still employs the B-grid.

In the southern hemisphere grid points align closely to the latitude and longitudes, but approaching the North Pole this breaks down as the model pole is shifted on to lie in Greenland in order to avoid singularities. The grid is thus cyclic in the x-direction and closed by continents along the northern edge of the model. The standard advection scheme is second-order centered finite difference scheme, while the time discretiazation follows a second-order-accurate modified leapfrog scheme. To dampen computational noise due to the leapfrog scheme, the "averaging timestep" procedure is used. The coarse resolution version of POP2 (see Shields et al., 2012), referred to as a 3° nominal resolution, has 100 grids in the x-direction and 116 in the y-direction. The model has been shown to perform worse than the nominal 1° resolution, however, it has a stable climate and can be used with respect to especially model experiments of implementation of new modules and model refinement, as its computational cost is considerably smaller than for the 1° resolution.

From the changed resolution towards the poles the grid sizes ranges from anything between $\mathcal{O}(15 \text{ km})$ to $\mathcal{O}(400 \text{ km})$. Thus it is apparent that the Rossby radius of deformation is not resolved many places in the ocean model. As such, there is a need for parameterizing effects of eddies.

## 5.2 Eddy parameterizations

The tracer transport equation in POP2 is

$$\frac{\partial}{\partial t}\varphi + \mathbf{U} \cdot \nabla\varphi = \mathcal{D}_H(\varphi) + \mathcal{D}_V(\varphi), \tag{27}$$

with $\varphi$ being the tracer, $\mathbf{U}$ the mean velocity, $\mathcal{D}_H$ and $\mathcal{D}_V$ being horizontal and vertical diffusion operators, respectively. The right hand side in equation 27 is representing all unresolved tracer transports, that is the transports not explicitly advected by the mean flow. Thus, it spans a very large suite of processes ranging from molecular scale to the mesoscale. In particular, eddy diffusion related to unresolved mesoscale eddies is included in these terms.

Eddy mixing is introduced in the tracer transport equation by combining isopycnal and thickness diffusivity as the sum of two matrices, the former derived in Redi (1982) and one representing the skew-flux form of thickness diffusivity described in Griffies (1998). The first one is implemented using small slope approximation, that is $\nabla_H \rho << \rho_z$. The use of the skew-flux form (as opposed to the advective form) of the thickness diffusivity has several advantages, including increased computational efficiency, decreased numerical dispersion and simplicity in the case where isopycnal and thickness diffusivities are set equal (for more insight, see Griffies, 1998). The combined isopycnal and thickness diffusivities transform the transport equation for a tracer, $\varphi$, to

$$\frac{\partial}{\partial t}\varphi + \mathbf{U} \cdot \nabla\varphi = \overline{R}(\varphi) + D_V(\varphi), \tag{28}$$

with

$$\overline{R}(\varphi) = \nabla \cdot \begin{pmatrix} \kappa_I & 0 & L_x(\kappa_{GM} - \kappa_I) \\ 0 & \kappa_I & L_x(\kappa_{GM} - \kappa_I) \\ -L_x(\kappa_I + \kappa_{GM}) & L_y(\kappa_I + \kappa_{GM}) & L^2 \end{pmatrix} \cdot \nabla_3\varphi, \tag{29}$$

where $\mathbf{L}$ is defined in eq. 15 and subscripts $x$ and $y$ refer to the zonal and meridional component of $\mathbf{L}$, respectively, and $\kappa_I$ and $\kappa_{GM}$ refer to isopycnal (Redi) and thickness (GM90) diffusivities, respectively.

In cases where the isopycnal slopes are too steep, a tapering function is applied to secure numerical stability of the solution. Such method is neccessary, yet the nature of it is beyond the scope of this project to go into further detail about.

The default setting of the isopycnal diffusivities in POP2 is a prescribed surface value which is constant in space and time, where diffusivities have variations with depth as a result of the local stratification changes (Danabasoglu and Marshall, 2007). The vertical profiles of diffusivity coefficients depends on the buoyancy frequency $N^2$, where the fraction $\frac{N^2}{N_{ref}^2}$ is applied to a reference value of the respective diffusivities for all depths below the surface diabatic layer. The definition of the layer depth depends on what parameterizations are used, but as the NSEF parameterization is used in this study, the surface diabatic layer is the same as the diabatic layer depth defined by this parameterization. The fraction of buoyancy frequencies is ensured to be positive by setting a minimum value of

$$N_{min} \leq \frac{N^2}{N_{ref}^2} \leq 1.0. \tag{30}$$

This ensures positive diffusivities in statically unstable regions. Reference values for all diffusivity coefficients are by default set to 3000 m$^2$ s$^{-1}$ and 4000 m$^2$ s$^{-1}$ for the nominal 1° and 3° resolution configurations, respectively.

Computationally, the model works by calculating a lateral and a vertical diffusivity. The final thickness diffusivity is then calculated by multiplying the two respective components. This is computationally efficient, as one can choose to combine the different schemes that are either changing horizontally or vertically.

For the horizontal diffusivity at the boundaries the model needs to define the depth of the boundary and transition layers. The boundary layer depth (BLD) is calculated in the KPP vertical mixing scheme as the first depth level where the bulk Richardson number exceeds a critical value (Large et al., 1994). The transition layer thickness (TLT) depends on two things: The possibly rather fast changing value of the BLD and the amount of heaving of isopycnals caused by eddies (Ferrari et al., 2008). Vertical displacement of a fluid particle close to the transition between interior and boundary layer will episodically experience diabatic mixing. The root-mean-square of the vertical displacement is then taken as contribution to the TLT of eddy heaving. In the model, this is approximated by the isopycnal slope, $|\mathbf{L}|$, times the barotropic Rossby deformation radius, $R$[2]. TLT is then calculated by finding the shallowest depth that is deeper than the sum of the BLD and the product of $|\mathbf{L}|$ and $R$. The difference between this depth and the BLD is then taken as the TLT. Danabasoglu et al. (2008) show, by envoking a model run with a 0-m TLT, that the model results are rather unsensitive towards the choice of TLT. They also analyze a model run where the TLT is simply set to be the difference between the mixed and boundary layer, which shows similar results as the run using the standard formalism for TLT.

In this study, the idea of interpreting the eddy diffusivities as a function of length scales and time scales are kept, but the calculations of the parameters are different. The idea of the eddy diffusivity as being a product of an eddy velocity and an eddy length scale is kept, the velocity scale, however, is kept fixed globally whereas the length scale is prescribed depending on the latitude. This is a very naive assumption,

[2] here set to $R = U/f$, with $U$ being a characteristic velocity scale set to 2 cm s$^{-1}$

but will be useful in considering the effect of polewards reduced eddy length scales. One can thus consider this study a test of the interpretation of $\kappa_{GM}$ as a product of length and velocity scales.

## 5.3 A latitudinally dependent diffusivity

The core of this study is to analyze the effect of a decreased diffusivity in the high latitude regions, especially focusing on the Arctic temperature bias. Estimates of eddy diffusivities have been performed using observations and eddy-resolving models. Liu et al. (2012) estimated eddy mixing coefficients using adjoint-based inverse methods and found diffusivities with high spatial variability. Their results showed thickness diffusivities to obtain the largest values in strong current systems such as the western boundary currents and the ACC. This was in agreement with the similar findings of Ferreira et al. (2005). Abernathy and Marshall (2013) used satellite altimetry to calculate ocean velocities and used this to infer geostrophic eddy diffusivities using the Osborn-Cox relation on the observed tracer variance in the ocean. This is a measure of local, irreversible mixing of tracers and is in general not directly translatable into thickness diffusivity coefficients, as they are defined to represent different mechanisms in mixing, but both studies point out that the eddy mixing is generally not well represented by a constant diffusivity value everywhere. The results of Abernathy and Marshall (2013) showed great diffusiviteis in the equatorial basins, with decreasing diffusivities when approaching the high latitudes. Their results showed that using a classic diffusivity of $\mathcal{O}(10^4 \mathrm{m}^2\mathrm{s}^{-1})$ would underestimate eddies significantly in the tropics and overestimate them in high latitudes such as the sub-polar gyres.

The studies of Ferreira et al. (2005) and Liu et al. (2012) suggest that eddy mixing strength is indeed a growing function of the available EKE, which is larger in regions of strong flow such as the Gulf Stream and the ACC. The findings of Abernathy and Marshall (2013), on the other hand, supports the idea of eddy diffusivities to be proportional to their respective mixing lengths, as we shall see now.

When more than one eddy length scale can be considered, the smallest should be used as the appropriate eddy length scale. Eden and Greatbatch (2008) considered the minimum of the Rossby radius of deformation and the Rhines scale, where the former is argued to be the smallest for latitudes north of 30°N. The Rossby radius of deformation is proportional to the scale depth and inversely proportional to the local coriolis parameter. Thus, it would be expected to decrease for the high latitudes as the coriolis frequency grows when approaching the poles and as the basin depth is in general smaller than at least the open equatorial ocean. In other words, to lowest order the Rossby radius deformation rate is a decreasing function of latitude. This is valid for both hemispheres, and agrees with the results of Abernathy and Marshall (2013). The low value of the deformation radius is confirmed by Nurser and Bacon (2014) who calculated the deformation radius for latitudes north of 60°N. Their results showed that the maximum annual value of the radius was found in the Canadian Basin with a value of $\mathcal{O}(15\text{ km})$ and that for large parts of the Arctic Ocean and Nordic Seas values rarely exceeded 10 km. Thus, if the Rossby radius of deformation is considered an appropriate length scale for eddies, the eddy diffusivities should decrease with latitude.

As mentioned earlier, the surface diffusivity in the closure for the thickness diffusivity of Danabasoglu and Marshall (2007) has the same value globally. Following the previous discussion, this choice seems poorly justified as there is no indication that the decrease in Rossby radius of deformation is compensated by an increase in the eddy kinetic energy. Thus, ignoring the spatial distribution of EKE, which is difficult to assess in a coarse resolution OGCM, an improved surface diffusivity should be obtainable by considering the Rossby radius of deformation. With this in mind, a very simple model can be set up for the surface diffusivity. All that is required is that the constant surface value is taken to be decreasing when approaching either of the poles, representing the change in $f$ as function of latitude. A very simple function that will accommodate this feature is a cosine function. With this simple framework a surface diffusivity is calculated by the simple model

$$[\kappa_{GM}]_{\text{ref}} = A_{ref} \cos\left(\theta\right), \tag{31}$$

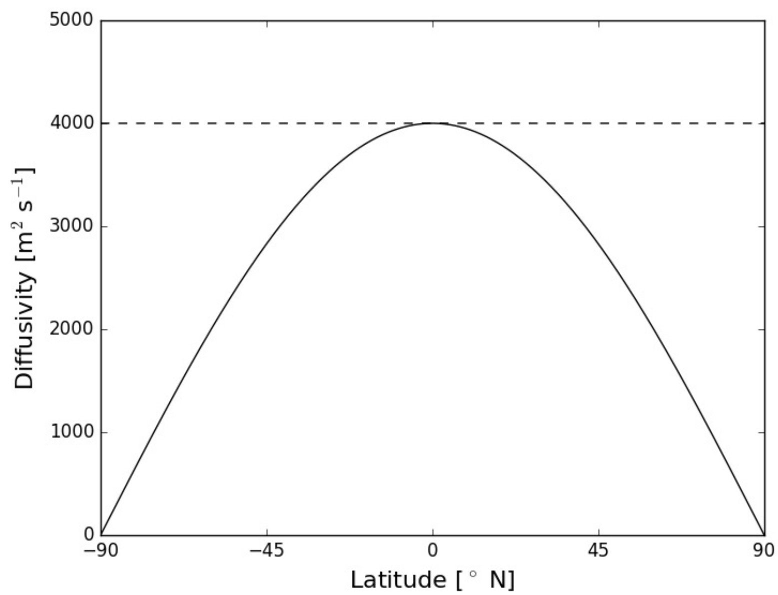


**Figure 7:** Surface diffusivities (m$^2$ s$^{-1}$) as function of latitude for DEFAULT (dashed line) and diffusivity reduced runs (solid line).

with $\theta$ being the latitude and $A_{ref}$ being a constant value, corresponding to a representative diffusivity in the equatorial region. This value is taken to be the same as the default surface value, 4000 m$^2$s$^{-1}$ in the coarse resolution POP2. This model is used in the surface reduced diffusivity runs described in section 5.4. The surface diffusivity from the model is represented in figure 7 along with the default surface diffusivity value. One might argue that the prescribed surface value could also be represented by the paramterization of Visbeck et al. (1997). However, their parameterization is influenced by the energetics of the current systems and as such might not necessarily decrease the mixing strength in the high latitudes. Remember that the working hypothesis is that too strong eddy mixing in the Nordic Seas is causing the Arctic temperature bias. With the simple model in equation 31 this hypothesis can be either rejected or supported, as eddy strength is reduced polewards by brute force by keeping the estimate of EKE, and hence the eddy velocity scale, fixed globally (as opposed to Visbeck et al., 1997).

## 5.4 Model runs

The further analysis is carried out using several different configurations of POP2. All these simulations will be described in this section. With the exception of one run that is fully coupled, all models use the forcing described in Large and Yeager (2004) with a surface fresh water correction of 0015. The model analysis is carried out for an average of model years 290-299, where the effects of the changed configurations should be distinguishable from the model spin-up. All model setups use the coarse, 3° nominal resolution of POP2 on a dipole grid with a displaced North Pole, except for one model run that is set up with a nominal 1° grid to inspect differences caused by changes in resolution. The settings are as follows: The first configuration, DEFAULT, uses the default settings of POP2, that is in particular the regular parameterization for $\kappa_{GM}$ along with standard values for all model constants. COSHOR is with the same settings as DEFAULT, but uses the prescribed surface diffusivity seen in figure 7 for the horizontal diffusivity, $\kappa_H$, whereas COSKAP uses the default horizontal diffusivity but the latitudinally dependent surface thickness diffusivity, $\kappa_{GM}$. COSKAPHOR combines COSHOR and COSKAP settings so that both thickness and horizontal diffusivities have the prescribed surface value seen in figure 7, but is otherwise similar to the settings of DEFAULT.

Besides the reduced diffusivity runs described above, some additional setups were initiated because analysis showed possible importance of other processes that needed to be investigated. Thus, VISC is like DEFAULT, but with a reduced viscosity parameter $c_2$ in equation 22[3]. B1850 is a fully coupled pre-industrial setup, provided to see to what extent the forced runs are comparable to the coupling with an active atmosphere. Because surface forcing and sea ice turned out to have importance, a run, CNYR, with prescribed sea ice was carried out for 100 years, otherwise exactly with settings like DEFAULT.

Finally, two more simulations were carried out with decreased eddy diffusivity. CONST uses the same setting as DEFAULT, but with constant thickness, horizontal and isopycnal diffusivities, fixed with a value of 800 $m^2s^{-1}$ globally. ZERO is run

[3] the parameter $c4$ was also increased to $10^{-8}$ m to compensate for the decreased $c2$, but this parameter is of questionable importance (Dion Häfner, personal communication)

**Table 2:** Summary of model setups. $\kappa$'s refer to surface diffusivity values, except for CONST where values are constant globally.
Case explanation: OCN/ICE: ocean-sea ice simulations. OCN: ocean only. FULL: fully coupled.

| | Case | Resolution | $\kappa_I$ ($m^2$ $s^{-1}$) | $\kappa_{GM}$ ($m^2$ $s^{-1}$) | $\kappa_H$ ($m^2$ $s^{-1}$) | $c2$ |
|---|---|---|---|---|---|---|
| DEFAULT | OCN/ICE | 3° | 4000 | 4000 | 4000 | 24.5 |
| COSHOR | OCN/ICE | 3° | 4000 | 4000 | 4000cos($\theta$) | 24.5 |
| COSKAP | OCN/ICE | 3° | 4000 | 4000cos($\theta$) | 4000 | 24.5 |
| COSKAPHOR | OCN/ICE | 3° | 4000 | 4000cos($\theta$) | 4000cos($\theta$) | 24.5 |
| VISC | OCN/ICE | 3° | 4000 | 4000 | 4000 | 0.5 |
| X1 | OCN/ICE | 1° | 3000 | 3000 | 3000 | 24.5 |
| B1850 | FULL | 3° | 4000 | 4000 | 4000 | 24.5 |
| CNYR | OCN | 3° | 4000 | 4000 | 4000 | 24.5 |
| ZERO | OCN/ICE | 3° | 4000 | 4000 | 0 | 24.5 |
| CONST | OCN/ICE | 3° | 800 | 800 | 800 | 24.5 |

with horizontal diffusivities set to zero everywhere. However, as these two runs were mainly used for initial analysis and they turned out to contribute little to the rest of the analysis, they will not be discussed much in the rest of this report. This is because CONST resembled the results of COSKAPHOR very much, whereas ZERO is very similar to COSHOR. All model runs are summarized in table 2.

Before we proceed the results in the next section it is important to keep in mind the model bathymetry compared to the observed bathymetry, as the coarsely resolved topography imposes limitations on numerical solutions to the primitive equations, and it may be important to relate the observed 2-dimensional fields to the model version of the bathymetry. The model bathymetry for the coarse resolution model setup is plotted in figure 8, and the model bathymetry of X1 is plotted in figure 9. When comparing this to the bathymetry map plotted in figure 1 in section 2 one finds that the model bathymetry is very simplistic, especially when it comes to features such as the Lomonosov Ridge and the Gakkel Ridge, and in general the steep slopes are poorly represented. The increased horizontal resolution clearly sharpens certain features of the ocean floor, although representation is still poor concerning especially the Nordic Seas and features such as the Gakkel Ridge. The black lines in figure 8 represent transects to be used in sections 6 and 7.

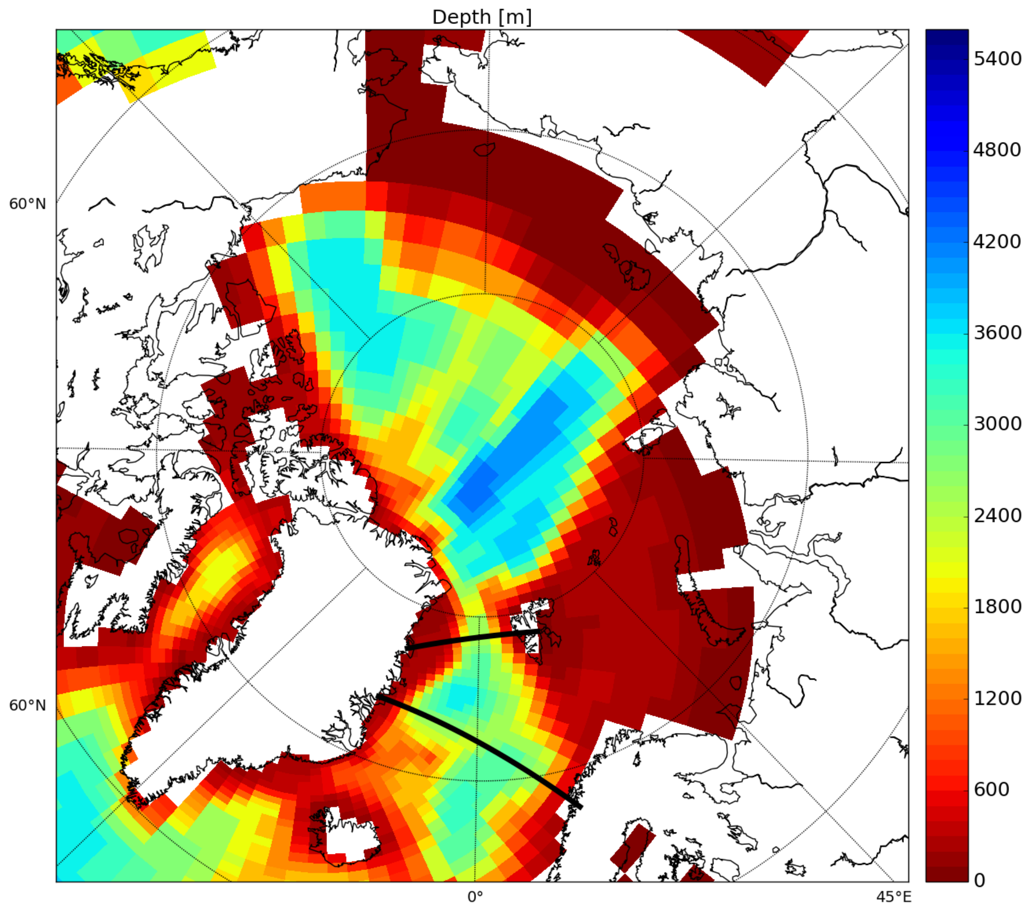


**Figure 8:** Coarse resolution model bathymetry (m). The black lines mark the Fram Strait (see section 6.3.2) as well as a transect through the Nordic Seas to be discussed in section 7. Coastlines are overlaid through third party software.

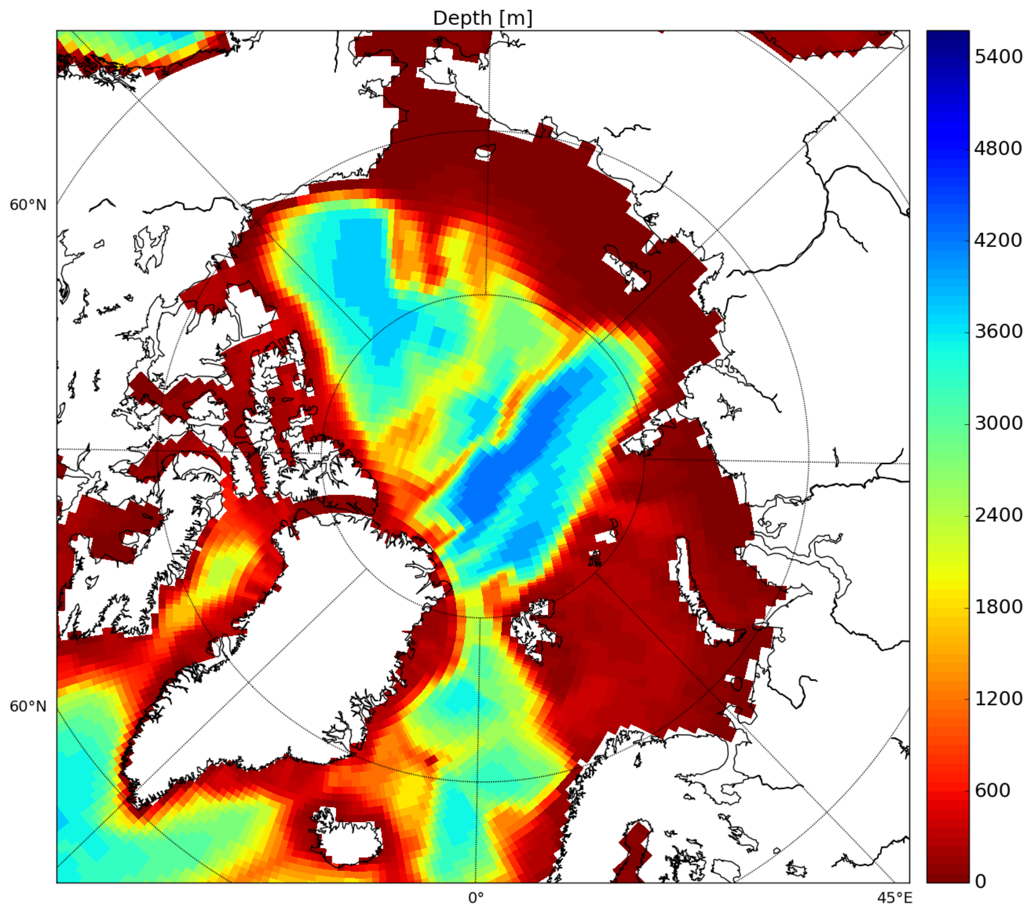


**Figure 9:** Standard resolution model bathymetry (m). Coastlines are overlaid through third party software.

# 6 Results

This section presents the main results of the study by presenting climatologies of the different model runs, primarily regarding the temperature of the Arctic Ocean and the Nordic Seas. Focus is put on the model runs regarding the control and reduced diffusivity experiments, i.e. DEFAULT, COSHOR, COSKAP and COSKAPHOR, as well as the reduced viscosity run, VISC, and in some respect the coupled simulation, B1850, and the nominal 1° simulation, X1. As mentioned before, two extra simulations, ZERO and CONST, were carried out, but these will only be mentioned briefly. This follows from the fact that these simulations show very similar behavior to the model runs COSHOR and COSKAPHOR, respectively. CNYR will only be discussed regarding surface forcing and used as reference to sea ice conditions.

Comparison will be made with the compiled observation map World Ocean Atlas 2009 (Locarnini et al., 2010, hereafter WOA). The temperatures in this dataset are in situ values, whereas the output of POP2 is potential temperature. Thus conversion is necessary for comparison. WOA data has been converted to potential temperature using the lapse-rate coefficients of Bryden (1973) and the algorithm of Fofonoff (1977). See appendix C for further details.

The section is presented as follows. Initially the surface and subsurface diffusivities of the simulations are presented in order to verify that the setup is correct. Hereafter follows a presentation of model spinup and global properties such as AMOC and ACC. Next is a presentation of the simulated Nordic Seas in the different model runs, followed by moving downstream along the Norwegian Current into the Arctic Ocean, presenting the simulated ocean properties here. The observed bias in the model has a temperature signal, and as such, focus will generally be on the structure of the temperature fields rather than other properties. However, the temperature structure is modified in the ocean in a complex suite of processes, some of which are most easily represented by other model output variables. When used, these will be explained in more detail.

## 6.1 Diffusivities

The starting point is to evaluate that the imposed diffusivities have the desired structure. The surface diffusivities[4] are plotted in figure 10. The left panel shows the thickness diffusivities for the cases DEFAULT, CONST and COSKAP, whereas the right panel shows the horizontal diffusivities in the runs DEFAULT, CONST and COSHOR. What is important to note is that the diffusivities in COSHOR and COSKAP have the desired poleward reduction, meaning the surface imposed diffusiv-

[4]Which for thickness diffusivity is defined as the first subsurface layer as $\kappa_{GM}$ is set to zero at the surface to avoid spurious across boundary mixing.

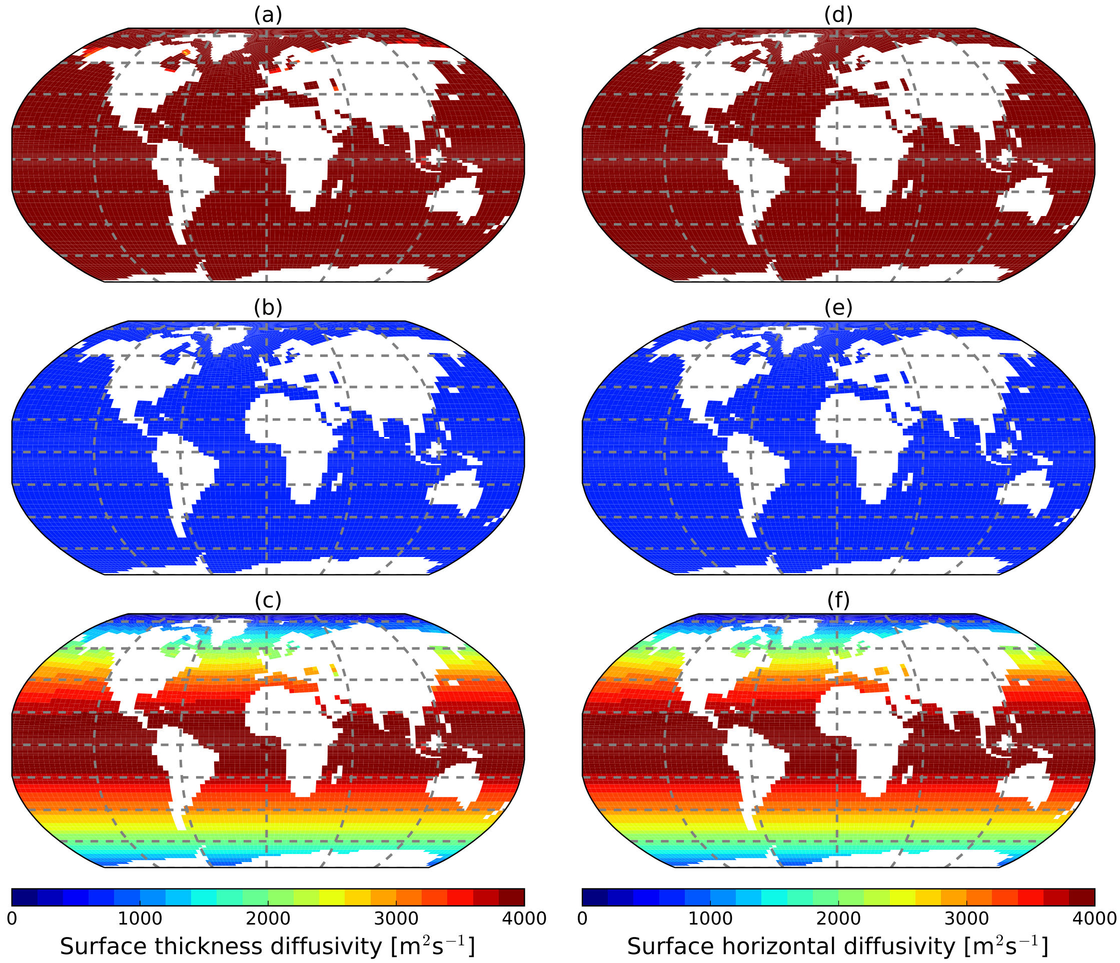


**Figure 10:** Left: Imposed surface thickness diffusivity structure for DEFAULT (upper), CONST (middle) and COSKAP (lower). Right: Imposed surface horizontal diffusivity for DEFAULT (upper), CONST (middle) and COSHOR (lower). Note that COSKAPHOR is a combination of COSKAP and COSHOR.

ity has the desired structure. The combined simulation, COSKAPHOR, incorporates a combination of the two diffusivities shown in the lowest row of figure 10. To illustrate the effect of the reduced diffusivities in the region of most importance, the Nordic Seas, the thickness diffusivity at a model depth of 197 m is plotted in figure 11 for DEFAULT and COSKAP. It is seen that the prescribed change in surface

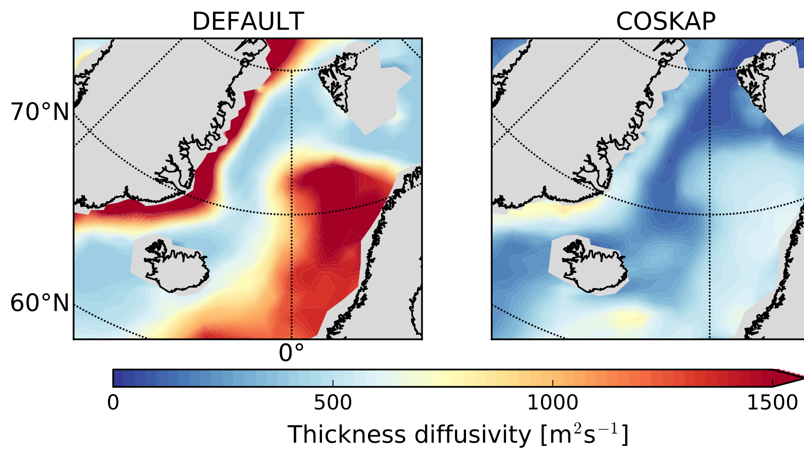


**Figure 11:** Thickness diffusivity (m$^2$ s$^{-1}$) in the Nordic Seas at a model depth of 197 m for DEFAULT (left) and COSKAP (right).

diffusivity significantly reduces the thickness diffusivity in this region, reducing the diffusivity from more than 1500 m$^2$s$^{-1}$ to around 600 m$^2$s$^{-1}$. This value might be too low (Andersson et al., 2011), but it will serve for our idealized simulations.

## 6.2 Spinup and global properties

To first get an overview of the simulations we look at the spinup of the DEFAULT simulation and at some global impacts of changing parameters in the subgrid mixing parameterizations. Some of the climatologies that are often the primary focus of OGCM improvements are the strength of the AMOC and the ACC. In this thesis, the former will be defined as the maximum value of the overturning at the equator, whereas the latter is defined as the maximum value of the barotropic streamfunction across the Drake Passage (the narrow passage between South America and Antarctica). Both are output fields in CCSM4.

In figure 12 the evolution of AMOC strength at the equator is plotted for the DEFAULT run over the course of the 300 model years. The model has a strong AMOC in the beginning but decreases towards very small values over the first century of the model run. A sort of equilibrium is reached by the second century at a very

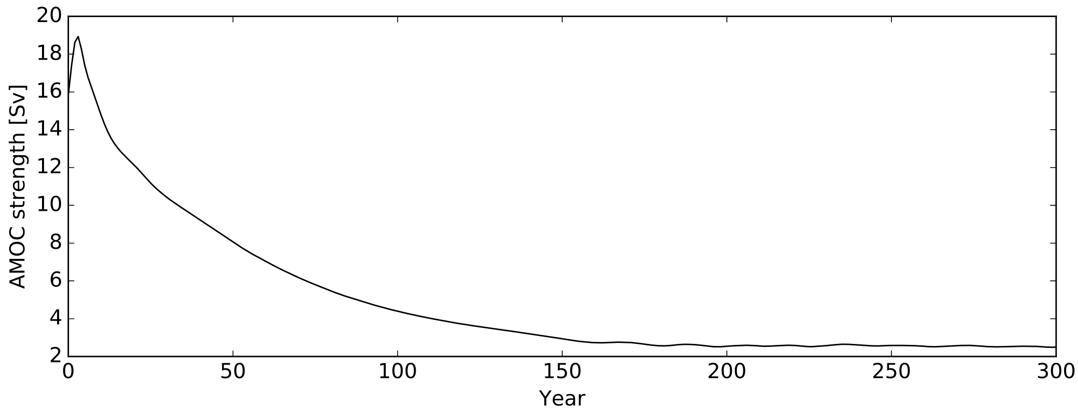


**Figure 12:** AMOC strength at the Equator (Sv) for the 300 years of the DEFAULT.

weak AMOC of about 2.5 Sv. The general pattern is similar for all the forced, coarse resolution runs, with the exception that COSHOR, COSKAP and COSKAPHOR all have small drifts by year 300. The maximum of the drift is in COSKAP which has a drift of -0.006 Sv yr$^{-1}$, i.e. a drift of about half a Sv per century, and it is therefore expected that this drift is too small to affect any of the results that will be discussed further.

The Drake Passage transport (from here ACC strength) of DEFAULT is plotted in figure 13. It is obvious that the model is not fully equilibrated after 300 years, as the ACC weakens. The weakening is, however, relatively weak, with a trend close to -0.05 Sv yr$^{-1}$, which corresponds to a weakening each year of about 0.03%. For our purposes, however, we assume that this drift is unimportant.

The AMOC and ACC transports in all primary model runs are listed in table 3. It is seen that decreasing the diffusivities towards the Poles result in increased AMOC and ACC transports. The latter is not surprising given that there has previously been noted an inverse relationship between ACC strength and eddy diffusivity (e.g Eden et al., 2009).

The AMOC is too small for all the forced runs. Only the coupled run and X1 have an AMOC strength that is close to the observationally estimated strength (18.7 Sv at 26.5°N according to Cunningham et al., 2007).

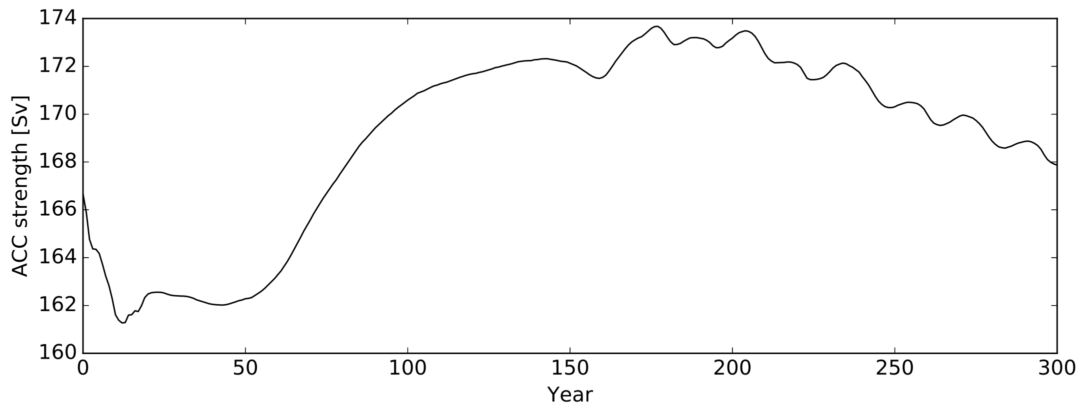


**Figure 13:** Drake Passage transport (Sv) for the 300 years of DEFAULT.

All forced coarse resolution runs have too strong Drake Passage transports. Meredith et al. (2011) estimated the mean ACC transports from 16 ADCP section measurements from 1993 - 2010 and found a value of $136.7 \pm 6.9$ Sv. The coupled run has a too weak ACC. Shields et al. (2012) found a similarly weak ACC and attributed it to an equatorward shift in the Southern Ocean storm track. In line with Jochum et al. (2008), reducing viscosity in VISC results in a weaker ACC closer to observed estimates, but still too strong. X1 captures an ACC strength much in line with observations. However, all forced simulations still have drifts by the end of year 300, and it is not known at what level they equilibrate, as this might take centuries or millenia to obtain, and for our purposes an equilibrated ACC is not required.

**Table 3:** AMOC and ACC strengths. All units in Sv.

| | DEFAULT | COSHOR | COSKAP | COSKAPHOR | VISC | B1850 | X1 |
|---|---|---|---|---|---|---|---|
| AMOC | 2.5 | 2.8 | 3.3 | 3.9 | 1.2 | 13.2 | 14.5 |
| ACC | 169 | 177 | 193 | 200 | 160 | 100 | 138 |

## 6.3 The High Latitudes

The primary region of interest is the Arctic Ocean and the Nordic Seas, where the temperature bias is observed and possibly generated. In this section, the climatologies of the different model runs are investigated for the high latitudes. The results are presented first for the Nordic Seas and then for the Arctic Ocean.

### 6.3.1 The Nordic Seas

Being the basin in which the temperature bias develops, the Nordic Seas is the region that seems most interesting to investigate. If the bias indeed develops in the Nordic Seas and propagates into the Arctic one can hopefully improve the model representation of the northernmost latitudes by preventing the bias formation in the Nordic Seas. As was introduced in figure 4 in section 4, the temperature bias in the Nordic Seas appears to spread from the Norwegian Current into the interior in DEFAULT. The first step in the analysis is to see if the different model runs limit this temperature spreading.

Figure 14 shows the potential temperature distribution at model a depth of 197m for the primary model runs. For comparison, the potential temperature from WOA is plotted for a depth of 200 m. These depths in models and WOA will in all further analysis be compared, despite their 3 m offset.

Figure 14 shows that there is a change in the temperature signal in all the reduced diffusivity runs. The temperature of DEFAULT is in the region between Iceland and Svalbard around 2-4°C, in COSHOR all is less than 3°C and in COSKAP the temperature range is 1-2°C. The warm Atlantic Water has a narrower structure in COSHOR and even narrower in COSKAP. COSKAPHOR has the coldest water East of Greenland and between Iceland and Svalbard in the range 0-1°C, as well as the narrowest Atlantic inflow. The temperature range in VISC is similar to DEFAULT, despite a colder inflow of water between Iceland and Norway. One interesting feature is the temperatures just along the coast of Greenland. Data from WOA suggest ocean temperaures of the order of 1 - 2°C, but both COSKAP, COSKAPHOR and B1850 have temperatures below -1°C.

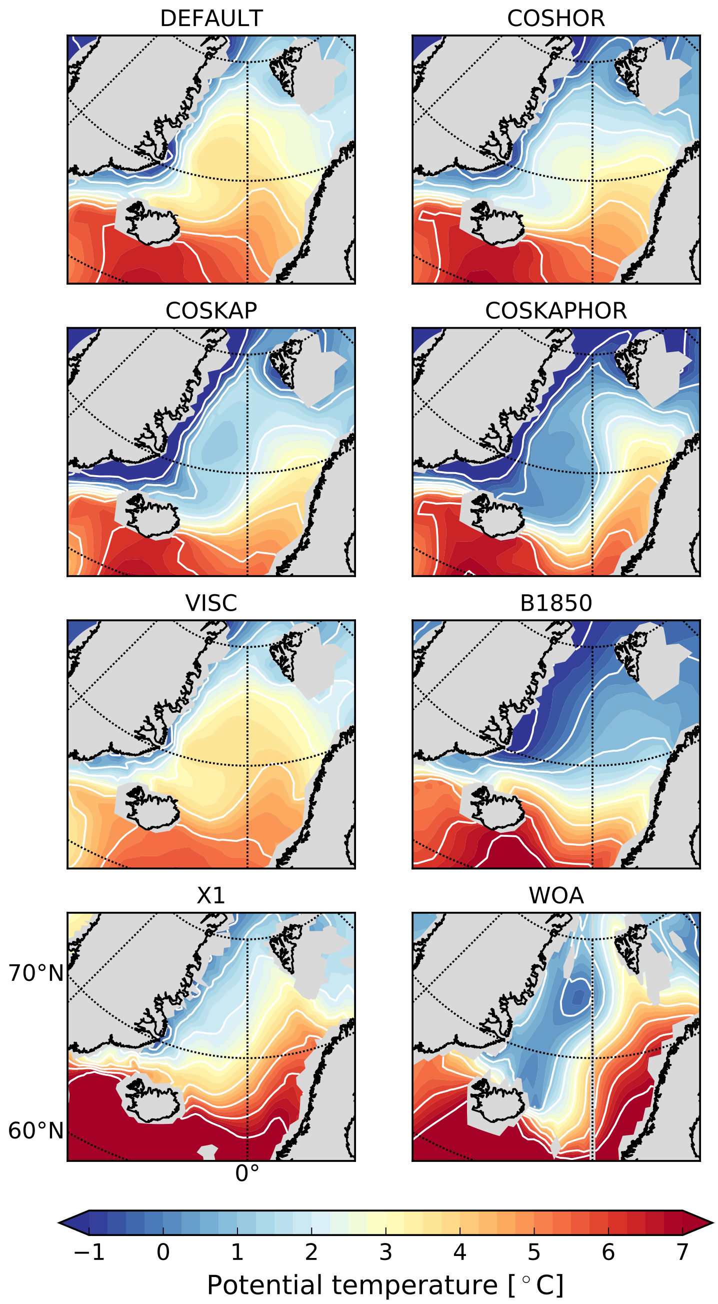


**Figure 14:** Nordic Sea potential temperature (°C) at a model depth of 197 m for primary runs. WOA data is at 200 m.

The Norwegian Current in B1850 has a large temperature gradient at the model depth of 197 m. The region East of Greenland spans temperatures from below -1°C to several degrees near Iceland, but is generally cold compared to DEFAULT.

X1 with increased horizontal resolution has a Norwegian Current temperature comparable to WOA, but west of the 0°E meridian the temperatures are comparable to those in COSKAP, but with a huge warm bias just north of Iceland.

It is interesting to also take a look at the potential temperature even deeper than the above presented 197 m, and as such the temperatures are again plotted for the same model runs, but at a model depth of 580 m and compared to WOA data at a depth of 600 m in figure 15. This depth is, as can be seen in figure 15, below sill depth of the Denmark Strait between Greenland and Iceland, and thus gives information on properties of the waters that overflow the Denmark Strait (Danabasoglu et al., 2010). The structure of temperatures is very similar to the structure at 197 m depth, however with an important difference compared to figure 14, i.e. that not only the temperature bias but also the absolute potential temperature is generally larger in all model runs, except for close the Norwegian coast. This shows that a temperature inversion in the Nordic Seas takes place in in the model. Of greatest importance is the temperature west of the Barents Sea and Spitzbergen, just south of 80°N, which suggests that the temperature inversion is not only present along the East Greenland shelf, but also in the Norwegian Current prior to its arrival at the Fram Strait. This will be discussed more in section 7.

The reduced warm bias in the diffusivity reduced runs smight be related to an increased heat loss to the atmosphere along the Norwegian Current. This will likely be accompanied by an increase in deep convection in the Nordic Seas. One way to assess the amount of deep convection or deep water formation is by looking at the model tracer ideal age. This is a passive ocean tracer which is set to zero whenever the water parcel reaches the surface. Thus, the younger the water, the more recently it surfaced. Ideal age is plotted in figure 16 for the same 7 model runs as in figure 14. The general patterns are similar to the observed temperature patterns. DEFAULT has waters in the central part of the basin of age around 80 years. COSHOR has a decrease in ideal age especially around Svalbard and in the middle of the Nordic Seas,

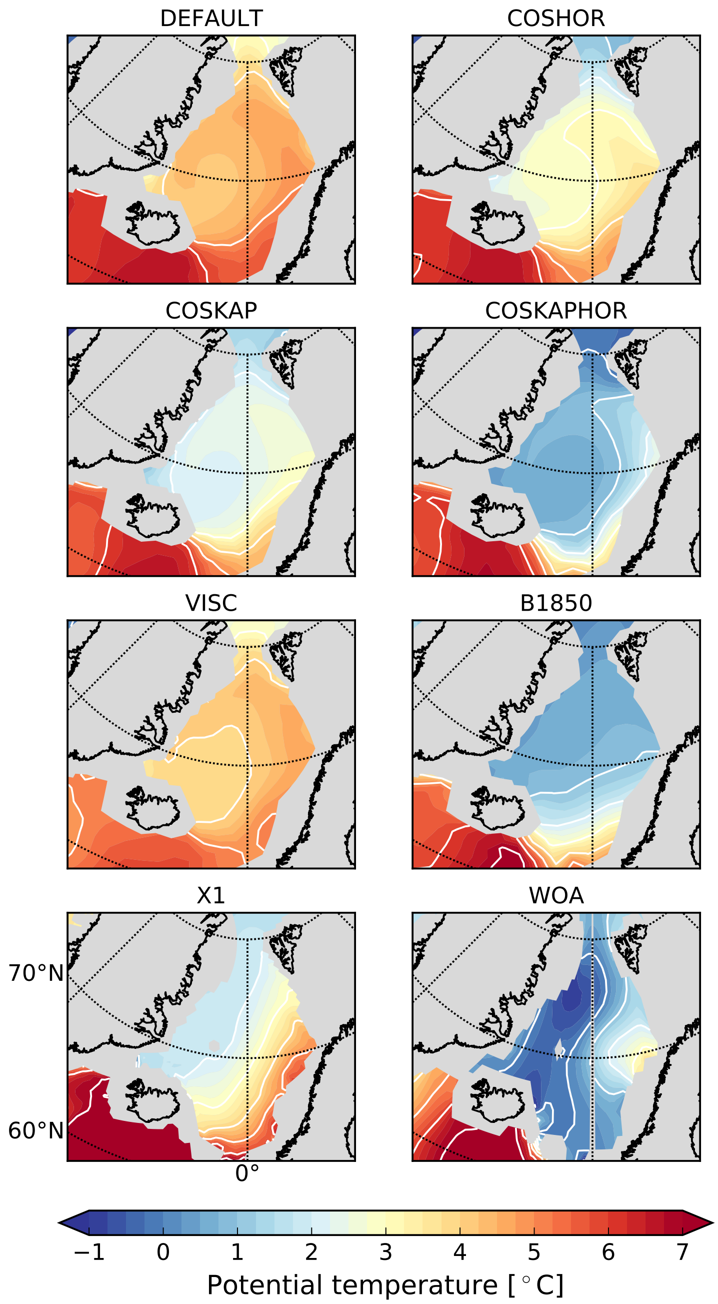


**Figure 15:** Nordic Sea potential temperature (°C) at a model depth of 580 m for primary runs. WOA data is at 600 m.

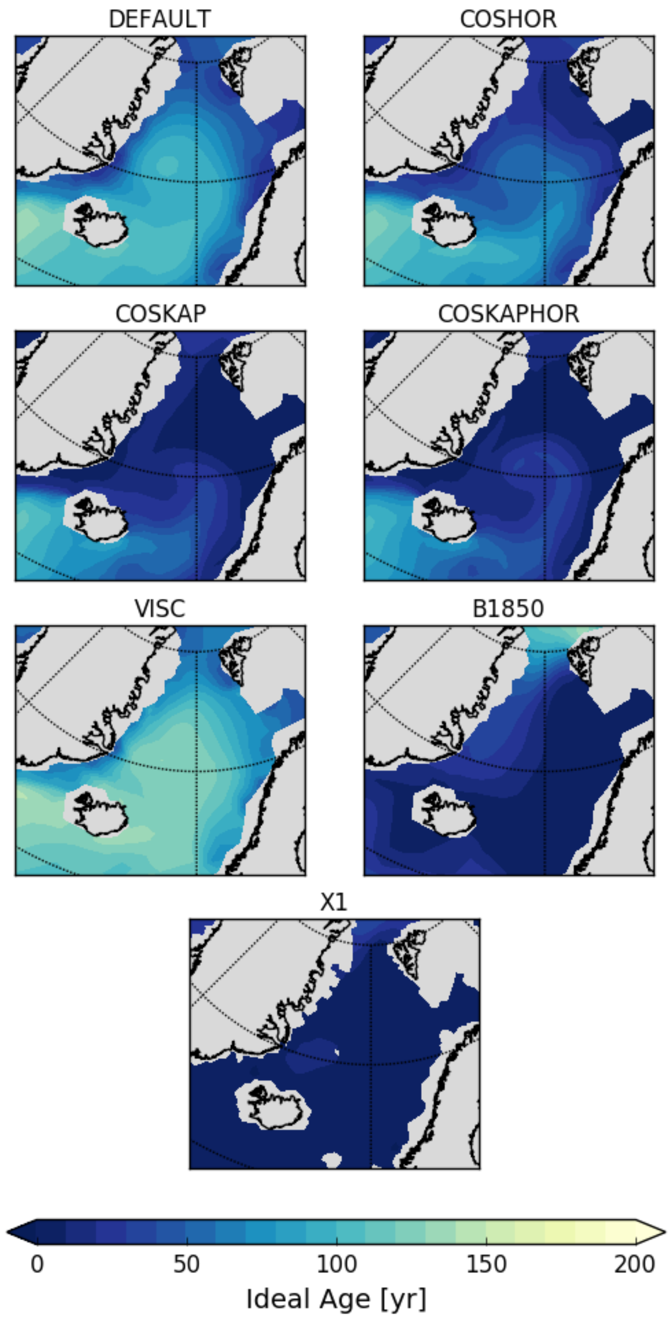


**Figure 16:** Nordic Sea ideal age at a model depth of 267 m.

whereas COSKAP and COSKAPHOR have reduced ideal age in the entire Nordic Seas, most prominent off Svalbard and near the Barents Sea Opening. VISC has increased ideal ages older than 100 years and B1850 has very young water masses everywhere in the Nordic Seas at the shown model depth. X1 has large ventilation all over the Nordic Seas, south and southwest of Iceland as well, unlike all the coarse resolution, forced runs.

### 6.3.2 The Fram Strait

The Fram Strait (FS) is along with the Barents Sea (BAS) the most important channels through which the Arctic Ocean is connected to the World oceans. Observations (e.g. Schauer et al., 2008; Beszczynska-Möller et al., 2012) reveal that the transport through the strait is characterized by a two-branched northward West Spitzbergen Current (WSC) and a southward East Greenland Current (EGC). The flow is strongly barotropic through the approximately 300 km broad, 2.5 km deep strait. Velocities in the Norwegian Current are of magnitudes up to 20 cm $s^{-1}$, but mostly lie below 5 cm $s^{-1}$ (Beszczynska-Möller et al., 2012). The temperature profile through the strait has warm surface waters in the WSC and cold surface waters in the EGC, but below the 400 m the isotherms follow depth, with the 1°C isotherm closely lying at a depth of approximately 600 m, and the 0°C isotherm at 800 m (Beszczynska-Möller et al., 2012; Schauer et al., 2008). Beszczynska-Möller et al. (2012) report observed transports inferred from a mooring array across the strait for several years, finding that the WSC transports are of $6.6 \pm 0.4$ Sv northward through the strait. Schauer et al. (2008) find a much larger transports of 12 Sv. The EGC transports waters southward from the Arctic to the Nordic Seas, resulting in a net transport of 2 Sv (Schauer et al., 2008; Beszczynska-Möller et al., 2011), meaning a range from 8.6 to 14 Sv. The discrepancies in estimates are speculated to arise in the addition of extra mooring equipment in the central part of the strait in the later period of the observation campaign (Rudels, 2015). As such, results will here be compared to those of Beszczynska-Möller et al. (2012) as these are the latest and include more data.

The model output temperatures in FS at a slightly varying latitude ranging from 77.5 to 78.7°N (see figure 8) for the primary model runs are plotted in figure 17 overlaid with velocity contours. Northward velocities are marked with solid contours, southward with dashed, and the contour interval is 0.5 cm $s^{-1}$. The 0-contour is highlighted. The horizontal axis extends from a western boundary, Greenland (left) to Spitzbergen on the East (right). All model runs show a too deep 0°C isotherm, for most runs lying close to a depth of 1.5 km, with the exceptions COSKAPHOR and B1850, which have depths of 1 km and 2 km, respectively. At the same time, all runs have a cold, approximately 100 m thick surface layer overlying the warm core, unlike observations that suggest the temperature to have its maximum in the surface. This suggests an early subduction of the WSC. Temperature maxima in DEFAULT and VISC reach 4°C in agreement with observations, whereas the temperatures of all other runs are too cold in general, 2°C in COSHOR and COSKAP and below 1°C in COSKAPHOR and B1850. In X1 the temperature maximum is rather shallow compared to the other runs, around 500 m depth. The deep waters are, however, very warm, with the warm bias extending all the way to the seafloor (compared to the results of Beszczynska-Möller et al., 2012). While the temperature magnitude is right in DEFAULT, it is displaced downwards and the warm core is not directly in contact with the atmosphere. These characteristics apply to all model runs.

Whereas the temperature structure is somewhat comparable to observations, despite being displaced downwards in the vertical, the flow structure parts completely from the observed barotropic structure (Schauer et al., 2008; Beszczynska-Möller et al., 2012). Instead, DEFAULT exhibits a strongly baroclinic flow structure, with the upper 1000 m flowing northward, the waters between 1000 and 2000 m flowing slowly southwards and the bottom waters having very slow, northward movement. In the surface on the Greenland shelf, waters flow strongly southward. The strength of the northward flow is much weaker than observations, with most velocities below 1.5 cm $s^{-1}$, much slower than the observed maximum of up to 20 cm $s^{-1}$ in the surface current. Reducing horizontal diffusivity weakens the flow, whereas the reduced thickness diffusivity increases the flow speed. This is both valid for the northward flow as well for the EGC along the Greenland shelf, and the deep southward flow,

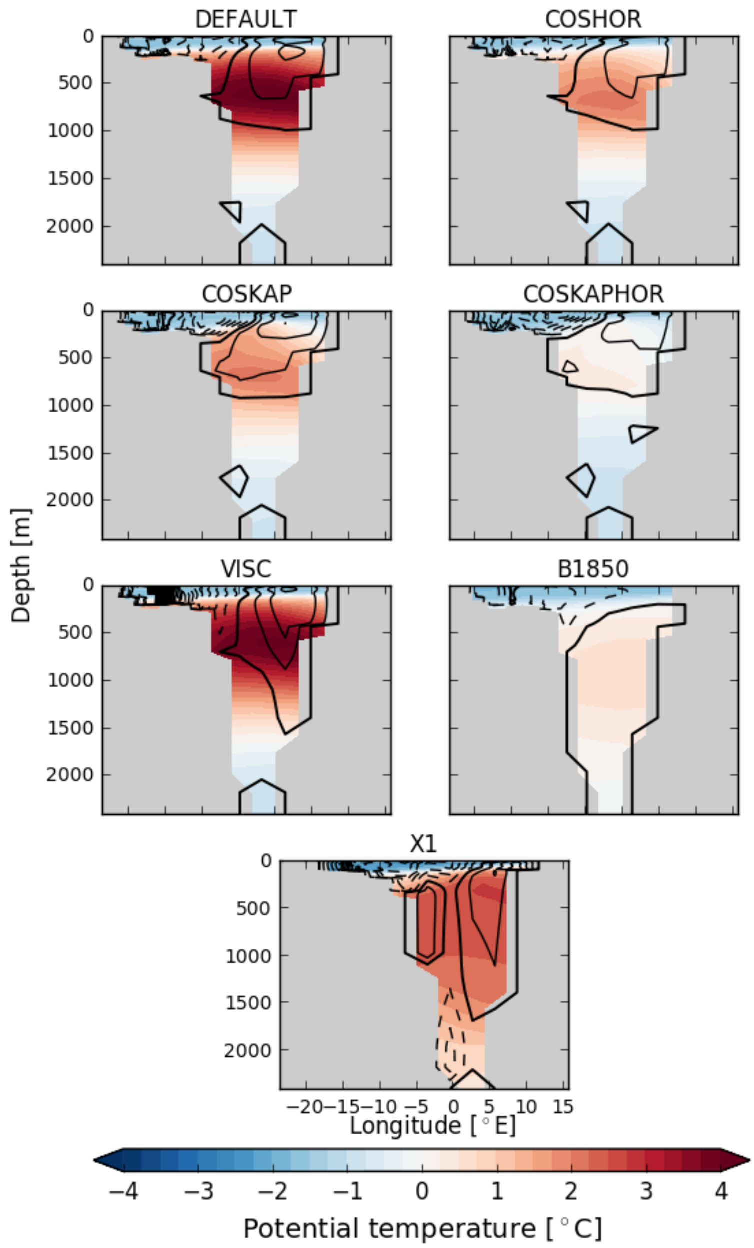


**Figure 17:** Fram strait transect. Colours indicate potential temperature (°C). Contours indicate velocities (cm $s^{-1}$). Solid contours indicate northward flow, dashed southward. Contour interval is 0.5cm $s^{-1}$.

although northward velocities are still far from observations. Reducing viscosity results in a shift towards a flow structure more comparable to that of the observed barotropic flow. The WSC penetrates deeper to 1500 m, but still maintains a somewhat baroclinic flow on the western boundary and below 1500 m. The flow of the WSC in B1850 is extremely weak, with no northward velocities greater than 0.5 cm $s^{-1}$, spanning the entire width of the strait below 500 m. This is accompanied by a rather weak return flow in the EGC.

The calculated transports are presented in table 4. It is evident that there is a tendency towards the transports being much too weak in both northward and southward directions. None of the simulations has a net outflow of 2.0 Sv, however all transports have a net southward volume transport. DEFAULT has an almost zero net flow, with both inflow and outflow around 1.5 Sv. COSHOR has reduced inflow and increased outflow, reaching a net outflow of about 0.9 Sv. COSKAP has an increase in both inflow and outflow, and COSKAPHOR has an increased inflow but decreased outflow, being the only simulation with above 1 Sv net outflow. VISC increases both current strengths yielding a net outflow of about 0.5 Sv, and B1850 has a decrease in both inflow and outflow and a net volume transport of 0.4 Sv southward. X1 has a stronger inflow and outflow than DEFAULT, but still only yields a net volume export from the Arctic below 1 Sv.

**Table 4:** Fram Strait transports. Positive values denote watermasses entering the Arctic Ocean. All units in Sv.

| | DEFAULT | COSHOR | COSKAP | COSKAPHOR | VISC | B1850 | X1 |
|---|---|---|---|---|---|---|---|
| In | 1.34 | 0.99 | 1.71 | 1.08 | 2.22 | 0.75 | 1.65 |
| Out | −1.48 | −1.71 | −2.13 | −2.31 | −2.69 | −1.15 | −2.47 |
| Net | −0.14 | −0.89 | −0.42 | −1.22 | −0.47 | −0.40 | −0.83 |

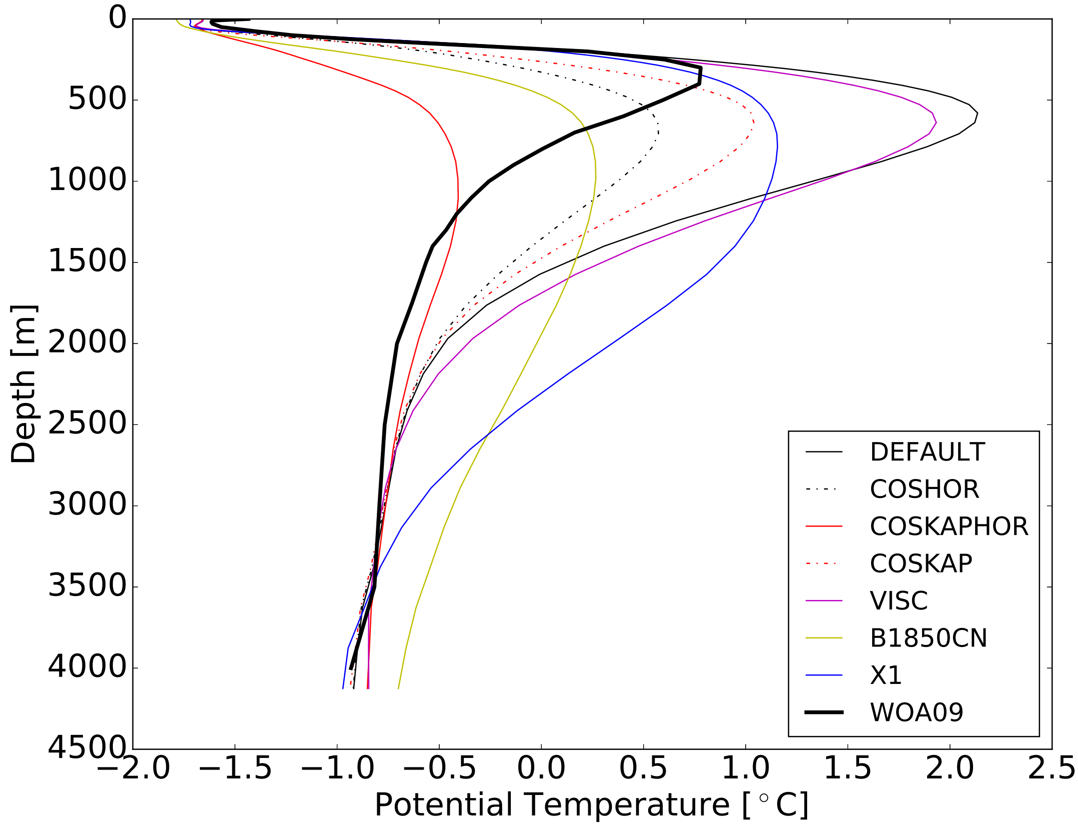


**Figure 18:** Potential temperature (°C) averaged between 80 and 90°N for primary model runs.

### 6.3.3 The Arctic Ocean

The goal of this study is to identify the cause of the Arctic temperature bias and to improve the representation of the Arctic Ocean, which is naturally the next region to inspect for the different model runs. Some important climatologies to look into are the Atlantic water core temperature, the upper Atlantic water depth and the flow of the Atlantic layer. Initially, however, it makes sense to compare the temperature-depth structure with observations. A similar plot to figure 12 of Jahn et al. (2012) is produced for the primary model runs in figure 18 showing the Arctic Ocean temperature averaged between 80 and 90°N. For comparison a profile obtained from WOA is also included. It is evident that none of the simulations captures the same structure seen in the observations from WOA. The structure of DEFAULT is similar to observations within the upper few hundred metres, but where observations suggest a maximum average temperature of approximately 0.75°C at a depth of 300-400m, DEFAULT has increasing temperatures until a depth deeper than 500 m and a maximum temperature almost 1.5°C warmer than WOA. All reduced diffusivity runs show a decrease in the maximum temperature, but with the maximum still located at a depth of some 600-700 m. COSKAP shows a maximum mean temperature just above 1°C, a reduction of more than 1°C compared to DEFAULT and only slightly warmer than the observed value from WOA. Reducing horizontal diffusivity in COSHOR decreases the maximum temperature even further to 0.5°C. The combined COSKAPHOR has a maximum mean temperature of -0.5°C and at a depth of 1000 m. Reducing viscosity in VISC results in a very similar profile as in DEFAULT, with a slightly colder maximum temperature, but with slightly warmer temperatures below 1000 m. In X1 the maximum temperature is shifted slightly downwards compared to DEFAULT, and with a maximum temperature comparable to COSKAP, but it has a large positive temperature bias at depths between 1000 and 3000 m, showing a very thick Atlantic layer. B1850 has a maximum temperature only slightly above 0°C, but like X1 has a large positive temperature in the deep waters. Unlike X1, however, the bias extends all the way to the ocean bed. Besides B1850, all model profiles are very similar below 3000 m. The thickness of the Atlantic layer appears to be the same in all forced, coarse resolution runs.

The first feature in the Arctic Ocean to inspect is one that is of particular interest to investigate in model simulations, the upper Atlantic water depth (UAWD). The definition here is adapted from that of Jahn et al. (2012), which is the depth of the upper 0°C isotherm in the Arctic Ocean. For model output and WOA data, this is defined as the shallowest depth at which water is above 0°C. The importance of the UAWD is that it can be used to identify the shallowest depth of water that has the potential to melt overlying sea ice. Thus, the UAWD represents the depth to which waters must be mixed in order to release a large heat reservoir, the Atlantic layer, capable of melting huge amounts of sea ice. Should the Arctic experience increased vertical mixing that brings up the warm Atlantic waters, the reduced sea ice cover following melting will potentially allow more mixing as the sea ice acts to shield the ocean from the wind stress. This constitutes a possible feedback mechanism in the Arctic: increased mixing reduces sea ice which increases mixing and so on. The importance of this feedback mechanism is not fully understood, but it is obvious that in order to assess the importance of the feedback mechanism from model studies, the UAWD has to be very similar to observations. A too shallow UAWD could cause an overestimation of the feedback, whereas a too deep UAWD would cause the opposite. Given that the Arctic is a very sensitive region in the climate system, the UAWD is very important to capture satisfactorily.

The UAWD is plotted in figure 19 for the primary model runs and for WOA data. Note that the UAWD for COSKAPHOR is ill-defined in most of the Arctic as it generally does not simulate any waters of temperatures greater than 0°C.

DEFAULT captures the structure of the UAWD rather well (compare to WOA), with shallow depths along the edge of the Barents Sea and deepening along the coast of Russia. The UAWD in the Canadian basin, though, is too shallow. WOA shows a maximum UAWD around 375 m, whereas DEFAULT has the deepest UAWD at a depth of just around 200 m. COSHOR generally deepens the UAWD. As a result, UAWD is somewhat deeper than WOA by some 50-75 m. COSKAP shows a structure very similar to that of WOA, however with a too deep UAWD in the central Arctic over the Lomonosov Ridge and in the Eurasian basin. VISC shows a UAWD structure very similar to DEFAULT, though slightly deeper in the Canadian Basin. The coupled B1850 has an extremely deep UAWD everywhere, with most of the entire Arctic Ocean having UAWD deeper than the maximum observed value. X1 has a structure comparable to VISC, only slightly deeper in the Canadian Basin, though still too shallow compared to WOA.

Figure 20 presents the Atlantic water core temperature (AWCT), defined as the maximum temperature in the subsurface water column. DEFAULT shows a clear warm bias as expected. The pattern almost shows a linear decrease in temperature as the distance to the Fram Strait increases. The temperature pattern is very similar in VISC, with the difference that VISC has a slight skewness so that temperatures are generally warmer follwing the shelf around Russia than around Greenland. The

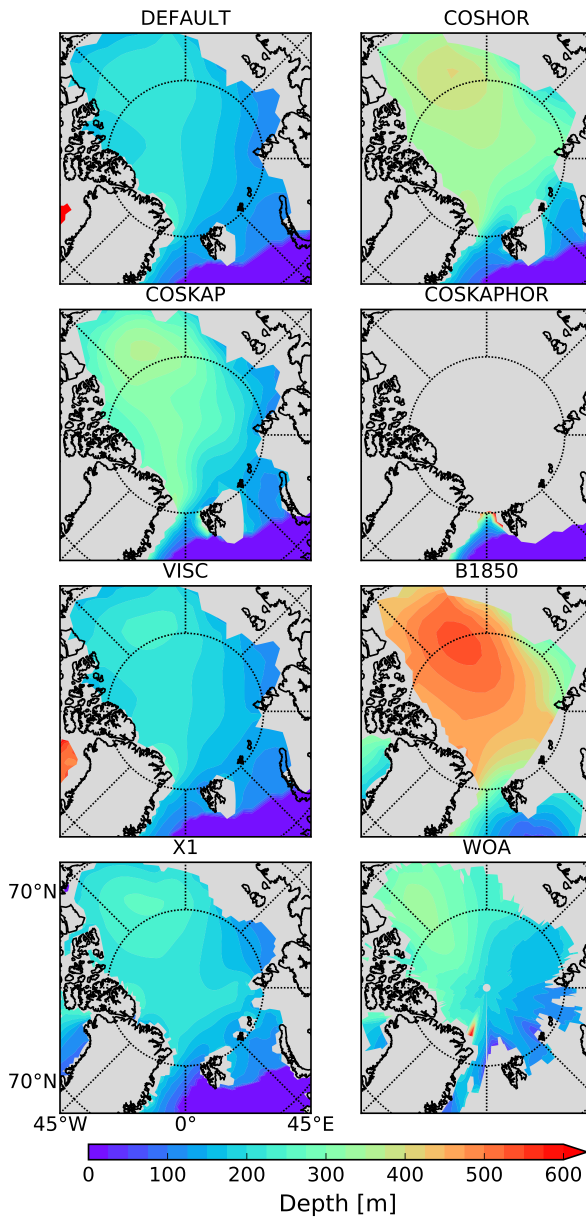


**Figure 19:** Upper Atlantic water depth, defined as the depth of the upper 0°C isotherm. Note that COSKAPHOR lacks a UAWD for most of the Arctic as there is no subsurface waters with temperatures above 0°C.

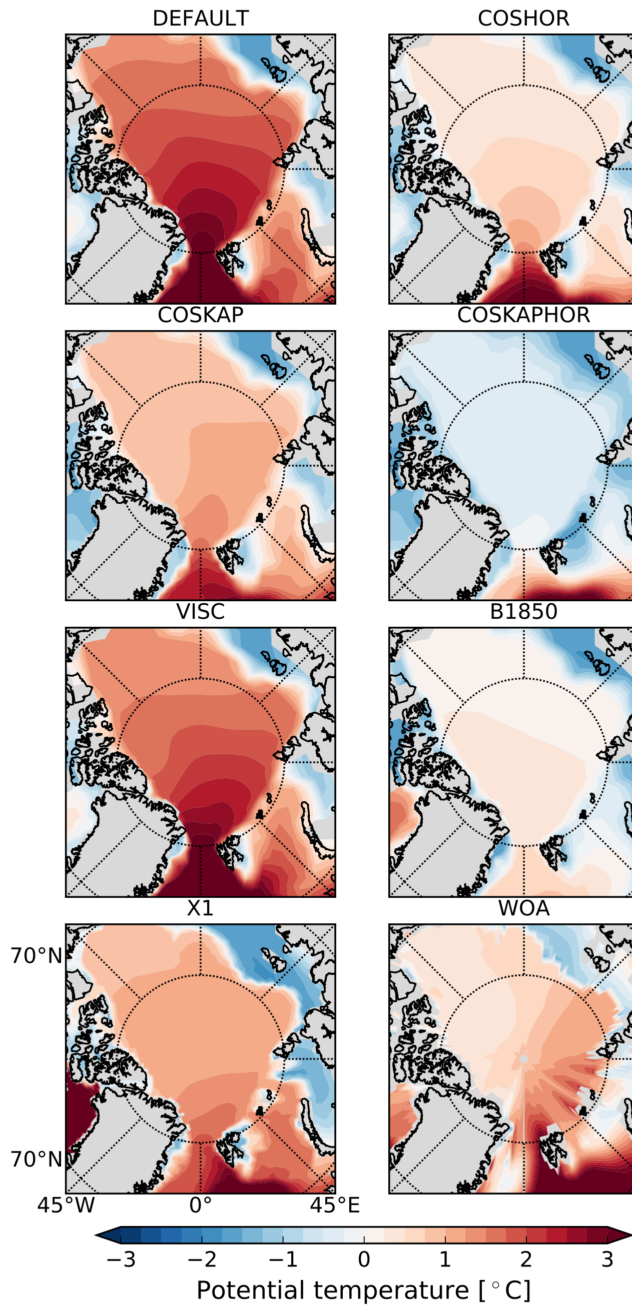


**Figure 20:** Atlantic water core temperature (°C) defined as the maximum subsurface temperature in the water column.

AWCT pattern in COSHOR is very similar to DEFAULT, but with greatly reduced temperatures, resulting in temperatures more comparable to WOA, especially in the Canadian Basin. COSKAP has a skewness like VISC, but with a reduction in the AWCT, resulting in temperatures closer to WOA in especially the Eurasian Basin, although still too warm in the Canadian Basin. COSKAPHOR has a very uniform AWCT of about -0.5°C. B1850 has a skewness opposite that of VISC and COSKAP, with the warmest waters along the northern Greenland coast, with an AWCT generally colder than WOA. X1 has a skewness like COSKAP and VISC, with slightly warmer temperatures than COSKAP.

Streamlines are plotted for the flow of the Atlantic layer in the Arctic in all primary model runs in figures 21 and 22. The Atlantic layer is here defined from a potential density surface, $\sigma$, which represents the density surface holding the warmest water in the Fram Strait inflow. Thus, slight variations in the potential density surface occur between the model. The potential density surfaces are listed in figure 21 as well. Below the streamlines the bathymetry is plotted in colors to compare with the flow. The observed flow is not plotted, but in general the flow follows the bathymetry cyclonically around the basins as well as along the ridges, constituting semi-closed circulations around the edge of the basins in both the Eurasian and Canadian Basins (Rudels et al., 1994). All model runs have very weak flow on the order of mm s$^{-1}$ in most of the Arctic (not shown). DEFAULT has waters emerging from the Fram Strait flowing into the middle of the Arctic to the Lomonosov Ridge, from where it flows in all directions. The flow is even anticyclonic along the Siberian shelf in the Canadian Basin as well as the interior of the basin, which agrees with the anticyclonic circulation in the Beaufort Gyre. COSHOR has an almost identical flow pattern. COSKAP is slightly different as most of the inflow from the Fram Strait follows around the bathymetry of the Eurasian Basin, until reaching the Lomonosov Ridge where it overflows into the Canadian Basin. Here, a circulation resembling the observed flow around the basin edge is present, but it lacks the anticyclonic Beaufort Gyre. COSKAPHOR has a flow like COSKAP. VISC has a representation of the Canadian Basin as DEFAULT. B1850 has a similar flow pattern as DEFAULT. X1 has a distinct flow which shows flow in the Eurasian Basin directed towards the Fram

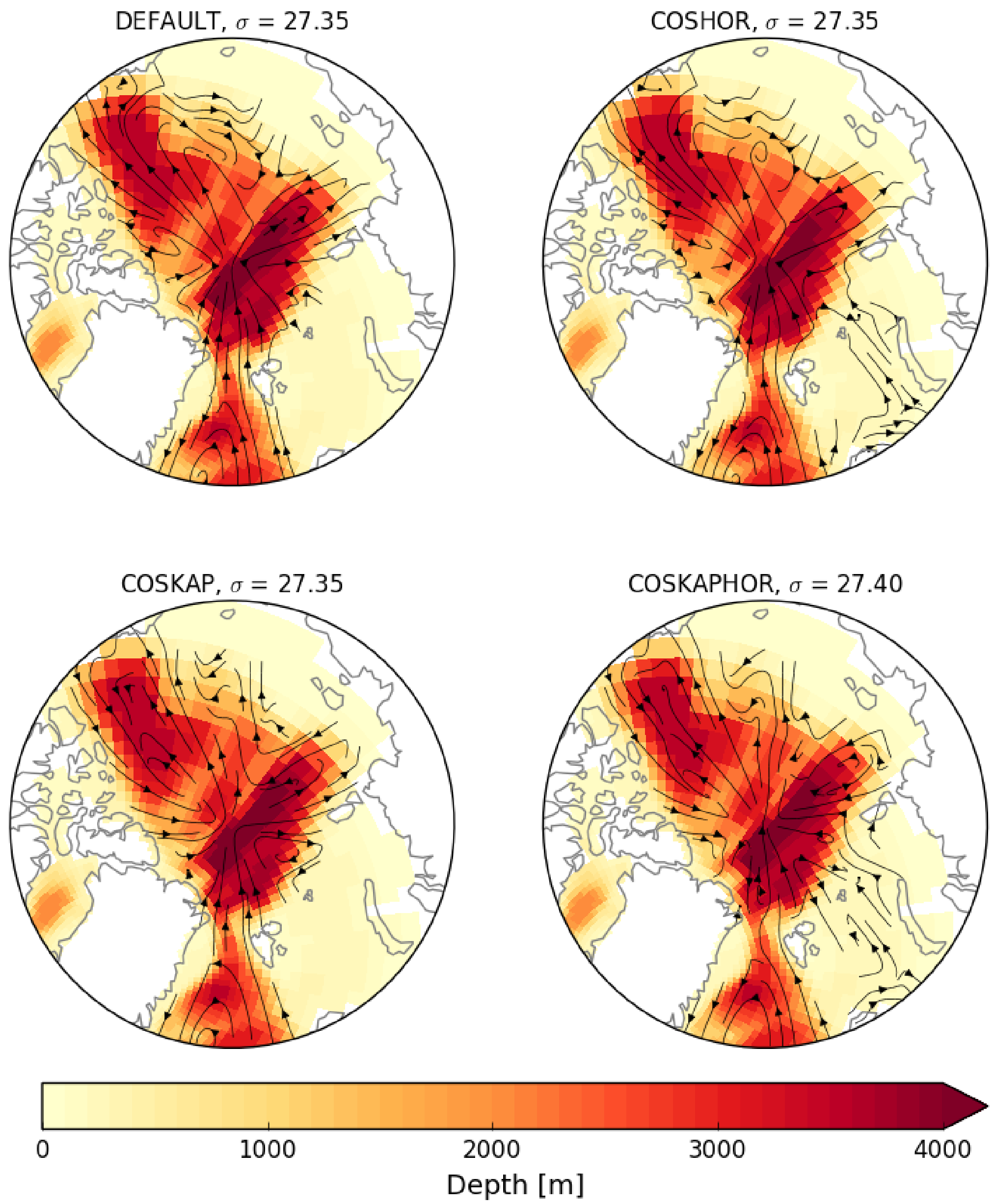


**Figure 21:** Streamlines of the Atlantic water, defined by the $\sigma$-surface indicated for DEFAULT, COSHOR, COSKAP and COSKAPHOR. The underlying colors indicate the model bathymetry (in m).

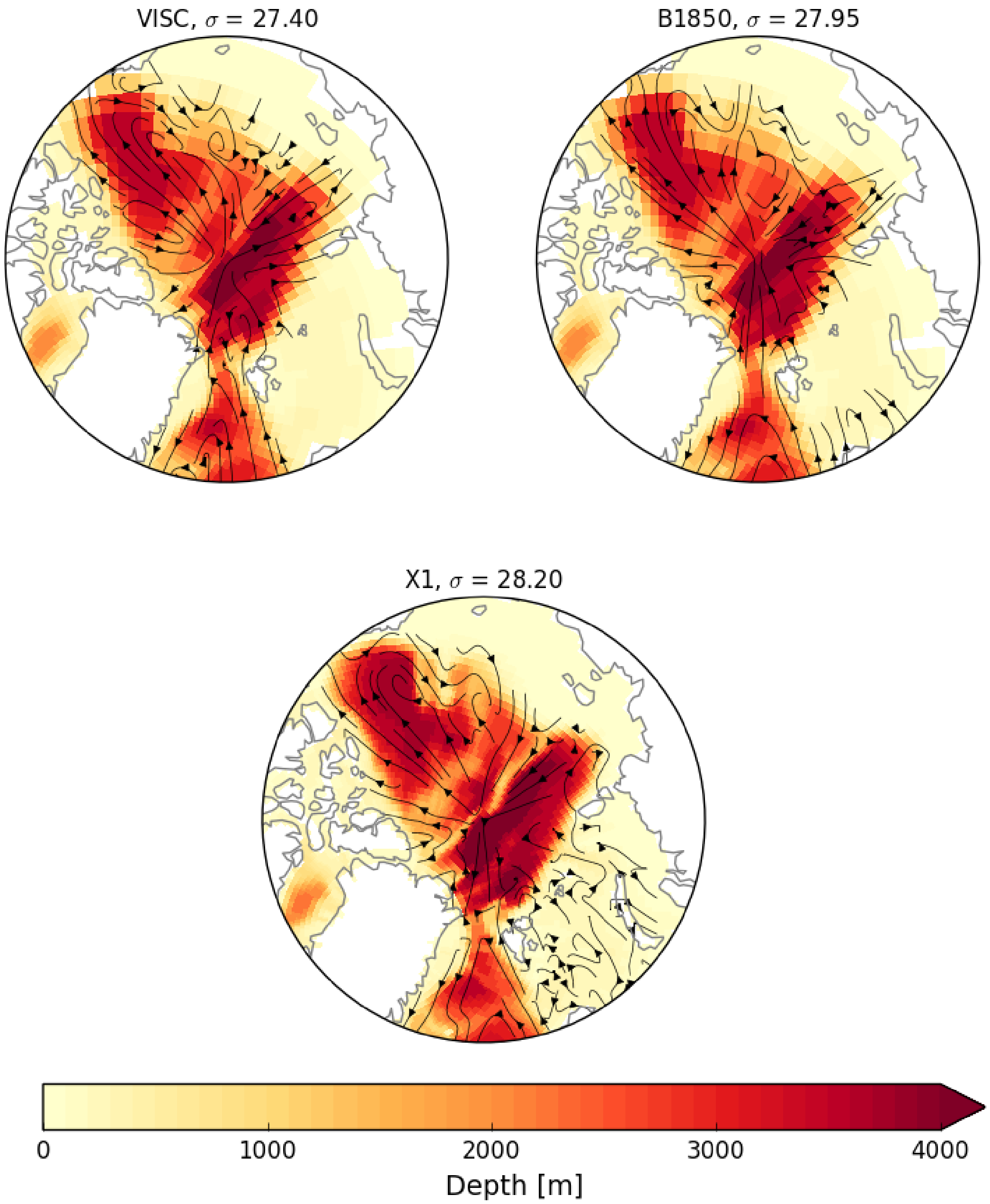


**Figure 22:** Same as figure 21 but for VISC, B1850 and X1.

Strait, and an anticyclonic flow in the Canadian Basin resembling of the Beaufort Gyre.

Ideal age for the model depth 267 m is plotted in figure 23. With B1850 as the only exception, all model simulations have a structure that resembles the youngest waters to form at the Fram Strait and Barents Sea outflow to the Arctic. In general, both COSHOR, COSKAP and COSKAPHOR have younger waters than DEFAULT and VISC, possibly related to a younger inflow waters from both Fram Strait and the Barents Sea, and possibly also more deep convection in the Arctic region itself. B1850 shows surprisingly old waters, suggesting that no deep convection reaches the depth of 267 m or lower. This old water is also present all the way the Fram Strait. The structure of ideal age follows that of the AWCT and the streamlines, suggesting a flow in the wrong direction along the Greenland shelf.

## 6.4 Sea ice

As surface forcing and deep convection are likely important in the simulations, the summer (September) and winter (March) sea ice concentration is plotted after 100 years for the primary model runs as well as X1 and a simulation with a prescribed sea ice, CNYR, in figures 24 and 25, respectively. The sea ice concentration is large throughout the entire Arctic region for all runs in March. Some important differences are very interesting to highlight, though. First of all, the sea ice maxima in the coupled B1850 shows very extensive sea ice concentrations east of (as well as southwest of) Greenland and completely ice covered Barents Sea. Another interesting feature is the ice cover in Fram Strait. DEFAULT and VISC have a completely ice covered (>95 %) Fram Strait, whereas the diffusivity reduced runs COSHOR, COSKAP and COSKAPHOR have slightly reduced sea ice concentrations in this region. The sea ice in CNYR is prescribed from satellite observations from 1978-1999 (Large and Yeager, 2004), and shows the eastern Fram Strait to be rather ice free and shows smaller ice concentrations in Barents Sea as DEFAULT. X1 shows a sea ice distribution very similar to that of CNYR.

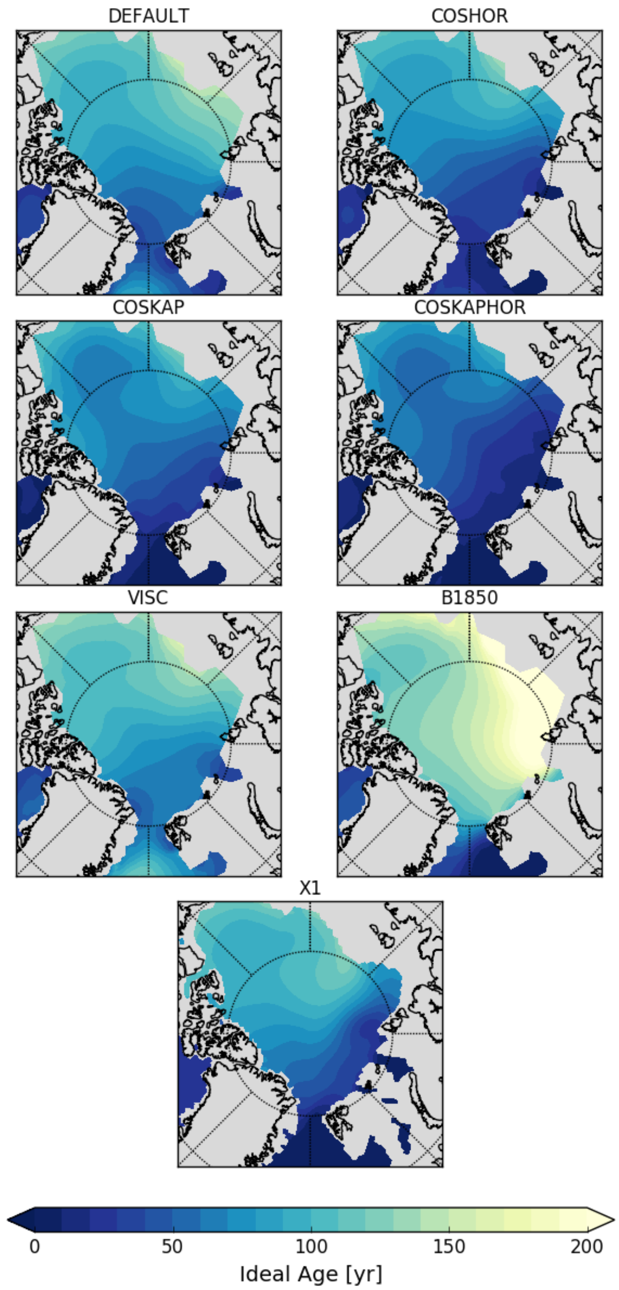


**Figure 23:** Ideal age at a model depth of 267 m in the Arctic basin of model runs.

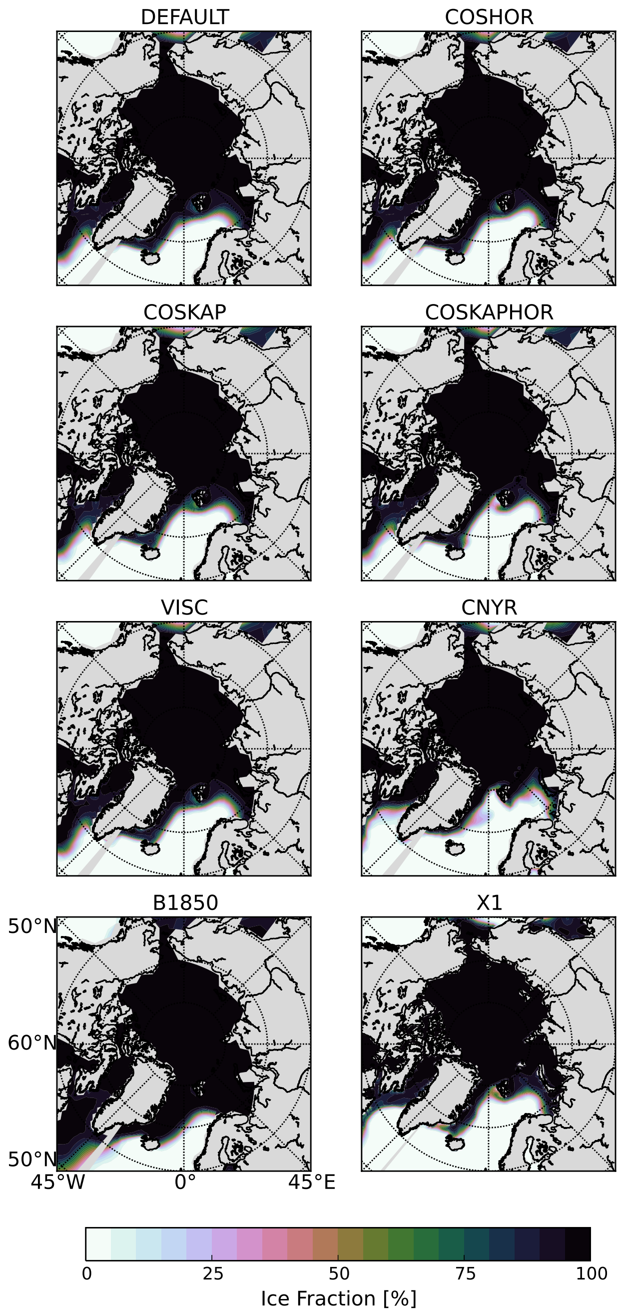


**Figure 24:** Sea ice fraction in March for primary model runs and CNYR averaged between years 90-99.

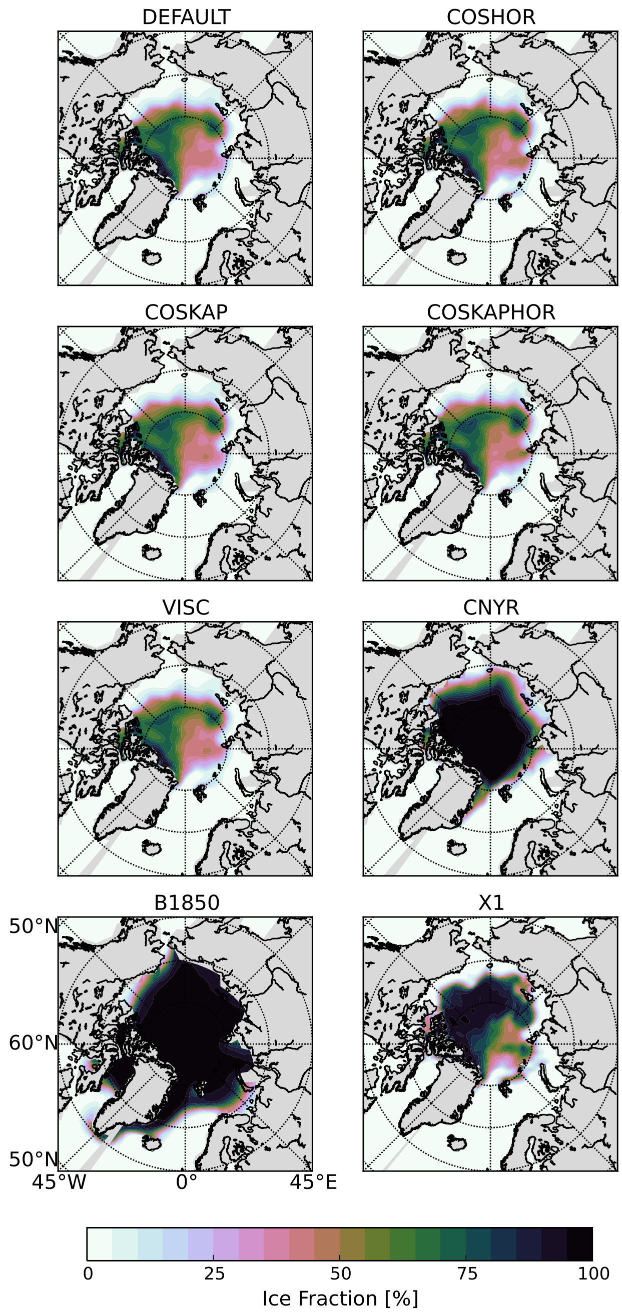


**Figure 25:** Same as figure 24 but for sea ice minimum in September.

Turning to the sea ice minimum in September, the model results are drastically different depending on forcing and resolution. All forced coarse resolution runs with an active sea ice model show a substantial low sea ice concentration throughout the Arctic Ocean when compared to the sea ice concentrations of CNYR. Sea ice concentrations are very low in especially the Eurasian Basin and along the Chuchki Shelf in the Canadian Basin. X1 has sea ice concentrations somewhere in between CNYR and the DEFAULT, with the same problems as the aforementioned, only less pronounced. On the other far end, B1850 has extensive sea ice, even in the Nordic Seas and Barents Sea which is ice free in CNYR.

# 7 Discussion

The previous section displayed results from a suite of different model runs that have been carried out. In the following section the previous results will be discussed and tied together in order to understand the observed differences between the different model runs. From here we should get a better understanding of the connection between reduced diffusivities and the observed reduction of the temperature bias in the Arctic and Nordic Seas which occur for all runs with decreased diffusivity. Finally some discussion is focused on the general idea of parameterizing eddy effects as tracer diffusion as well as other mechanisms of importance in setting the Arctic temperature bias, namely resolution and forcing.

## 7.1 Eddy mixing

The primary interest is to see how the eddy mixing parameterizations influence the temperature bias. In the following, both horizontal and thickness diffusion will be discussed, but before this it is insightful to investigate possible remote effects of reducing the diffusivity globally.

### 7.1.1 Remote effects

The observed reduction in the Arctic temperature bias from reducing diffusivities makes it tempting to claim a straightforward connection between the two. However, such conclusion is not valid as a global reduction of the diffusivity might have dynamic, global effects, especially it might have crucial implications connected to the Gulf Stream, its strength, temperature structure and its path, which would impact the Norwegian Current, and we are thus interested in roughly assessing to what extent the observed reduction of the temperature bias in the Nordic Seas and Arctic Ocean are caused by the local reduction in diffusivity rather than remote effects. For such rough comparison, a test run was made where thickness diffusivity was reduced in the Nordic Seas only. This case will be referred to as KNSEA. This model run has very sharp, horizontal gradients in the thickness diffusivity on the Nordic Seas boundary, and this sharp transition is not realistic and might cause spurious effects, which is why the run is only discussed as a secondary simulation in this section rather than the previous, but it does serve a useful purpose of trying to give a rough estimate of the importance of the local and the remote reductions of $\kappa_{GM}$. It might be viewed as a mix between DEFAULT and COSKAP, as it contains the same diffusivities in the Nordic Seas as COSKAP, but the same diffusivities as DEFAULT everywhere else. The temperature difference between KNSEA and DEFAULT and KNSEA and COSKAP at a model depth of 580 m are plotted in figure 26. For reference, the reader might want to look back at figure 14 and compare the figures. As can be seen, KNSEA is about 1°C colder everwhere than DEFAULT, and about 1°C warmer everywhere in the Nordic Seas than COSKAP. This suggests that one might attribute around half of the reduction in temperature bias in the Nordic Seas to the local reduction in the diffusivity in COSKAP, whereas remote effects can be attributed the other half. This is a very rough estimate, and the respective effects can be both larger or smaller as the climate system is very complex. For instance, it is not at all clear that the same result would be obtained if one were to make the reverse experiment and keep diffusivities large in the Nordic Seas and reduce them everywhere else. However, it is important to note that with a local reduction in thickness diffusivity only we still get a reduction in the temperature bias, and the connection between Nordic Seas eddy diffusion and the temperature bias is evident. At the same time it is important to note that the global changes in the model also do play a role. How or why is beyond the scope of this thesis to discuss, but it is important to keep in mind when analyzing the results.

When discussing remote effects of reducing the diffusivity towards the Poles it is also of interest to shortly discuss the observed changes in the global circulations, the AMOC and the ACC. The observed impact of decreasing (thickness and horizontal) diffusivities towards the Poles show that AMOC strength increases slightly. The AMOC is specifically dependent on the watermass properties of the waters in Denmark Strait and the Faroe Bank Channel. In POP2, a parameterization for the Nordic Seas overflows has been implemented (see Danabasoglu et al., 2010). The parameterization calculates the density of the product water after the source water

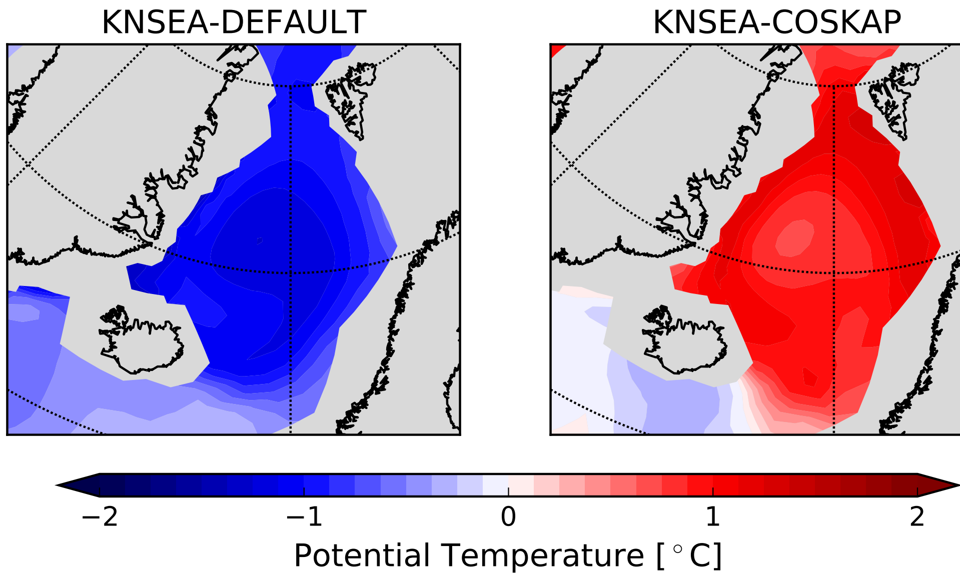


**Figure 26:** Potential temperature difference (°C) in the Nordic Seas at depth 580 m between KNSEA and DEFAULT (left) and KNSEA and COSKAP (right).

(at the sill level of the Denmark Strait) has mixed with entrainment water and leaves the overflow region at the appropriate isopycnal. The source water density depends on the salinity and temperature in the southwestern part of the Nordic Seas, which has been shown to be too warm. Decreasing the diffusivity should cause source water to be colder, but the eddy diffusion of tracers also mix salinity from the Norwegian Current to the Denmark Strait and Faroe Bank Channel. Hence, although the source water is colder than in DEFAULT, it is also fresher (not shown). As a result, the small improvement in AMOC strength is likely a result of the decreased ocean temperatures East of Greenland, but the issue of the very weak AMOC in all coarse, forced runs, is likely caused by a great salinity anomaly (also connected to the weak surface restoring), which may get worse from reducing the diffusivities as we expect that the reduced diffusivity not only brings less heat, but also less salt from the Atlantic waters in the Norwegian Current to the East Greenland Current.

The ACC increases with decreased diffusivity, which is expected as the strength of the ACC is very dependent on the diffusion of tracers. The physical reasoning behind reducing diffusivities in the Southern Ocean follows from the reduction of the Rossby radius of deformation, but the ACC is higly energetic and contains huge amounts of EKE, which is not taken into account when reducing the diffusivity. As such, a more ideal setup would not decrease eddy diffusivities as much in the Southern Ocean as has been done in the present study, but as focus of this thesis is in the Nordic Seas and the Arctic Ocean, no effort has been made to accommodate this.

### 7.1.2 Horizontal diffusivity

It is evident that reducing the horizontal eddy diffusivity in COSHOR causes changes in the high latitudes. Starting with the Nordic Seas, the temperature bias is reduced in both 200 and 580 m, but still exists in a pronounced form (see figure 14 and 15). This suggests that too strong horizontal mixing cannot be the only cause of the observed temperature bias. This view is further supported by the fact that the temperature bias was also observed in a simulation with zero horizontal diffusivity (ZERO) which was run for 100 years. The results are very similar to the first 100 years of COSHOR, with the major difference being that the changes between COSHOR and DEFAULT were only slightly enhanced in ZERO, and as such the simulation was discarded for further analysis. However, the existence of the temperature bias in ZERO clearly suggests that excess horizontal diffusion of tracers is not the full story of the temperature bias. Nevertheless, reducing the temperature bias is also followed by a reduction of the Arctic temperature bias itself as well as a deepening of the UAWD (see figure 19). The deepening of the UAWD is likely related to a general deepening of the Atlantic layer, seen in figure 18 as the temperature maximum is slightly deeper than in DEFAULT. Reducing the horizontal diffusivity appears to have very little impact of the circulation of the Atlantic water in the Arctic and is therefore not the reason for the poor representation of the flow seen in DEFAULT (figure 21). This is not a big surprise as we expect the horizontal diffusion to occur only in the surface boundary layer, and as the Atlantic core is pretty deep it is not expected that horizontal diffusion should affect it directly, although indirect dynamic effects might.

#### 7.1.3 Thickness diffusivity

The absolute drop in thickness diffusivity in the Nordic Seas in COSKAP compared to DEFAULT is larger than that of the horizontal diffusivity in COSHOR as seen in figures 11 and 5. It is also evident that temperatures in the Nordic Seas are generally lower in COSKAP than in COSHOR (see figures 14, 15). However, at the same time the Arctic temperature-depth profile shows that the Arctic is warmer in COSKAP than in COSHOR. This appears to be caused by a change in the volume and heat transports through the Fram Strait. The volume transports through Fram Strait are increased in COSKAP compared to DEFAULT, whereas COSHOR had decreased inflow of Atlantic water. At the same time, Atlantic water core temperatures are slightly warmer in COSKAP (figure 17). As a result, the net heat transport is increased in COSKAP compared to COSHOR. One would expect a warmer Norwegian current when reducing the diffusivities, as the temperature is confined to the narrow region of the current. However, as both the waters of the Nordic Seas and the Arctic are colder than DEFAULT when reducing the diffusivities, the heat must be going somewhere. From the increased deep water formation seen in the ideal age in figure 16, it is indicated that the energy is lost to the atmosphere instead of transported to the Arctic. This will also explain the colder Arctic profile in COSHOR compared to COSKAP, as COSHOR has in increased ventilation within the Arctic (see figure 23). Thus, reducing the diffusivities cause a greater temperature loss to the atmosphere, cooling the waters below observed temperatures. In this respect there seems to be at least two different explanations for the reduction of temperature bias by reducing diffusivities: (1) too large eddy diffusivities smear out the isopycnals and transport the warm Atlantic waters to the subsurface interior of the Nordic Seas where it is not in contact with the atmosphere and hence does not lose enough energy prior to entrance into the Arctic; (2) Reduced heat loss from the Norwegian Current to the atmosphere caused by the Atlantic water being isolated from the atmosphere, possibly by a fresh surface layer, causes too warm subsurface temperature to mix into the interior through eddy diffusion. In general this is a "chicken and egg" question. Does the temperature mix to the interior so that the water loses contact to the atmosphere, or does the water lose contact with the atmosphere and therefore mix excess temperature? This will be discussed more below.

The reduction of $\kappa_{GM}$ also improves the circulation of the Atlantic water in the Arctic, resembling the flow along the topography in the Canadian basin, but at the cost of the Beufort Gyre structure that might be present in DEFAULT. As such, one might speculate that the poor representation in the flow properties in the Arctic Ocean in the coarse resolution setup is related to the temperature bias and/or excess eddy diffusion within the Arctic Ocean. No matter the reason, it is interesting that we do see a change in direction in the Canadian basin in COSKAP.

### 7.1.4 Combined effects

Reducing both thickness and horizontal diffusivities adds some more dynamics to the entire problem than just decreasing one of the two. First of all, COSKAPHOR has no water masses warmer than 0°C in the Arctic, and as such the hydrography is ill represented, with no defined UAWD or AWCT (figures 19, 20). This is caused by the inflowing waters through Fram Strait being weaker and colder than DEFAULT, resulting in a weak heat transport through the strait and thus small heat import to the Arctic. Despite the waters being too cold, the circulation, like in COSKAP, does improve as compared to DEFAULT and observations (Rudels et al., 1994). That the temperature is much colder in COSKAPHOR than in the COSKAP, but the flow structure is similar, does point towards too large thickness diffusivity in the Arctic is partly causing the anticyclonic flow around the Canadian basin seen in DEFAULT. There is a question, though, as to which circulation is preferred. Obviously, none of the models capture the observed cyclonic boundary current and the anticyclonic Beaufort Gyre at the same time. Which one is preferred will probably depend on the specific experiment.

The Nordic Sea temperature structure in COSKAPHOR is the most accurate of all the forced simulations compared to WOA. This supports the idea that the temperature bias is indeed connected to excessive eddy diffusion of tracers. However, the strong resemblance to observations break down upon reaching the Fram Strait when COSKAPHOR is strongly cooled. This gives rise to speculation that COSKAPHOR indeed loses too much of its temperature on its way to the Fram Strait as well as after passing it, seen in the the decrease in ideal age in both the Nordic Seas and the Arctic. This suggests that there is a complicated interplay between the ocean-atmosphere interactions, the eddy diffusion and the temperature bias.

#### 7.1.5 Understanding the reduction of the temperature bias

The previous analysis brings up the important question of whether the Atlantic water spreads out in the Nordic Seas and gets shielded from the atmosphere or if it is the other way around. This question is difficult to assess, but nevertheless an attempt must be made. In figure 27 is plotted the potential temperature along the transect shown in figure 8 for DEFAULT (left panel) and in the first year of DEFAULT (right panel). The first year of the model is used instead of direct observations. This choice has been made as the model is initialized with observed January temperature fields, a dataset very similar to WOA. Using the first model year in place of observation comes at a cost as the model bias starts to develop already in the first year. The reason to use it here instead of using WOA is that model drift within the first year is likely smaller than possible errors obtained from interpolation of WOA data or model output on to a grid so that one can compare a transect in the model with the observed data.

As can be seen in figure 27, the structure of the Norwegian Current is very different after 300 years than what observations suggest. First of all one might notice that in the right panel there is only one branch in the Norwegian Current, unlike observations (Raj et al., 2015). This is likely caused by the coarse resolution setup. As seen in section 6.3 the temperature below the upper 100 m has spread out all the way to the western boundary (Greenland) and the Atlantic waters ($\theta > 2°$C)

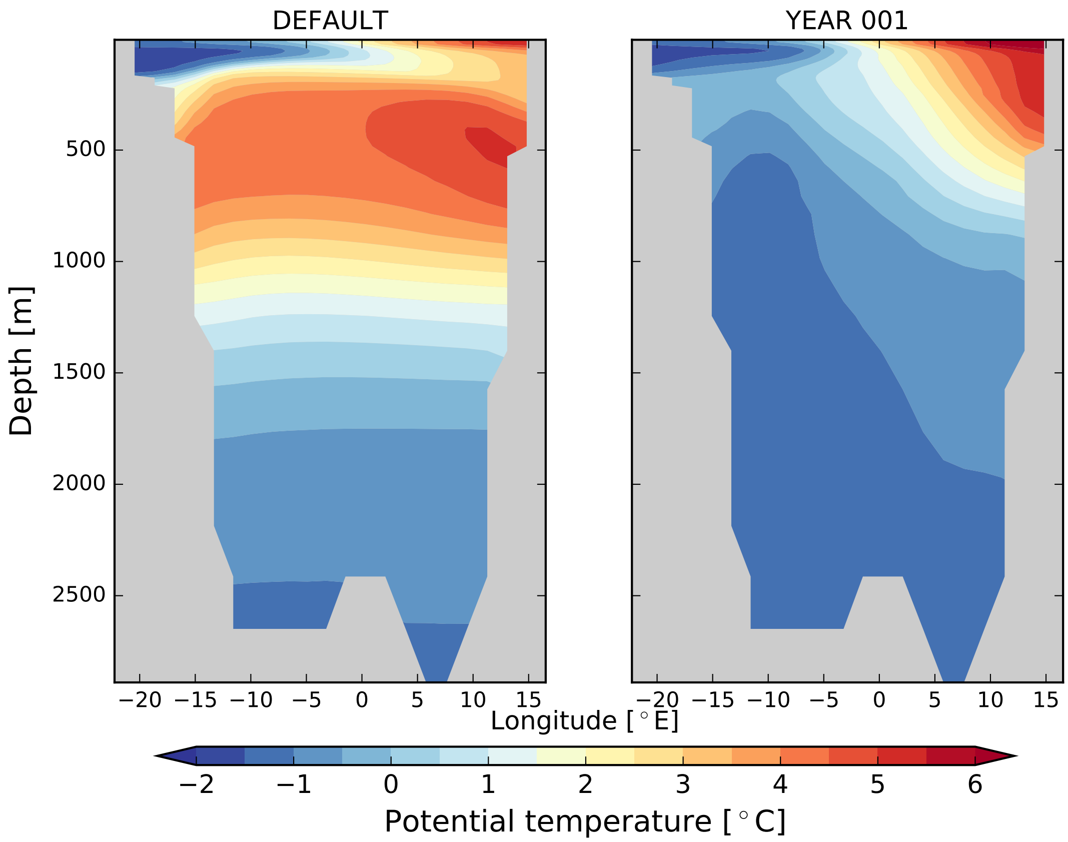


**Figure 27:** Nordic Seas potential temperature (°C) transect in DEFAULT (left) and in the first year of DEFAULT (right).

stretch more than a kilometer deep in the water column. The most interesting feature, however, is that the Atlantic water has seemingly split into a surface and a subsurface part, the subsurface core having a maximum temperature close to 500 m depth. This sort of 2-core structure is accompanied by a strong stratification, shielding the lower core from interaction with the atmosphere. This can be compared to an early subduction of the Atlantic water, which should not happen until much closer to the Fram Strait (Beszczynska-Möller et al., 2012). This would explain the temperature bias in the Arctic as discussed above.

A similar 2-core structure is present in all coarse resolution, forced runs, which is partly illustrated in figure 28 where the same transect is plotted for COSKAP (left) and B1850 (right). This means that even when both horizontal and thickness diffusivities are reduced, the Atlantic water inflow separates in two branches. The difference is that the vertical temperature gradients are smaller, which causes a weaker stratification (in figure 28 it is hardly captured by the colorbar). As such, by reducing diffusivities the separation of the two cores becomes weaker, and the lower core is more likely to lose heat to the surface through ventilation, also indicated by the decrease in ideal age in these model runs (figure 16). That reducing diffusivity reduces the stratification makes sense, as diffusion is parameterized to flatten isopycnals by transporting tracers down gradient, which in this case is away from the Norwegian Shelf. By reducing the diffusivities the warm waters are kept close up against the Norwegian shelf instead of spread out in the interior. So instead of flattening the isopycnals and isotherms, these are kept fairly steep along the Norwegian shelf.

However, it is not evident from the simulations if the origin of the 2-core structure is too strong diffusion. In fact, the existence of the structure even in COSKAPHOR suggests that the splitting might even be unrelated to mixing. As such, there is a caveat to the results presented in this thesis: While reducing the diffusivity, the Arctic temperature bias is indeed reduced, but the actual cause of the bias, the 2-core structure shielding the Atlantic inflow of water from losing heat to the atmosphere, may be happening due to other model misrepresentation. As a result, while reducing diffusivities, reduces the temperature bias in the Arctic and partly improves important features such as the UAWD in the Canadian basin, it cannot be ruled out that it is a result of treating the symptom rather than the disease itself, which is the 2-core structure of the Norwegian Current. Whether or not this structure is caused by excessive eddy diffusion or if it is the other way around is not clear, but the fact that it is present even in COSKAPHOR does suggest the latter. However, reducing the diffusivities does improve simulation of the Arctic in several ways. Therefore it is of continued importance to understand the implications of present eddy parameterizations on the model representation of the Northern High Latitudes.

It is important to further note the difference between the plotted transects of the coupled B1850 and DEFAULT in figures 28 and 27, respectively. The coupled run

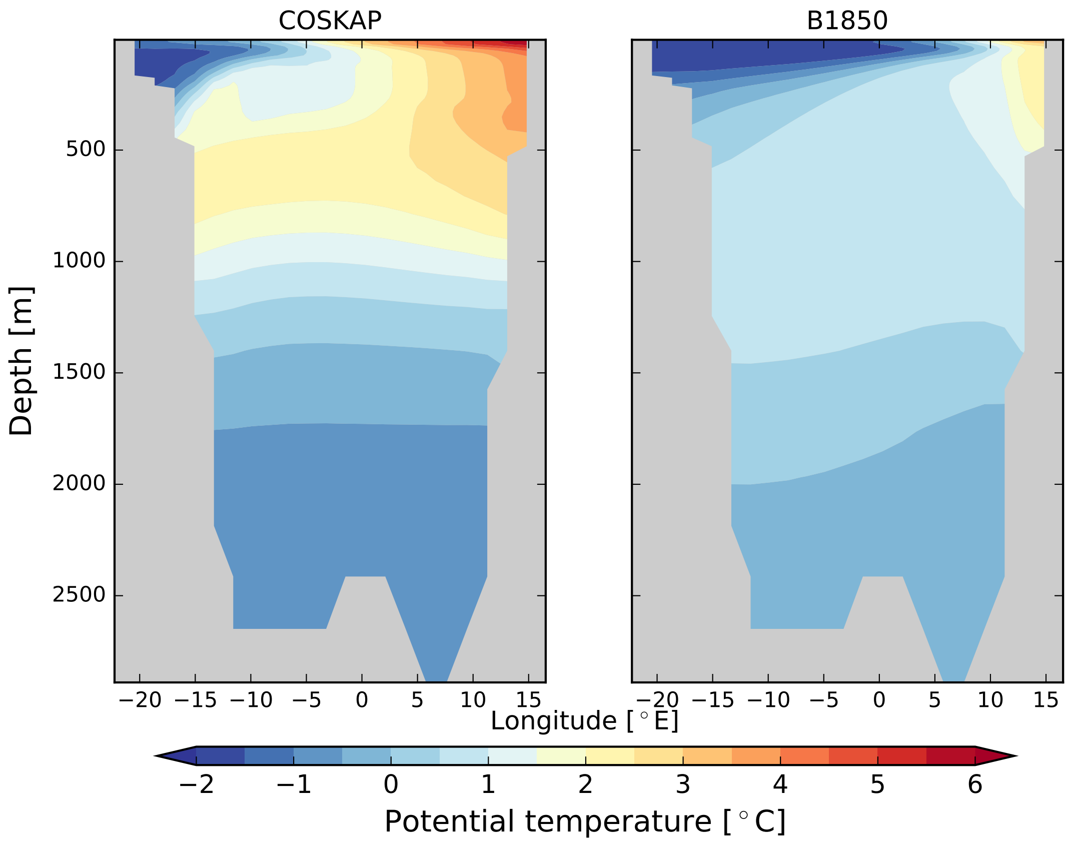


**Figure 28:** Nordic Seas potential temperature (°C) transect in COSKAP (left) and in B1850 (right).

has a slightly different structure than the coarse resolution, forced runs. Here, a very weak separation is also present in the Norwegian Current (mostly visible between 5 and 10°N), forming again a 2-core structure, but the waters are much colder in the Norwegian Current than observations suggest, with surface temperatures several degrees colder than seen in the right panel of figure 27. The interior is seen to have a similar, warm spreading of temperature as observed in the forced runs, only with a much smaller amplitude, in line with the colder Norwegian Current. This suggests that the process that causes the temperature bias in the forced and coupled simulations may be the same in both settings. The difference in the structure of the bias lies in the fact that it goes deeper and is not as warm, possibly because a lot of heat is lost to the atmosphere on the current's way along the Norwegian shelf. In B1850 the 2-core structure also causes a temperature bias. The upper branch loses its heat to the atmosphere, where the lower branch can be seen as an early subduction of the Atlantic layer, shielding it from the surface to spread out the temperature to the interior of the Nordic Seas, resulting in the observed deep water temperature bias in the Arctic. That the Norwegian Current is so cold in the coupled setup is out of the scope of this thesis to explain, but it is well known that there is a cold bias in the surface waters of the coupled coarse resolution CCSM4, and this is likely related to the present results (Shields et al., 2012). That the Norwegian current is thus colder than observed is not a surprise, whereas surface temperatures in the forced runs are only allowed small excursions away from the imposed atmospheric surface temperatures. If one was to reduce the mixing in a coupled setup, it is likely that the deep warm bias would be reduced in line with COSKAP or COSKAPHOR, but the Arctic would then likely have even less incoming heat transport as the Norwegian Current would lose more heat to the atmosphere. This would possibly result in the opposite of a warm bias, a cold bias like in COSKAPHOR where there are no waters above 0°C, and thus no warm, Atlantic layer.

## 7.2 Secondary experiments

### 7.2.1 Viscosity

The reason why viscosity has been investigated is the fact that the flow through the Fram Strait in DEFAULT is found to be largely baroclinic, where observations such as those described in Beszczynska-Möller et al. (2012) suggest a more barotropic flow. Simultaneously, the flow is generally too weak. The weak, baroclinic flow is possibly a result of too high viscositites. The reduction in VISC happens is in the eddy viscosity coefficient, which would overall lead to a reduced viscosity given that the eddy viscosity in these areas is the largest of the different viscosity parameters (and smaller than the viscous CFL number). The increase in $c4$ somewhat opposes this effect, but only very little around the Fram Strait as the distance to the western boundary is too small to give large effects from the change in e-folding length scale.

The resulting flow through the Fram Strait (see figure 17) might be characterized as slightly more barotropic than DEFAULT and all other runs, as the inflow to the Arctic is more confined to the Spitzbergen boundary and extends deeper than in DEFAULT, but the resulting changes in the Arctic are tiny. The main conclusion drawn from VISC is that the transports through Fram Strait do increase, bringing them closer to observations. The resulting transports, however, are still much smaller than observational estimates. This suggests that one of the problems regarding simulation of the Arctic watermasses is the narrow passage which is simply too coarsely resolved, even in X1. Instead of reducing viscosity one might try to develop a parameterization for the Fram Strait transports. This, however, unnecessary unless the properties in the Nordic Seas are captured better, as the parameterization would then still propagate the warm bias into the Arctic, just at a different rate. If VISC was combined with a run with reduced tracer diffusion the effect might be larger, but this is speculative and beyond the scope of this project.

#### 7.2.2 Resolution

As with most other climatologies it turns out that resolution is an important factor in the temperature development. As most of the cases in this study is concerned with the coarse resolution version of POP2 it is important to discuss if what is happening in the model is simply fixed by increasing the horizontal resolution. This claim does not appear valid if one takes a brief look at the temperature-depth profiles in figure 18, where the standard 1° resolution, X1, performs poorly just as the coarse resolution DEFAULT, having a maximum temperature almost 0.5° C too warm, and in the deeper ocean between 1 and 2 km the temperature bias is even worse than in DEFAULT. One place where the increase in resolution might have the biggest impact is, as mentioned above, the representation of the Fram Strait, but as can be seen in figure 17 the resolution of the Fram Strait below 500 m is similar in the coarse and the standard resolution model setup. More specifically, the width of the strait is only increased by one grid point when going from coarse to standard resolution. This obviously has consequenses for the flow, which as with the coarse resolution is largely baroclinic unlike the observed barotropic structure, although the flow characteristics are slightly different and transports are different. The temperature structure in the Nordic Seas is improved in X1 compared to DEFAULT, but a large temperature bias still exists. As a result, the temperature bias is also in the standard resolution run occuring in the Nordic Seas and transported to the Arctic, and is not a property caused by the Arctic processes alone. The standard 1° and coarse 3° resolution models have different surface diffusivity coefficients, $A_{ref}$, being 3000 and 4000 m$^2$ s$^{-2}$, respectively. This may explain some of the improved temperature in the upper km in the Nordic Seas. It is therefore not impossible that a reduction in diffusivities in the 1° setup will also improve the temperature bias.

Though the higher resolution simulation is not performing particularly better than DEFAULT in this study, it is important to note that in the coupled setup analyzed in Jahn et al. (2012) the flow properties in the Arctic and UAWD are fairly well represented, and as such part of the poor performance, in particular the flow of the Atlantic water in the Arctic, might be explained by issues with the simple ocean-ice setup. Furthermore, one might still speculate that increasing horizontal resolution even further will improve the simulation of the Arctic. As such, it is a natural next step, but left for others, to analyze higher resolution output and find if the representation of the Arctic is improved. This will also greatly enlighten the understanding of the temperature bias and its relation to sub-grid mixing parameterizations. If moving to eddy-resolving or eddy-permitting resolution completely annihilates the temperature bias, comparing the coarse and fine resolution output might reveal previously undiscovered processes important to the Northern high latitudes. Another option is to use nested grids in the Nordic Seas and Arctic. However, POP2 is inflexible in this sense which makes nesting difficult and is thus unlike to be worth while. Furthermore, nested grids will inherit whatever biases that occur outside the nested grid. As has been discussed, the changes in the model are not necessarily caused by the local changes in the model only.

#### 7.2.3 Surface forcing

As the heat loss to the atmosphere is important in cooling the Norwegian Current, and as sea ice changed slightly by reducing diffusivities, it is interesting to investigate the effect of fixing the sea ice, done in the case CNYR. This thought occured because of the way the forcing fields try to fix surface temperatures to a given level. Removing sea ice in one place might then have serious impact on the results. Fixing sea ice in CNYR, however, cooled the Norweigian Current excessively, reducing intermediate water temperature in the Arctic to below -1° C (not shown). As a result, it did not make sense to analyze the simulation any further. However, the CNYR sea ice distribution did point out a huge difference in the model setups, with far too little sea ice in the forced, coarse resolution setups. This might have an impact by capping the Atlantic water with a cold, fresh layer, also observed by the North Atlantic halocline catastrophe evident in the extremely weak AMOC, and might be important in shielding the Norwegian Current from the atmosphere. However, as has been shown in the previous sections, the observed structure in the forced, coarse resolution runs is similar to the standard resolution and the coupled run despite their increased sea ice cover. The coupled run stand out with its general cold surface bias (Shields et al., 2012), but it is important to note that even with the excessive sea ice observed in B1850 the Arctic temperature bias occurs with an associated bias in the Nordic Seas found through a 2-core structure. In the initial phase of the project an increased salinity restoring was used which mixed the Atlantic layer too heavily vertically (as mentioned in section 4). What this and CNYR tells us is that the atmosphere-ocean interactions in the surface layers are very important in the process of forming the Atlantic layer in the Arctic. Getting the cooling of the Norwegian Current right is of crucial importance for getting the Arctic and Nordic temperature structures right. This means that getting the latitude of subduction of the Atlantic water right is very important, something that all model runs in this study fail to. Understanding this might be the key in getting the full understanding of the Arctic temperature bias.

## 7.3 Parameterizing eddies

The discussion above calls for a more general discussion of the concept of eddy diffusivities, in particular $\kappa_{GM}$. While some studies (Visbeck et al., 1997; Eden and Greatbatch, 2008) interpret the eddy diffusivity as a product of the important scale parameters (time, length and/or velocity), the default setting in POP2 (DEFAULT) calculates the diffusivity based solely on the local stratification with no consideration of e.g. available eddy kinetic energy, EKE. While the CCSM4 default settings in a coupled setup generally produces good results[5], it is physically flawed as the eddy strength in general takes no considerations towards the global eddy pattern such as the poleward reduction of a characteristic eddy length scale. As is also observed in the above results, enforcing this reduction (in e.g. COSKAP) leads to a better simulation in the Arctic. This, however, comes at the cost of a too strong ACC, but as $\kappa_{GM}$ in the interpretation of e.g. Eden and Greatbatch (2008) should also be a function of the available EKE, this flaw might in fact be compensated if one included the energy contribution in the calculation as is done in their scheme. This would be a large study in itself, and is after all what has been done in the scheme of Eden and Greatbatch (2008). For this study it would have been interesting to use this parameterization, but numerical problems occured in the implementation in the coarse resolution setup, and it is left for others to solve this.

With the current situation it might be time to pause and reflect. The implementation of the GM90 parameterization was a huge improvement in CCSM (Danabasoglu et al., 1994), but it has some severe drawbacks. Current parameterizations are generally based on eddy dynamics such as mixing length and characteristic velocities or timescales (Visbeck et al., 1997; Eden and Greatbatch, 2008). However, it is important to note that the parameterization by construction can only transport energy from the mean APE to the EKE. This downscale energy cascade is representative of baroclinic instabilities, but the reverse energy cascade from EKE to mean potential energy is also observed in ocean and fluid dynamics in barotropic instabilities, backscatter and jet rectification (see e.g. Porta Mana and Zanna, 2014). This impor-

[5]Despite the errors in the model such as the one analysed in this study one should never forget that CCSM4 still overall is an extremely well-performing climate model

tant eddy effect is not present in the downgradient thickness diffusion of GM, and thus the parameterization is incomplete. This is also obvious when analyzing the results of Ferreira et al. (2005) (see their figure 12), who by their adjoint model found several large regions in the world oceans to have negative diffusivities. In the development of their parameterization, these large areas were completely ignored (Ferreira et al., 2005; Danabasoglu and Marshall, 2007). The parameterization may be well suited for representing baroclinic downscale energy cascades, but clearly neglects important physics connected to mesoscale eddies.

Trying to calculate the EKE budget and using this in an eddy parameterization such as that in Eden and Greatbatch (2008) might be a step in the right direction, but only if the energy is allowed to propagate both ways. Another idea might be to acknowledge the success of GM, but also accept that the parameterization is more than two decades old and that it might be time to think of new ideas. With the advance in computer technology and eddy-resolving and eddy-permitting models, way has been made for different ways to parameterize eddies, such as stochastic parameterizations (Porta Mana and Zanna, 2014). However, the use of coarse resolution models will be present for several years to come, and this calls for a rethinking of the present way to parameterize eddies. One idea could be to develop separate parameterizations for the different eddy dynamics such as baroclinic and barotropic instabilities as well as backscatter. However, with every addition of a new parameterization there is a computational cost, and this approach might not be feasible.

## 7.4 Using CCSM4 in the Arctic

The general topic of this thesis has been to discuss how poorly the Arctic is represented in the CCSM4 and POP2 and what problems are present in the model, with the major focus being the subsurface temperature bias. As discussed above, reducing the diffusivities polewards improves the overall simulation of the Arctic when one compares COSKAP to DEFAULT on both Nordic Seas and Arctic temperature, UAWD and possibly Arctic flow properties. Yet, despite its improvements, reducing diffusivities may be getting the Arctic better for the wrong reasons, as evidenced by the 2-core structure and the still too warm Arctic below 500 m. The reader can thus be tempted to ask whether the model is even useful in simulating climate in the Arctic environment. The answer to this is that despite its errors, the model is still useful in certain ways. For one, the ocean-atmosphere interactions are not affected greatly by the warm bias, as the temperature bias is mainly present below more than 100 m. Of course, as discussed earlier, with sea ice retreat in the Arctic and increased mixing in the upper ocean, the model might have shortcomings in this sense. However, one might also gain something from the current setup.

Current research in paloeclimate regarding abrupt warming events in the past glacial called Dansgaard/Oeschger (DO) events have been hypothesized to be related to a subsurface warming in the Nordic Seas and Arctic Ocean that accumulates until the warm water through a yet to be determined mechanism is brought to the surface and melts away a large area of sea ice (Dokken et al., 2013). Although the current setup of the model is meant to simulate pre-industrial climate, the warm bias might be viewed as representing the hypothesized warm Atlantic layer causing the DO events. This might be exploited by using the current setup of the model (with the excessive sea ice seen in B1850) to investigate the plausibility of this hypothesis concerning DO events by testing mechanisms of how to get the warm waters to the surface and investigate how the sea ice responds[6]. Another alternative could be to remove part of the sea ice to see if the warm subsurface water will be brought up and release its heat to the atmosphere. Such use of the model might be illuminating and as such the current model performance might be put to exciting use. This is, however, speculative and is left for other people to investigate.

[6]The temperature bias in B1850 presented here is in the deepest ocean, though, but the model is still warming (compare e.g. to figure 2).

# 8 Conclusion

A series of ocean simulations have been carried out using the coarse resolution CCSM4 and its ocean component POP2 in order to investigate the development of the Arctic temperature bias. Analysis has included poleward reductions in either horizontal or thickness surface diffusivities or both, reduced ocean eddy viscosity, and forced coarse 3° resolution setups have been compared to both a forced 1° resolution setup as well as a coarse coupled setup. From the results it is evident that reducing the diffusivities in the high latitudes results in a reduced subsurface temperature bias. The reduced temperature bias is attributed to an increased temperature loss to the atmosphere due to a confinement of the Norwegian Current to the shelf slope. This weakens the stratification in the spurious 2-core structure of the model Norwegian Current, causing an increase in heat loss to the atmosphere. Reducing diffusivities is connected to an improvement of the representation of both Nordic Seas and Arctic temperature, and reduced thickness diffusivity is also related to a reversed flow of intermediate, Atlantic waters in the Canadian basin in the Arctic which compares with observations.

Despite the promising results of the reduced diffusivities, it is not possible to conclude that strong diffusion is in fact the cause of the 2-core structure of the Norweigian Current, and that the chain of events actually happen the other way around. The 2-core structure shields the Atlantic water from losing its heat to the atmosphere, causing it to spread out in the interior instead. Thus, it cannot be ruled out that the reduction in the Arctic temperature bias following a reduction in eddy diffusivities is not just a result of treating secondary effects of a 2-core structure of the Norwegian Current.

The inspection of reducing viscosity suggests that an improved simulation of the transport through the Fram Strait might improve the overall simulation of the Arctic, as the transports in the current default model settup are not consistent with observations. Together with a model run with increased resolution it appears that the Fram Strait is too poorly resolved in both POP2 setups to properly simulate transports, which generally are too weak.

The key conclusions remain that while it may not be the optimal solution, reducing the thickness diffusivity does improve simulation of the Nordic Seas and the Arctic Ocean in the current setup of the coarse resolution POP2. This calls for better parameterizations than the currently available ones, preferably including the possibility of reverse energy cascades which the current GM parameterization does not include. Getting the full understanding of the temperature bias, however, requires even more extensive research than this study presents. One obvious next step is to compare the coarse resolution setups described in this thesis with an eddy-resolving or at least eddy-permitting model. This will both reduce the importance of eddy parameterizations and increase horizontal resolution in the vicinity of the Fram Strait and thus shed a much needed light on the relative importance of sub-grid mixing parameterizations in the Nordic Seas.

# References

Aagaard, K. (1981). On the deep circulation in the arctic ocean. *Deep Sea Res. 28A*, 251–268.

Aagaard, K. and E. C. Carmack (1989). The role of sea ice and other fresh water in the arctic circulation. *J. Geophys. Res. 94*, 14485–14498.

Abernathy, R. and J. Marshall (2013). Global surface eddy diffusivities derived from satellite altimetry. *J. Geophys. Res. 118*, 901–916.

Anderson, L., G. Björk, O. Holby, E. Jones, G. Kattner, K. Koltermann, B. Liljeblad, R. Lindegren, B. Rudels, and J. Swift (1994). Water masses and circulation in the eurasian basin: Results from the oden 91 expedition. *J. Geophys. Res. 99*, 3273–3283.

Andersson, M., K. Orvik, J. LaCasce, I. Koszalka, and C. Mauritzen (2011). Variability of the norwegian atlantic current and associated eddy field from surface drifters. *J. Geophys. Res. 116*, C08032.

Arakawa, A. and V. Lamb (1977). Computational design for the basic dynamical processes of the ucla general circulation model. Volume 17 of *Methods in Computational Physics*, pp. 174–265. San Diego: Academic Press.

Beszczynska-Möller, A., E. Fahrbach, U. Schauer, and E. Hansen (2012). Variability in atlantic water temperature and transport at the entrance to the arctic ocean, 1997-2010. *ICES Journal of Marine Science 69*, 852–863.

Beszczynska-Möller, A., R. Woodgate, C. Lee, H. Melling, and M. Karcher (2011). A synthesis of exchanges through the main oceanic gateways to the arctic ocean. *Oceanography 24(3)*, 82–99.

Bryan, K. (1969). A numerical model for the study of the circulation of the world oceans. *J. Comput. Phys. 4*, 347–359.

Bryden, H. L. (1973). New polynomials for thermal expansion, adiabatic temperature gradient and potential temperature of sea water. *Deep-Sea Res. 20*, 401–408.

Cunningham, S., T. Kansow, D. Rayner, M. Baringer, W. Johns, J. Marotzke, H. Longworth, E. Grant, J.-M. Hirschi, L. Beal, C. Meinen, and H. Bryden (2007). Temporal variability of the atlantic meridional overturning circulation at 26.5n. *Science 317*, 935–938.

Danabasoglu, G., S. Bates, B. Briegleb, S. Jayne, M. Jochum, W. Large, S. Peacock, and S. Yeager (2012). The ccsm4 ocean component. *J. Climate 25*, 1361–1389.

Danabasoglu, G., R. Ferrari, and J. C. McWilliams (2008). Sensitivity of an ocean general circulation model to a parameterization of near-surface eddy fluxes. *J. Climate 21*, 1192–1208.

Danabasoglu, G., W. G. Large, and B. P. Briegleb (2010). Climate impacts of parameterized nordic sea overflows. *J. Geophys. Res. 115*, C1105.

Danabasoglu, G. and J. Marshall (2007). Effects of vertical variations of thickness diffusivity in an ocean general circulation model. *Ocean Modell. 18*, 122–141.

Danabasoglu, G., J. McWilliams, and P. Gent (1994). The role of mesoscale tracer transports in the global ocean circulation. *Science 264*, 1123–1126.

Dokken, T., K. Nisancioglu, C. Li, D. Battisti, and C. Kissel (2013). Dansgaard-oeschger cycles: Interactions between ocean and sea ice intrinsic to the nordic seas. *Paleoceanography 28*, 491–502.

Eden, C. and R. Greatbatch (2008). Towards a mesoscale eddy closure. *Ocean Modell. 20*, 223–239.

Eden, C., M. Jochum, and G. Danabasoglu (2009). Effects of different closures for thickness diffusivity. *Ocean Modell. 26*, 47–59.

Ferrari, R., J. C. McWilliams, V. M. Canuto, and M. Dubovikov (2008). Parameterization of eddy fluxes near oceanic boundaries. *J. Climate 21*, 2770–2789.

Ferreira, D., J. Marshall, and P. Heimbach (2005). Estimating eddy stresses by fitting dynamics to observations using a residual-mean ocean circulation model and its adjoint. *J. Phys. Oceanogr. 35*, 1891–1910.

Fofonoff, N. (1977). Computation of potential temperature of seawater for an arbitrary reference pressure. *Deep Sea Res. 24*, 489–491.

Gent, P. R., G. Danabasoglu, L. J. Donner, M. M. Holland, E. C. Hunke, S. R. Jayne, D. M. Lawrence, R. B. Neale, P. J. Rasch, M. Vertenstein, P. H. Worley, Z.-L. Yang, and M. Zhang (2011). The community climate system model version 4. *J. Climate 24*, 4973–4991.

Gent, P. R. and J. C. McWilliams (1990). Isopycnal mixing in ocean circulation models. *J. Phys. Oceanogr. 20*, 150–155.

Gent, P. R., J. Willebrand, T. J. McDougall, and J. C. McWilliams (1995). Parameterizing eddy-induced tracer transports in ocean circulation models. *J. Phys. Oceanogr. 25*, 463–474.

Griffies, S. M. (1998). The gent-mcwilliams skew flux. *J. Phys. Oceanogr. 28*, 831–841.

Griffies, S. M., A. Biastoch, C. Böning, F. Bryan, G. Danabasoglu, E. Chassignet, M. England, R. Gerdes, H. Haak, R. Hallberg, W. Hazeleger, J. Jungclaus, W. Large, G. Madec, A. Pirani, B. Samuels, M. Scheinert, A. Gupta, S. C.A., H. Simmons, A. Treguier, M. Winton, S. Yeager, and J. Yin (2009). Coordinated ocean-ice reference experiments (cores). *Ocean Modell. 26*, 1–46.

Holton, J. R. (2004). *An introduction to Dynamic Meteorology* (5 ed.). Elsevier Inc.

Ilicak, M., H. Drange, Q. Wang, R. Gerdes, Y. Aksenov, D. Bailey, M. Bentsen, A. Biastoch, A. Bozec, C. Böning, C. Cassou, E. Chassignet, A. C. Coward, B. Curry, G. Danabasoglu, S. Danilov, E. Fernandez, P. G. Fogli, Y. Fujii, S. M. Griffies, D. Iovino, A. Jahn, T. Jung, W. G. Large, C. Lee, C. Lique, J. Lu, S. Masina, A. J. G. Nurser, C. Roth, D. S. y. Mélia, B. L. Samuels, P. Spence, H. Tsujino,

S. Valcke, A. Voldoire, Z. Wang, and S. G. Yeager (2016). An assessment of the arctic ocean hydrography in a suite of interannual core-ii simulations. *Ocean Modell. 100*, 141–161.

Jahn, A., K. Sterling, M. M. Holland, J. E. Kay, J. A. Maslanik, C. M. Bitz, D. A. Bailey, J. Stroeve, E. C. Hunke, W. H. Lipscomb, and D. A. Pollak (2012). Late-twentieth-century simulation of arctic sea ice and ocean properties in the ccsm4. *J. Climate 25*, 1431–1452.

Jakobsson, M., L. Mayer, B. Coakley, J. A. Dowdeswell, S. Forbes, B. Fridman, H. Hodnesdal, R. Noormets, R. Pedersen, M. Rebesco, H.-W. Schenke, Y. Zarayskaya A, D. Accettella, A. Armstrong, R. Anderson, P. Bienhoff, A. Camerlenghi, I. Church, M. Edwards, J. Gardner, J. Hall, B. Hell, O. Hestvik, Y. Kristoffersen, C. Marcussen, R. Mohammad, D. Mosher, S. Nghiem, P. Pedrosa, M.T. Travaglini, and P. Weatherall (2012). The international bathymetric chart of the arctic ocean (ibcao) version 3.0. *Geophys. Res. Let. 39*, 12609.

Jochum, M., B. Briegleb, G. Danabasoglu, W. Large, N. Norton, J. S., M. Alford, and F. Bryan (2013). The impact of near-inertial waves on climate. *J. Climate 26*, 2833–2844.

Jochum, M., G. Danabasoglu, M. Holland, Y. Kwon, and W. Large (2008). Ocean viscosity and climate. *J. Geophys. Res. 25*, C06017.

Koszalka, I., J. LaCasce, M. Andersson, K. Orvik, and C. Mauritzen (2011). Surface circulation in the nordic seas from clustered drifters. *Deep Sea Res. 58*, 468–485.

Large, W. and S. Yeager (2004). *Diurnal to decadal global forcing for ocean and sea-ice models: the data sets and flux climatologies.*

Large, W. G., J. C. McWilliams, and S. C. Doney (1994). Oceanic vertical mixing: A review and a model with a nonlocal boundary layer parameterization. *Reviews of Geophysics 32*, 363–403.

Liu, C., A. Köhl, and D. Stammer (2012). Adjoint-based estimation of eddy-induced tracer mixing parameters in the global ocean. *J. Phys. Oceanogr. 42*, 1186–1206.

Locarnini, R. A., A. V. Mishonov, J. I. Antonov, T. P. Boyer, and H. E. Garcia (2010). World ocean atlas 2009, volume 1: Temperature. s. levitus, ed. noaa atlas nesdis 68. Online. U.S. Government Printing Office, Washington, D.C.

Meredith, M. P., P. Woodworth, T. Chereskin, D. Marshall, L. Allison, G. Bigg, K. Donohue, K. Heywood, C. Hughes, A. Hibbert, A. Hogg, H. Johnson, L. Jullion, K. B.A., H. Leach, Y.-D. Lenn, M. Maqueda, D. Munday, A. Garabato, C. Provost, J.-B. Sallee, and J. Sprintall (2011). Sustained monitoring of the southern ocean at drake passage: past achievements and future priorities. *Rev. of Geophys. 49*, RG4005.

Nurser, A. and S. Bacon (2014). The rossby radius in the arctic ocean. *Ocean Science 10*, 967–975.

Olbers, D. and C. Eden (2013). A global model for the diapycnal diffusivity induced by internal gravity waves. *J. Phys. Oceanogr. 43*, 1759–1779.

Porta Mana, P. and L. Zanna (2014). Toward a stochastic parameterization of ocean mesoscale eddies. *Ocean Modell. 79*, 1–20.

Raj, R., L. Chafik, J. Nilsen, T. Eldevik, and I. Halo (2015). The lofoten vortex of the nordic seas. *Deep Sea Res. 96*, 1–14.

Randall, D. A. (1994). Geostrophic adjustment and the finite-difference shallow water equations. *Mon. Weather Rev. 122*, 1371–1377.

Redi, M. H. (1982). Oceanic isopycnal mixing by coordinate rotation. *J. Phys. Oceanogr. 12*, 1154–1158.

Rudels, B. (2015). Arctic ocean circulation, processes and water masses: A description of observations and ideas with focus on the period prior to the international polar year 2007–2009. *Progress in Oceanography 132*, 22–67.

Rudels, B., E. P. Jones, L. G. Anderson, and G. Kattner (1994). On the intermediate depth waters of the arctic ocean. In O. M. Johannesen, R. D. Muench, and J. E. Overland (Eds.), *The Polar Oceans and their role in shaping the global environment: The Nansen Centennial Volume*, Volume 85 of *Geophysical Monograph*, pp. 33–46. Washington D.C.: American Geophysical Union.

Schauer, U., A. Beszczynska-Möller, W. Walczowski, E. Fahrbach, J. Piechura, and E. Hansen (2008). Variation of measured heat flow through the fram strait between 1997 and 2006. In R. Dickson, J. Meincke, and P. Rhines (Eds.), *Arctic-Subarctic Ocean FLuxes*, pp. 65–85. Dodrecht: Springer.

Shields, C. A., D. A. Bailey, G. Danabasoglu, M. Jochum, J. T. Kiehl, S. Levis, and S. Park (2012). The low-resolution ccsm4. *J. Climate 25*, 3993–4014.

Smith, R., P. Jones, B. Briegleb, F. Bryan, G. Danabasoglu, J. Dennis, J. Dukowicz, C. Eden, B. Fox-Kemper, P. Gent, M. Hecht, S. Jayne, M. Jochum, W. Large, K. Lindsay, M. Maltrud, N. Norton, S. Peacock, M. Vertenstein, and S. Yeager (2010). *The Parallel Ocean Program (POP) reference manual.*

Spall, M. A. (2013). On the circulation of atlantic water in the arctic ocean. *J. Phys. Oceanogr. 43*, 2352–2371.

Steele, M., J. H. Morrison, and T. B. Curtin (1995). Halocline water formation in the barents sea. *J. Geophys. Res. 100*, 881–894.

Visbeck, M., J. Marshall, T. Haine, and M. Spall (1997). Specification of eddy transfer coefficients in coarse-resolution ocean circualtion models. *J. Phys. Oceanogr. 27*, 381–402.

Woodgate, R. A. and K. Aagaard (2005). Revising the bering strait freshwater flux into the arctic ocean. *Geophys. Res. Lett. 32*, L02602.

# A List of symbols

| | |
|---|---|
| $A_{visc}$ | Parallel viscosity parameter |
| $B_{visc}$ | Perpendicular viscosity parameter |
| $\beta$ | Meridional change in coriolis parameter |
| $b$ | Buoyancy |
| $c_n$ | Viscosity tuning parameter $n$ |
| $\Gamma$ | Adiabatic lapse-rate |
| $f$ | The local coriolis-parameter |
| $g$ | The gravitational acceleration |
| $H$ | Depth |
| $\mathbf{K}$ | 3-dimensional mixing tensor |
| $\kappa_{GM}$ | Thickness diffusivity coefficient |
| $\kappa_H$ | Horizontal diffusivity coefficient |
| $\kappa_I$ | Isopycnal diffusivity coefficient |
| $\mathbf{L}$ | 2-dimensional slope vector |
| $L_r$ | The first baroclinic Rossby radius |
| $L_{Rhi}$ | Rhines length scale |
| $N$ | Brunt-Väisälä frequency |
| $P$ | Pressure |
| $\rho$ | Density |
| Ri | The Richardson number |
| $S$ | Salinity |
| $\sigma$ | Potential density |
| $T$ | Temperature |
| $\theta$ | Potential temperature or latitude |
| $\phi$ | Longitude |
| $\mathbf{U}$ | Horizontal effective velocity |
| $U$ | Horizontal scale velocity |
| $\mathbf{u}$ | Horizontal large-scale velocity |
| $\mathbf{u}^*$ | Horizontal eddy-induced velocity |

| | |
|---|---|
| $W$ | Vertical effective velocity |
| $w$ | Vertical large-scale velocity |
| $w^*$ | Vertical eddy-induced velocity |
| $\varphi$ | An arbitrary tracer |
| $\nabla$ | The 3-dimensional gradient operator |
| $\nabla_H$ | The horizontal gradient operator |
| $\mathbf{\Psi}$ | Vector stream function |

# B List of acronyms

| | |
|---|---|
| AB | Amundsen Basin |
| ACC | Antarctic Circumpolar Current |
| ADCP | Accoustic Doppler Current Profiler |
| AMOC | Atlantic Meridional Overturning Circulation |
| APE | Available Potential Energy |
| AR | Alpha Ridge |
| AWCT | Atlantic Water Core Temperature |
| BAS | Barents Sea |
| BES | Bering Strait |
| BB | Baffin Bay |
| BLD | Boundary Layer Depth |
| CA | Canadian Archipelago |
| CAB | Canadian Basin |
| CCSM4 | Community Climate System Model |
| CFL | Courant-Friedrichs-Lewy |
| CS | Chuchki Shelf |
| CTD | Conductivity-Temperature-Depth |
| EGC | East Greenland Current |
| EKE | Eddy Kinetic Energy |
| EUB | Eurasian Basin |
| ES | East Siberian Shelf |
| FS | Fram Strait |
| GB | Greenland Basin |
| GCM | General Circulation Models |
| GM90 | Gent-McWilliams 1990 parameterization |
| GR | Gakkel Ridge |
| KPP | K-Profile Parameterization |
| KS | Kara Shelf |
| LB | Lofoten Basin |

| | |
|---|---|
| LR | Lomonosov Ridge |
| LS | Laptev Shelf |
| MB | Makarov Basin |
| NAB | Nansen Basin |
| NOB | Norwegian Basin |
| NS | Nordic Seas |
| NSEF | Near Surface Eddy Flux |
| OGCM | Ocean General Circulation Models |
| POP2 | Parallel Ocean Program |
| TLT | Transition Layer Thickness |
| TS | Temperature-Salinity |
| UAWD | Upper Atlantic Water Depth |
| WOA | World Ocean Atlas |
| WSC | West Spitzbergen Current |

# C Converting WOA temperature to potential temperature

As the World Ocean Atlas 2009 data has in situ temperatures listed, it needs to be converted to potential temperature in order to be compared to POP2 output. This is done by using the algorithm described by Fofonoff (1977) using the polynomial coefficients for adiabatic lapse-rate of Bryden (1973). The latter fits the adiabatic lapse rate to observations, yielding the following formula for the adiabatic lapse-rate:

$$\Gamma(^{\circ}\mathrm{C}/1000\mathrm{dbar}) = \sum_i \sum_j \sum_k A_{i,j,k} P^i (S-35)^j T^k. \tag{32}$$

Here, $T$ is in situ temperature, $P$ is pressure and $S$ is salinity. The coefficients $A_{i,j,k}$ are listed in Bryden (1973). The Fofonoff (1977) algorithm efficiently calculates the integral over the adiabatic lapse-rate:

$$\theta_r(P_0, T_0, S_0, P_r) = T_0 + \int_{P_0 P_r} \Gamma \mathrm{d}p, \tag{33}$$

with subscript 0 refers to in situ values and $P_r$ is the reference pressure, here chosen to be the surface pressure (0). The algorithm evaluates the integral in steps of d$p$'s, which can be resolved to be small or large, depending on the needed precision. For comparing with model output, the number of integration steps need only be 1 (Fofonoff, 1977, shows that the error is of order 0.1 mdeg C). Bryden (1973) also presents a formula for the integral in eq 33, with an error value of 2 mdeg C, slightly worse than the following algorithm. For the purpose of this study, the formula of Bryden (1973) would most likely be satisfactory, but for the sake of minimizing errors, the following method was used. The algorithm follows:

$$
\begin{aligned}
\Delta\theta_1 &= \Delta P \cdot \Gamma(P_0, \theta_0, S_0); & \theta_1 &= \theta_0 + 0.5 \cdot \Delta\theta_1 \\
\Delta\theta_2 &= \Delta P \cdot \Gamma(P_0 + 0.5\Delta P, \theta_1, S_0); & \theta_2 &= \theta_1 + (1 - 1/\sqrt{2})(\Delta\theta_2 - q_1) \\
\Delta\theta_3 &= \Delta P \cdot \Gamma(P_0 + 0.5\Delta P, \theta_2, S_0); & \theta_3 &= \theta_2 + (1 + 1/\sqrt{2})(\Delta\theta_3 - q_2) \\
\Delta\theta_4 &= \Delta P \cdot \Gamma(P_0 + \Delta P, \theta_0, S_0); & \theta_4 &= \theta_3 + \tfrac{1}{6} \cdot (\Delta\theta_4 - 2q_3)
\end{aligned}
\tag{34}
$$

where

$$
\begin{aligned}
q_1 &= \theta_1 \\
q_2 &= (2 - \sqrt{2})\Delta\theta_2 + (-2 + 3/\sqrt{2})\Delta\theta_1 \\
q_2 &= (2 + \sqrt{2})\Delta\theta_3 + (-2 - 3/\sqrt{2})\Delta\theta_2 \\
\Delta P &= P_r - P_0,
\end{aligned}
\tag{35}
$$

with $\Delta P = P_r - P_0/N$, where $N$ is the number of iterations. In this study $N = 1$. The biggest uncertainty in the method is calculating the correct pressure, which is here simply taken to be equal to the hydrostatic pressure at the data depth using a constant density of 1000 kg m$^{-3}$.